# Thermal Management of a Dual Active Bridge Converter for Smart Home Applications: Design of An Optimal Integrated Forced Air Heat-Pipe Embedded Heatsink Cooling System

# THERMAL MANAGEMENT OF A DUAL ACTIVE BRIDGE CONVERTER FOR SMART HOME APPLICATIONS: DESIGN OF AN OPTIMAL INTEGRATED FORCED AIR HEAT-PIPE EMBEDDED HEATSINK COOLING SYSTEM

BY

MARYAM ALIZADEH, B.SC.

A THESIS

SUBMITTED TO THE DEPARTMENT OF MECHANICAL ENGINEERING

AND THE SCHOOL OF GRADUATE STUDIES

OF MCMASTER UNIVERSITY

IN PARTIAL FULFILMENT OF THE REQUIREMENTS

FOR THE DEGREE OF

MASTER OF APPLIED SCIENCE

Master of Applied Science (2019) McMaster University

(Mechanical Engineering) Hamilton, Ontario, Canada

TITLE: Thermal Management of a Dual Active Bridge Converter for Smart Home Applications: Design of An Optimal Integrated Forced Air Heat-Pipe Embedded Heatsink Cooling System

AUTHOR: Maryam Alizadeh

B.Sc., (Mechanical Engineering)

Amirkabir University of Technology, Tehran, Iran

SUPERVISORS: Dr. Ali Emadi,

Dr. Jennifer Bauman

NUMBER OF PAGES: $cxv$, 115

*To my mother and father*

# Abstract

Due to significant progress in power density and miniaturization in the field of power electronics, point of converter packaging is becoming an important issue. Thermal management techniques should be implemented in design of a converter cooling system for ensuring robust functionality during the device operation. The thermal deign of a power converter under specific power loss is mainly determined by the maximum allowable temperature of the power switches. During operation, these switches experience rapid power transitions and therefore reliable thermal management must be used to prevent device failures.

The objective of this research is to design a reliable, efficient, small cooling system for a power converter using in smart home applications. Considering the limitations in the converter's size an integrated forced air heat pipe heat sink cooling system is proposed. A thermal model for the proposed cooling system is developed. In addition, the accuracy of the model in combination with multiple heat sources is verified with simulation and validated experimentally by building a setup for the proposed cooling system with multiple heat sources. Finally, the validated model is used in optimization algorithms for finding the optimal design of the cooling system.

In this thesis the geometrical configurations of the heat sink along with the fan selection options is optimized. Two objective functions, volume and efficiency of the cooling system, have been selected as the design space. The optimization problem has been limited to six degrees of

freedom represented by number of fins, fin height, fin thickness, heat sink width, base plate thickness and fan selection options.

The optimization is carried out using two different algorithms, Teaching Learning Based Optimization (TLBO) and Particle Swarm Optimization (PSO). Comparisons of the results of these two algorithms presented in this study show that TLBO algorithm requires less evaluations to find the optimal design compare to PSO. It has also been found that TLBO is more robust since it does not have any algorithm-controlling parameters. The improvement from robustness of the TLBO algorithm comes at the reliable results in terms of finding the optimum design more accurately.

# Acknowledgements

This research was undertaken thanks to funding from Canada Excellent Research Chair Program. I would like to take the opportunity to thank some very special people; without their help I could not do any of this.

I would like to express my deepest gratitude to my academic supervisor, Dr. A. Emadi whose expert advice, knowledge and guidance, motivated me throughout my research. It was a great honor to work with him and I'm very thankful for all the support he gave me over the last two years.

I am most grateful to my co-supervisor Dr. J. Bauman, for her much needed guidance, insight and expertise which greatly improved my research. I would also like to thank the faculty of mechanical engineering department especially Dr. Koshy and Dr. Habibi. I learnt a lot from these great people.

Thank you to Elvir Kahrimonovic for giving me the opportunity to have the wonderful experience of working at Infineon technologies based in Austria for the industry exchange program.

Thanks to Romina Rodriguez for her expertise, guidance and challenging detail questions as we worked together in different projects on the power electronics thermal management in these past two years.

And, thanks to all my colleagues and friends at McMaster Automotive Resource Centre (MARC) for their supports and friendship. Special thanks to Carin Yeghiazarian for his friendship and technical insight in engineering design.

Last but by no means least, I would like to express the profound gratitude from my deep heart to my father and my mother again, for which my mere expression of thanks likewise does not suffice. Without their unconditional love and consistent support through all the years, all my achievements have simply been impossible. And here goes my special thanks to my sister, Sara for being always not only a sister but being a true friend.

# Contents

# List of Figures

# Chapter 1

# Introduction

## 1.1. Motivation

Electronics devices are inseparable components of modern living and reach into all aspects of daily human life. They are growing into more and more advance and exceedingly compact devices. This trend leads to higher heat loss generation of electronic chips caused by electric current in even smaller surface areas. High heat flux of electronic components requires more efficient cooling methods to prevent component failure and ensure the device's reliable functionality. Advances in the field of power electronics have led to significant progress in power density and miniaturization. In order to keep up with the progress of compact and high-power density for electronic devices, more effective thermal management techniques and designs need to be applied to ensure the reliability of the new electronic systems while occupying small volume in the device's package.

The main goal of this work is to study the thermal performance of forced air cooling in a power converter used in smart grids for home applications by implementing an integrated heat pipe heat sink for dissipating the power loss of discrete power switches of the device. The objective

of the proposed forced air-cooling system in this study is to suggest an optimal integrated heat pipe heat sink design in terms of thermal performance, minimal volume and increasing the power efficiency of the cooling system.

Investigating the thermal performance of cooling system at different power loss ranges and finding the optimal design for a large number of different cooling system parameters and objectives with heat transfer software simulations (i.e. ANSYS Icepack) is very time consuming. Therefore, a thermal resistance network model for the cooling system has been developed for multiple heat sources. The thermal model is verified with ANSYS Icepack simulation and validated experimentally.

Another important factor for finding the optimal design of the cooling system is to utilize a reliable optimization algorithm. In 2011, Teaching Learning Based Optimization (TLBO) algorithm is proposed by R.V. Rao [1]. The algorithm is based on the influence of a teacher on the output of learners in a class. The most wide-used evolutionary optimization algorithms like PSO (Particle Swarm Optimization) or GA (Genetic Algorithm) require algorithm-specific controlling parameters. In contrast, TLBO is a more robust algorithm and doesn't need algorithm-specific controlling parameters [2]. In addition, this algorithm is for seeking global solutions for continuous non-linear functions, which also has low computations and high consistency [1]. Therefore, TLBO is implemented in this study to find the optimal design in terms of thermal performance, minimum volume and maximum power efficiency. The results are compared and disused with PSO algorithm and verified by simulating the optimal design in ANSYS Icepack.

## 1.2. Research Contributions

The main contributions of this research are as the following:

1. Design a forced air heat-pipe embedded heat sink cooling system for managing the thermal losses of a power converter using in smart grids for home applications.
2. Development of a thermal model for the proposed cooling system based on thermal resistance network.
3. Verification of the proposed thermal model with ANSYS Icepack simulation.
4. Experimental validation of the developed thermal model by using direct temperature measurements.
5. Finding the optimal design for the cooling system applying reliable optimization algorithms.
6. Implementing the optimization algorithm for finding the optimum design for the cooling system in terms of lowest volume and highest power efficiency.
7. Analysis of the optimized design for the maximum power loss of the converter.
8. Verifying the optimum cooling system design by simulating the design in ANSYS Icepack.

## 1.3. Outline of the Thesis

This research study concentrates on thermal management of the discrete power switches of a power converter for smart home applications by designing an optimal cooling system including heat pipes, heat sink and fan. The next chapters of this research are organized as followed:

Chapter two describes the fundamentals of heat transfer for thermal management. Then, it briefly introduces different techniques for thermal management in power electronics.

Chapter three explains the fundamentals of heat pipe systems. Afterwards, it explains the fundamentals of forced air cooling, design configurations and reviews the previous studies on forced air cooling system designs and reviews the previous work that has been done for thermal management of power electronic devices.

In chapter four, the dual active bridge converter is described. The objectives and challenges for thermal management of converters using in smart home applications are discussed.

In chapter five, the cooling system approach for the converter is explained and the design configuration is shown. Afterwards, the schematic of the cooling system is explained in detail. The heat pipe design criteria are explained and capable heat pipes for this research are selected. The thermal network model for the forced air cooling is defined and lastly the total thermal resistance network for the entire cooling system is achieved.

In chapter six, the selected heat pipes from chapter five are characterized for evaluating their thermal performance. The results are used in the developed thermal model for the proposed integrated forced air heat pipe heatsink cooling system. A setup is built and tested for validating the proposed thermal model from chapter five, experimentally. Later, the model is verified with the simulated model in ANSYS Icepack. And finally, the results are compared, and the accuracy of the model is discussed.

In chapter seven, the validated model is used for finding the optimal cooling system design in terms of volume and cooling system power efficiency. The optimization is implemented using two different algorithms, one a wide-used method (Particle swarm optimization) and the other a recently proposed algorithm (Teaching Learning Lased Optimization). The performance of each algorithm is discussed and compared, and lastly the optimal design is simulated and verified in ANSYS Icepack.

Chapter eight summarizes the main conclusions and suggests possible future research for the next generation of the converter's cooling system design.

# Chapter 2

# Fundamentals of Thermal Management

## 2.1. Introduction

Power electronics is the study of utilization of electronics components for controlling, converting and using the electrical power. Power converter devices are widely used in transportation, electrification, renewable energy applications [3]. The critical component in power converters is power semiconductor devices. However, due to the increasing demand of high power density and miniaturization, thermal management for the power converters is becoming more challenging and critical in the last decade [4],[5].

Thermal management solution for power electronics prevents the destruction of electronics due to their overheating. Thermal management techniques come in many forms, but all are based on the fundamentals of heat transfer for removing undesired heat. Junction of the electronic components is the most critical part that should not exceed the maximum allowable temperature provided by the manufacturers.

In general, heat transfer occurs whenever there is a temperature difference within a system or between the system and its surroundings. Heat transfer is classified into four broad mechanisms; thermal conduction, convection, radiation and transfer of heat by phase transitions [6].

## 2.1.1.Thermal Conduction

When the temperature difference exists in a stationary solid or fluid element, conduction heat transfer occurs along the temperature gradients. Conduction can happen only in one element at different points or between two elements that are in direct contact.

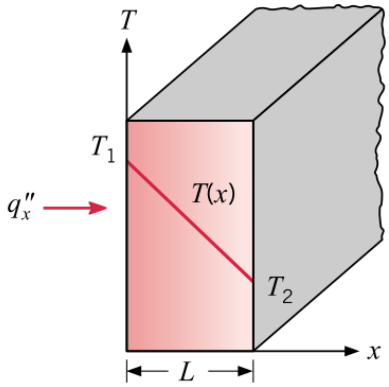


Figure 2.1: one dimensional conductive heat transfer [6]

The rate of heat moving from a surface (per unit area) is called heat flux. Heat conduction rate equation was introduced by Fourier's law in 1822. From Fourier's law, thermal conductivity in x-direction (Figure 2.1) is disproportional to the magnitude of the temperature gradient and opposite to its sign (Equation 2.1) [6]. Thermal conductivity (k) for each material is a unique

number and the unit is $\frac{W}{mK}$. And, the total heat output (q) in Watts is the product of the heat flux and the normal surface area ($A$) (Equation 2.2).

$$k_x = -\frac{q''_x}{\partial T/\partial x} \qquad \text{Equation 2.1}$$

$$q = A \,.\, q'' \qquad \text{Equation 2.2}$$

## 2.1.2.Thermal Convection

Convective heat transfer is the transfer of heat from one place to another via mass transfer, which dominantly is the movement of fluids. Convection is distinguished with two different mechanisms; natural convection and forced convection. When the fluid is forced to flow over a surface by external means such as a fan, pump, blower, etc. forced convection occurs. On the other hand, natural convection is caused by buoyancy forces which are the results of temperature difference in the fluid.

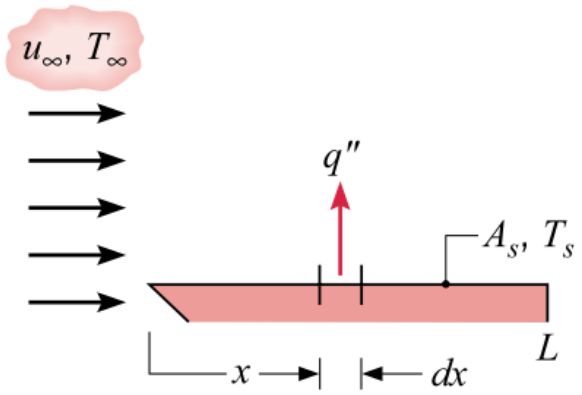


Figure 2.2: Convection heat transfer on a flat plate's surface [6]

Figure 2.2 shows the heat transfer convection over a plate with the surface area of $A_s$ and temperature of $T_s$, by considering an average convection heat transfer coefficient ($\bar{h}$) for the entire surface, the total heat transfer rate is calculated using Equation 2.3 [6].

$$q = \bar{h}.A_s(T_s - T_\infty) \quad \text{Equation 2.3}$$

It is known that in steady state conditions, when there is no change in latent energy, and thermal energy is not generating within an open system, energy equation can be described as Equation 2.4.

$$q = \dot{m}\, c_p\, (T_{out} - T_{in}) \quad \text{Equation 2.4}$$

## 2.1.3. Thermal Radiation

Thermal radiation happens when the kinetic energy of one surface travels to another surface via electromagnetic waves. Radiant energy can be emitted from any surface that has a temperature above absolute zero and since the energy is transported by electromagnetic waves, this type of heat transfer doesn't need the presence of any material like thermal convection or conduction [3].

Thermal radiation is dependent on the emissivity (ε) of the object, surface temperature and the capability of the surroundings for absorbing the energy (α)[4].

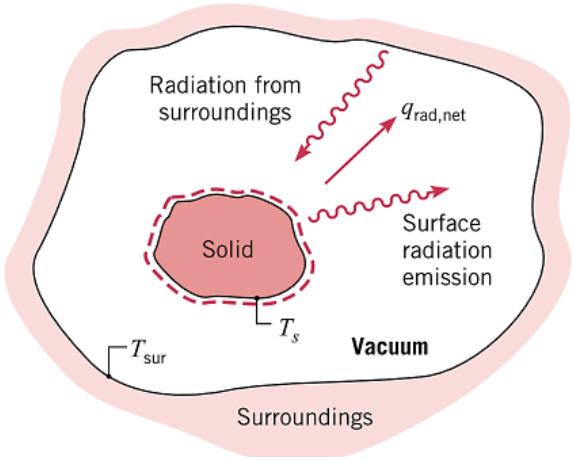


Figure 2.3: Radiation heat transfer between a surface and its surroundings [6]

Equation 2.5 describes the amount of heat transferred via radiation, where $\sigma$ is the Stefan-Boltzmann constant $5.67 \times 10^{-8}\,\mathrm{W/m^2K^4}$ and A surface area of the object [3].

$$q_{rad} = A.\varepsilon.\sigma(T_s^4 - T_{sur}^4) \qquad \text{Equation 2.5}$$

## 2.1.4. Phase Changes

Phase changes heat transfer occurs at a solid-liquid, solid-vapor or solid-solid interface. The transition from fluid to vapor form on a solid surface due to boiling causes transferring of the heat from the solid surface. Similarly, phase change from solid to fluid state on a surface due to melting causes the heat transfer from the surface and results in cooling the surface. In contrast, heat transfers to the surface when the vapor condenses to liquid state. So, phase changes heat transfer is involved with fluid motion and happens in almost no temperature difference. Phase change effectiveness is dependent on the latent heat of melting or vaporization $(h)$, surface tension at the interface $(\sigma)$ and the density difference of the two phases $(\rho_l - \rho_v)$.

## 2.2. Thermal Management Methods

Cooling electronic systems for reliable performance of the device is a key. For the last decades, a large variety of solutions are proposed for thermal management of power electronics systems [7]. However, cooling techniques are classified into two broad categories; active and passive cooling methods. These methods can involve the combination of any of four heat transfer mechanisms or just applying one of them [5].

### 2.2.1. Passive Cooling

Passive cooling is the application of available natural energy rather than consuming the conventional energy resources for transferring the heat [8]. In passively cooled systems, conduction and radiation are mostly utilized, especially for space-shuttle cooling. In space-based power generating systems the devices are in a vacuum environment, so convection methods are no longer applicable and the only mechanism for dissipating the heat is applying thermal radiation methods. One of the ways of utilizing passive cooling is applying heatsinks, heat spreaders (conductive plate to spread the heat), and thermal interface materials for natural cooling mechanisms [7]. For instance, in [9] flat-plate thermal spreaders and finned heat sinks are applied for thermal management of circuit board applications. Thermal interface materials play a key role in thermal management solutions in terms of providing proper connection between the cooling system components [10]. In [11] thermal interface material is used in the electronic components packages in order to ensure adequate heat transfer between the die and heat spreader of the component. A widely used passive cooling system is thermal energy storage with Phase Change Materials (PCM) [12]. PCM technology is mainly applied with other cooling systems like heat

sinks or heat spreaders for thermal management of devices with cyclic power dissipation [13]. PCMs also are widely used in thermal management of electronics [14] and automotive applications, specially cooling the battery systems in electric and hybrid vehicles [15]. PCMs are also applied in cooling of buildings in a way that cool air during night time solidifies the PCM storage and the warm weather during day time melts the PCM and extracts the accumulated cold [16]. Another common passive cooling system is heat pipes. In applications with limited space, heat pipes are the most used method for transferring the heat from the device to a location with larger space that heat dissipation is available. Heat pipes can be embedded in conductive plates or heat sinks for increasing heat spread or transfer capabilities [7]. Integrating heat pipes in electronic devices have been done widely in automotive applications [17], data centers cooling [18] and medical devices[19] due to their high conductivity, efficiency, flexibility and suitable range of working temperature without consuming any additional electric energy [20].

In general, passive cooling are very practical, energy-efficient and cost-effective techniques. However, they are limited in terms of relatively low level of heat dissipation compare to active cooling systems[5], [8].

### 2.2.2. Active Cooling

Active cooling methods involve an external device to enhance the cooling system performance, which mostly relies on conventional energy resources. Active solutions including forced air cooling, liquid cooling, spray cooling, jet impingement are commonly means of active cooling in power electronics systems. Forced air cooling usually is the combination of fans and heat sinks. The fans are implemented for lowering the thermal resistance between the ambient air and the heat sink. This method is the most commonly used cooling system in power converters

due to easy implementation [21]. While, for higher power densities liquid cooling is suggested over air cooling due to higher thermal conductivity of the liquids in comparison to gases. Liquid cooling technologies classifies into indirect and direct cooling methods. Cold plates are the most widely used indirect liquid cooling systems in power electronics and used in many applications such as automotive [22], solar power satellites[23], and data centers thermal management [24]. Jet impingement cools the device directly by very highspeed liquid streams. This technique is widely used for cooling power electronic modules [25] due to its high efficiency and high power working range. However, the performance of jet impingement systems is dependent on a large number of design parameters and the systems are costly compare to the other conventional liquid cooling systems [7]. Spray cooling is shattering forced liquid though a narrow outlet to a hot surface. The forced liquid becomes very small droplets when exiting the outlet. The droplets spread on the hot surface and by evaporating causes direct heat removal from the surface at even low temperature. Although this technology is very complex and dependent on many parameters, it is of interest for electronic cooling with high heat flux applications [26]. In general, leakage, corrosion, electrical conductivity and design complexity are the disadvantages of liquid cooling in comparison to air cooling technologies [7].

Mainly, active cooling solutions are more costly compare to passive cooling due to power energy consumption for their performance, however, they can provide higher cooling capacity and better thermal management in high power density devices [5].

# Chapter 3

# Heat Pipes and Forced Air Cooling Systems for Power Electronic Converters

In this chapter, initially fundamentals of heat-pips, their applications and working specifications are explained. Afterwards, forced air cooling systems due to their high applications in power converters are explained in detail and previous researches on forced air cooling systems are studied.

## 3.1. Heat Pipes

Among the passive cooling techniques for transferring the heat, heat pipes are considered as one of the most suitable technologies. A heat pipe is a passive two phases heat transfer device with a very high thermal conductivity, which is capable of transferring large quantities of heat with a minimal temperature drop in a very fast speed. Heat pipes are known as one of the most efficient passive heat transfer methods in terms of energy saving due to their high heat transfer effectiveness, zero need of electric power consumption, the ability to separate the hot and cold

sources completely, very low manufacturing costs in the last years and having no moving parts [27], [28]. Heat pipes have been used in very diverse applications such as electronics, food processing, spacecraft, plastic injection molders, mechanical, transportation, chemical and medical industries [29] [30].

### 3.1.1.Fundamental of Heat Pipes

Heat pipe structure made by an evacuated tube which is partially filled with a working fluid before evacuation. Heat pipes consist of three sections: evaporator, adiabatic (insulated), and condenser section (Figure 3.1). The working fluid changes its phase during the heat pipe operation; at the heat source, the working fluid absorbs the heat in the evaporator section and phase-changes to vapor due to latent heat of evaporation. Because of the higher vapor pressure of the working fluid at the evaporator than the condenser, the vapor flows rapidly towards the condenser. At the condenser, the latent heat of condensation is released to the heat sink and the vapor returns back to the liquid phase. The liquid moves back from the condenser to the evaporator in the opposite direction of vapor flow. The liquid movement carries by wicking structure of the heat pipe due to the capillary force of the wicks (Figure 3.1) or the gravity force. In general, wicks cause capillary pressure on the condensed working fluid to move back to the evaporator section. The wick structure is not necessary for the heat pipes in the cases that gravity or other sources can overcome the surface tension, and cause the liquid to return to the evaporator end [20].

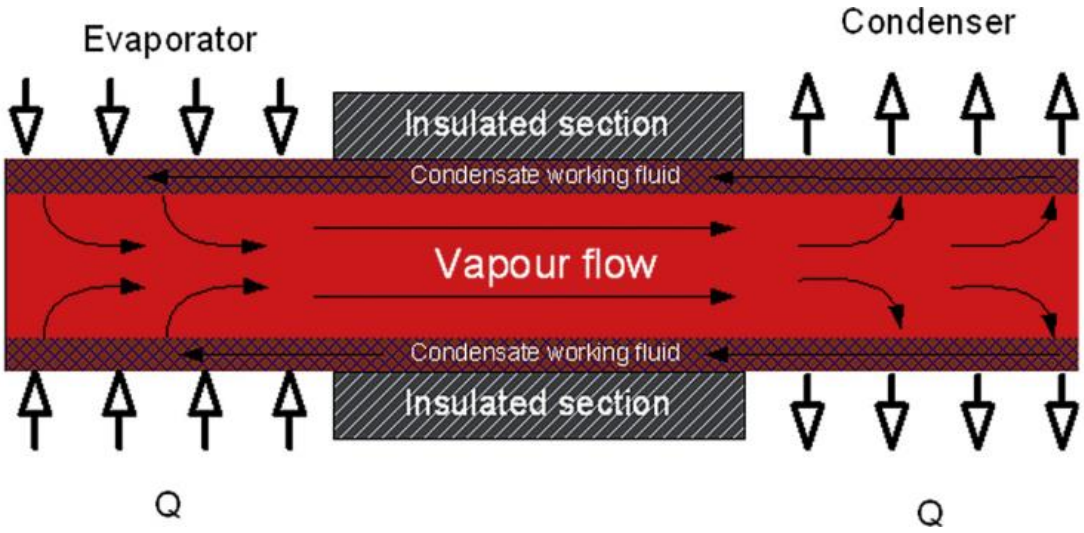


Figure 3.1: Heat pipe operation [28]

## 3.1.2.Heat Pipe Specifications

The working fluid can be different based on the operating temperature that is needed for the application. The author in [31] categorized the heat pipes according to their operating temperature range into four broad groups. The possible working fluids of each group are given in Table 3.1 [29].

Table 3.1: Possible working fluid for each category of heat pipes based on the operating temprature

| Group number | Temperature range (Kelvin) | Possible Working fluids |
|---|---|---|
| 1 | More than 700 | Liquid metals |
| 2 | 550-700 | Naphthalene and biphenyl, etc. |
| 3 | 200-550 | Water, ammonia, ethanol, methanol, etc. |
| 4 | 1-200 | Noble gasses, oxygen and nitrogen |

Usually, the selected materials for heat pipe casing are metals because of their high thermal conductivity and mechanical strength. The most commonly used metals are aluminum, copper, and stainless steels. However, recently silicon is presented as the best alternative for metals in terms of simpler fabrication process and good compatibility with semiconductor devices [32]. In general, aluminum is used in cases that low weight is critical, copper is mostly selected for the operating temperature range of (0,200) ℃. On the other hand, stainless steels cannot be used while having the water as the working fluid due to the reason that water reacts to steel and reduces the effectiveness of the heat pipe by the time. So, the working fluids and selected material of the heat pipe casing must be compatible to prevent chemical reactions such as oxidation. In [28], the author provided a table that shows the compatibility of different working fluids with different casing materials.

## 3.2. Forced Air Cooling

Forced convection is applied by implementing external mechanical apparatus such as fan, blower, pump, etc. when natural cooling is not adequate. Forced air cooling is one of the simplest and most widely used methods of high heat flux thermal management for a large variety of electronics systems ranging from personal computer to very large data centers. The advantages of forced air cooling compare to the other methods of active cooling are simpler design, less costs, ease of application and a wide range of availability for selecting off the shelf components in the last years. Usually, hot components are extended by mounting heat sinks in order to provide more heat dissipation area. In addition, for assuring more effective thermal management and lowering total thermal resistance between the heat sink and the ambient, devices that provide forced air such as fans are implemented to the cooling system. Fan selection is very critical aspect of the air

cooling designs. Not only the flow rate of the fan should be adequate for the cooling purpose, but also the static pressure (system's thermal resistance) that occurs by air flow passing through the heat sink's channels should not exceed more than the range of cooling requirements. The heat transfer coefficient of air forced convection is mainly in the range of 25 to 250 $W/m^2.K$ which can typically be used for applications with tens to hundreds watts heat loss [6], [7]. In the following of this section, we briefly explained different designs for the heatsinks, the performance specifications of fans and previous studies that have been done for designing forced air cooling systems in power electronics.

## 3.2.1. Heat Sink Designs and Specifications

Heat sinks are passive cooling devices that transfer the heat to the ambient air or fluid with the concept of extending the heat generating surface area of the heat source with their fins to the surrounding cooling medium. Due to the possible existence of air gaps between the heat sink and the heat spreader of the device, there is a need for thermal interface materials between them to fill the air gaps and by that improve the cooling system performance.

In general, heat sinks are classified into two broad categories based on the fin types; pin fins (Figure 3.2.a) and plate fins (Figure 3.2.b), the fins can be parallel or flared (Figure 3.2.c). Mainly, a heat sink with larger surface area has better performance. Pin-fin heat sinks are capable of having more surface area than parallel plate heat sinks with the same dimensions. In [33], pin and plate-fins are compared and it is found that for the same surface areas, pin-fins heat sinks have better cooling performance over plate-fins heat sinks. [34] ,[35] and [36] investigate the heat transfer performance of pin-fin heat sinks for different pin-fin configurations.

(a) (b) (c)

Figure 3.2.a: Pin-fin heat sink with round shape fins. b: Parallel plate heat sink. c: Flared plate heat sink [37]

Authors in [38] and [39] studied the heat dissipation performance of flared fin heat sinks, they observed that total heat dissipation capability of flared fin heat sink is higher than the parallel plate fin heat sink. With the equal effective surface area for heat sinks Figure 3.2.b and Figure 3.2.c, we can see that due to smaller channel width of parallel plate fins to flared fin ones, flow resistance in parallel plate fins is higher. So, flaring the fins decreases the heatsink thermal resistance and improves the total thermal performance. However, heats sinks with parallel plates are widely used for thermal management of electronics due to their easy manufacturing, design configurations and thermal model development. Thermal resistance of a heat sink simplifies its design criteria. Figure 3.3 represents a parallel-plate fin heat sink configuration. Thickness, length and height of the fin, number of fins, width and baseplate thickness of the heat sink, and thermal conductivity of the heat sink material are the parameters that define the thermal performance of a parallel-plate heat sink.

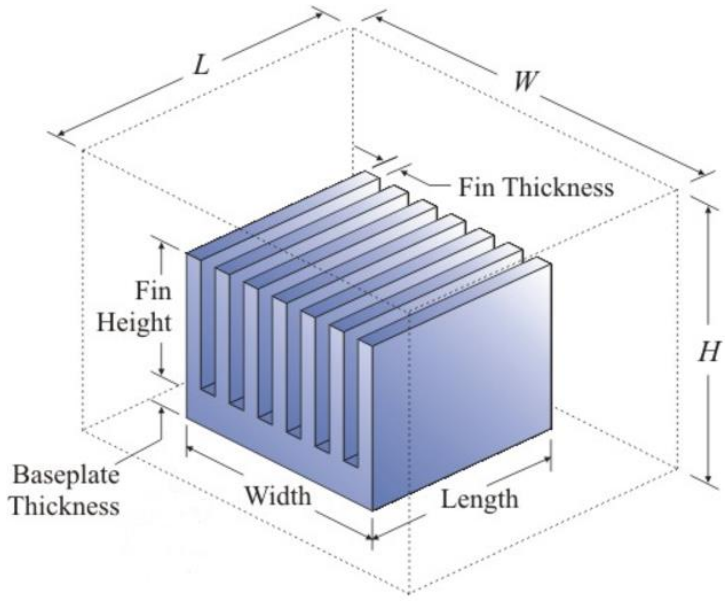


Figure 3.3: Design parameters for a parallel-plate fin heat sink

## 3.2.2. Fan Specifications

In the forced air cooling systems, the fan is the device for delivering the air flow to the heat sink's channels. The fan has an inlet to enter the air in the fan and an outlet which direct the air flow to the heat sink. The fan's motor transfers energy to the air. The delivered energy from the motor to the air flow is the energy difference between the air's energy at the outlet and inlet. The energy difference can be defined as the change in pressure between the two openings [40], [41].

Fan manufacturers usually define the performance of a fan in the form of pressure drop versus the volumetric air flow [42]. However, while implementing a fan in a system, in addition to the fan's pressure drop, losses occur whenever there is a change in cross section or direction of the fan. Therefore, in order to estimate the air flow of a fan while is faced to a heat sink, due to the change in cross section are of the air flow, the pressure drop-volumetric air flow curve of the fan has to be multiplied with the fin spacing ration of the heat sink [43].

The mechanical output power ($P_{out}$) for a fan is defined by the product of air volume flow (Q) and total pressure rise in the fan ($P_T$) (Equation 3.3), and the fan efficiency $\eta_f$ is the ratio between mechanical output power and actual power used by the fan ($P_{in}$) (Equation 3.4) [44], [43].

$$P_v = \frac{\rho . v^2}{2} \quad \text{Equation 3.1}$$

$$P_T = P_v + P_s \quad \text{Equation 3.2}$$

$$P_{out} = P_T . Q \quad \text{Equation 3.3}$$

$$\eta_f = \frac{P_{out}}{P_{in}} \quad \text{Equation 3.4}$$

The total pressure drop consists of two components; dynamic and static. Dynamic (Velocity) pressure ($P_v$) is in the direction of flow and occurs due to the velocity of the air flow, and the static pressure ($P_s$) is perpendicular to the air flow that is usually provided by the manufacture. Therefore, the total pressure of a fan is the sum of static and dynamic pressure (Equation 3.2).

The selection of fans for a system must be done by matching the fan performance with the system requirements [41]. So, finding the operating point of the fan is very dependent on the system properties. As a result, since operating point of each fan changes based on the properties of the system, we can find an optimized way of cooling system design or fan selection which leads to a better operating point, which induces lower thermal resistance, lower power consumption and higher efficiency of the cooling system.

## 3.3. Previous Studies for Forced Air Cooling System Design

In [27], a heat pipe finned heat exchanger model for energy recovery of air conditioning systems is presented and validated experimentally for different working fluid and working conditions. Several reviews have been done on heat pipe heat exchanger cooling system modeling and design [45]. Different designs have been done using heat pipes in cooling plates for increasing heat spreading on the surface and conductivity such as [46], [47] and [48]. Heat pipes are used in [49] for transferring the heat to the heat sink which can also be used as the enclosure of the electric devices. The theoretical power converter limits for forced convection thermal management is discussed in [50]. The authors in [51], studied the thermal barriers in converter systems in order to estimate the maximum possible power density of the device. These studies are implemented experimentally and validated in [52]. Forced air cooling system model developed and implemented by the authors in [50]–[53] are extended for designing a high ambient temperature forced air cooling in an automotive inverter system [54].

The design of a cooling system in power converters is not only for preventing the electric components from overheating, but also is pursuing an optimal design which is in desire of the converter design purpose such as minimizing the weight, the volume, height, the price or maximizing the efficiency for the desired working conditions, etc. An optimization approach is usually developed to find the optimal design which is in line with the objective function of the system.

The authors in [52], designed the forced convection cooling system for minimized weight. Optimizing the cooling system conductivity for different heat sink material has been done in [43]. The authors in [55], studied and compared the efficiency of forced and natural convection cooling systems for high power density converters. However, these researches did not take into account

the actual mechanical power consumption of the fan during its performance for optimizing the efficiency of forced air cooling systems. Also, in most of the thermal management problems in power electronics, researchers used genetic algorithm or other evolutionary algorithms to find the optimal design for the cooling system [55], [43], [52]–[54]. However, these algorithms are based on the algorithm-controlling parameters, which lead to un-robustness of the optimization mechanism [56]. On the other hand, some other algorithms exist which are more robust like Teaching Learning Based Optimization (TLBO) that can be applied for mechanical design problems [1],[57].

In this study, we applied TLBO algorithm for finding the optimal design of a forced air heat-pipe embedded heat sink cooling system for multiple heat sources. The optimization has been done for finding the minimum thickness and the actual mechanical power consumption of the cooling system. The optimization results are compared to the results applying Particle Swarm Optimization (PSO) which is an evolutionary algorithm, and lastly the optimum design is verified with ANSYS Icepack.

# Chapter 4

# Dual Active Bridge Converter for Smart Home Applications

## 4.1. Power Electronics in Smart Home Applications

In electric power systems, high flexibility in delivering the power is a must, especially in smart grid applications. High flexibility in delivering power is widely used in the integration of power source (for instance renewable energy source) and dynamic loads. The behavior of the source and load is in a way that is following a conveying path that ensures a reliable operation due to its design, that's why this type of source and load integration is known as smart grid technologies [58].

One of the very popular applications of using smart grids is in the houses with photovoltaic panels for producing electricity. Generating electricity using solar energy as the renewable power source has been very promising in the last decades. Photovoltaic panels accumulate solar energy and the system must convert the harvested energy to DC voltage or current. To obtain the fast

response and high flexible power delivery in the grid condition an efficient power converter is required [59].

## 4.2. Thermal Management Challenges for Power Converters in Smart Home Applications

Generally, volume and efficiency are the two key factors that are important for the converter packages in smart home applications. High volume requires more space for installation in the house and uses more material for the converters packaging especially in mass production. Low efficiency demands high power electricity consumption for the converter performance, which is not in favor of any consumer.

Advances in the field of power electronics had a huge progress in power density and miniaturization [7]. One of the critical components that are used in designing the power converters is power switches. Although, silicon power switches have been used widely in power electronics industry for the last few decades, silicon-based technology has some limitations for the increasing demand of high power density usages. One of the critical limitations of silicon-based power switches is their relatively low junction temperature operation capability, which also follows by costly cooling systems. However, the invention of silicon carbide (Si-C) based power switches results in higher thermal conductivity which follows by higher junction temperature operation capability [58], [5]. Therefore, more efficient cooling techniques are preferred to manage the thermal requirements of high power density components.

## 4.3. Introduction of the Dual Active Bridge Converter Using in Smart Home Applications

The designed power converter in this research is for smart home applications, which is using solar power as the renewable energy source. This converter consists of a dual active bridge converter and an inverter (Figure 4.1). The dual active bridge part includes the low voltage and high voltage side. The electricity from solar energy as the voltage input enters the high voltage side, and it either can be stored in a battery passing through the low voltage side or be used for one phase load applications as the house devices power electricity source.

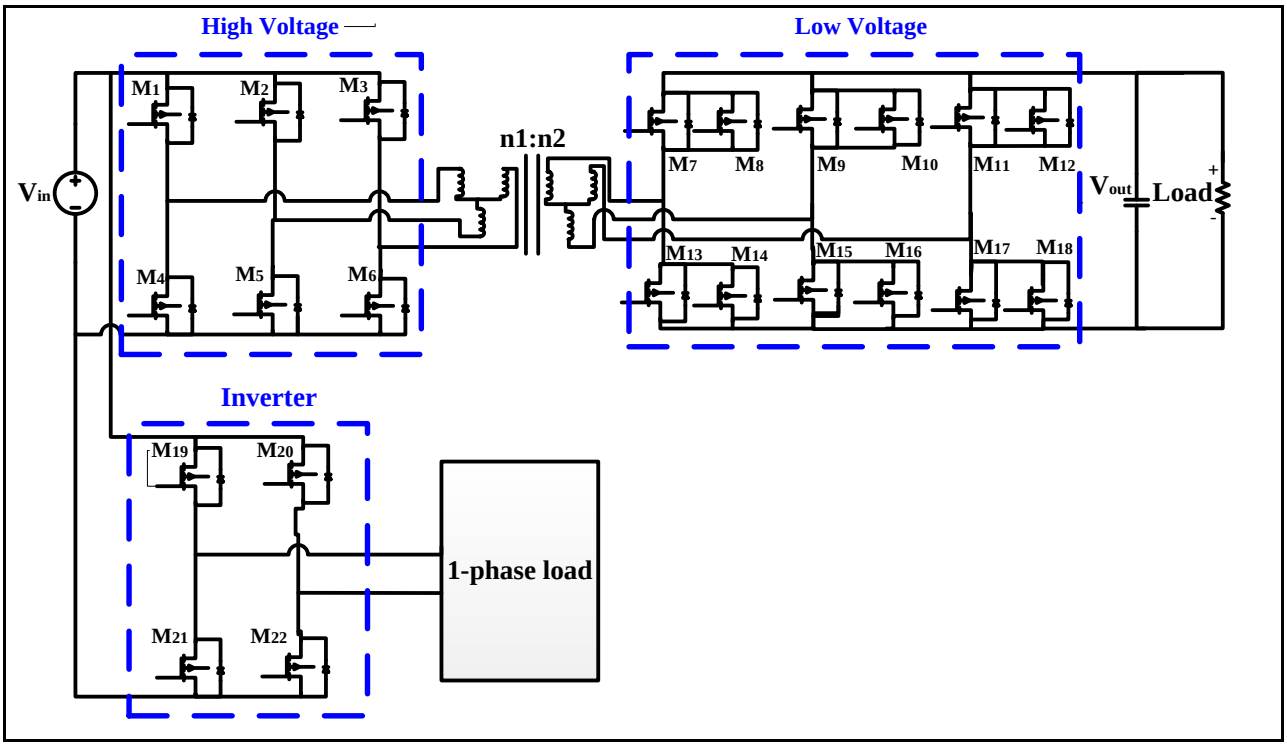


Figure 4.1: Schematic of the inverter with the Dual Active Bridge power converter

As already mentioned, one of the very critical components in power converters is switches. The switches that are used in this study is Metal-Oxide-Semiconductor Field-Effect Transistor (MOSFET). In our power converter, there are 6 power MOSFETs ($M_1 - M_6$) in the high voltage side, 12 MOSFETs ($M_7 - M_{18}$) in the low voltage side and 6 MOSFETs ($M_{19} - M_{22}$) for the inverter (Figure 4.1). The selected MOSFETs for this study are Silicon Carbide (Si-C) based power switches. In General, Si-C MOSFETs have higher junction temperature capability compare to silicon based switches. The Si-C based MOSFET that is used for the low voltage side is TO-220 and for the inverter and high voltage side is TO-247 power semiconductor package. The MOSFET types that are used in this design are as the following:

1) TO-247 (Silicon Carbide power MOSFET from CREE) [60] and [61].
2) TO-220 (OptiMOS3 power transistor from Infineon) [62].

## 4.4. Cooling System Objectives and Challenges

Power switches have the most heat loss in the converters and if their heat losses cannot be dissipated, they destruct permanently due to overheating. The physical location of the MOSFETs and different sides of our converter is shown in Figure 4.2.a.

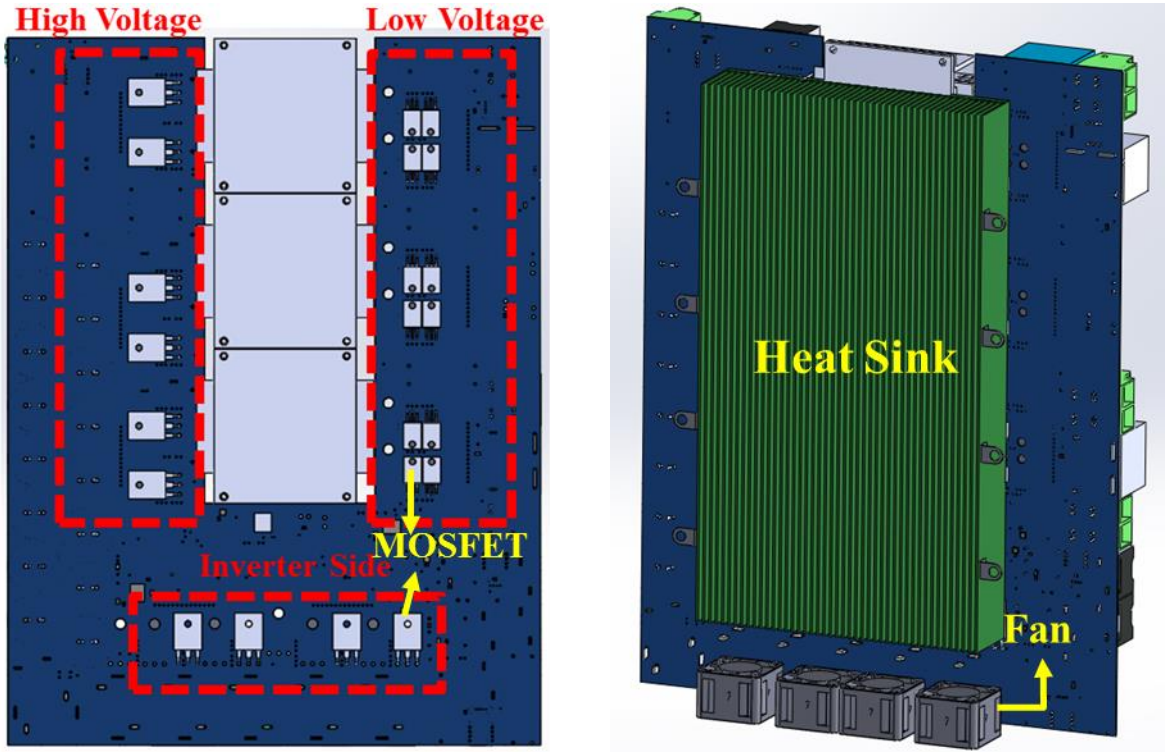


(a) (b)

Figure 4.2.a: The front view of the converter while is mounted on the wall, b: Possible cooling system for MOSFETs heat dissipation.

This converter is designed for 10 kW and tested up to 3 kW power output. The cooling system in this study is designed based on the experimental results of the tested converter for 3 kW. During the converter operation, maximum power loss for each side is measured experimentally and is used for the cooling system design as an input. The measured values for the power loss of each part of the power converter are shown in Table 4.1.

Table 4.1: Power loss heat dissipation in the converter

| | Max TOTAL power loss [W] | Max power loss of each MOSFET [W] |
|---|---|---|
| Low voltage side | 129.37 | 11 |
| High voltage side | 89.7 | 15 |
| Inverter side | 158.68 | 40 |

The power loss for each part should be divided between the groups of MOSFETs in them. According to Table 4.1, the maximum total power loss for low voltage side is 129.37 W and there are 12 MOSFETs located in this side, so the power loss of each MOSFETs in this group ($M_7 - M_{18}$) can be calculated using Equation 4.1. Similarly, the power loss for the MOSFETs in high voltage side ($M_1 - M_6$) and inverter side ($M_{19} - M_{22}$) is measured using Equation 4.2 and Equation 4.3, respectively.

$$\text{Power loss}_{\text{MOSFET,low voltage}} = \frac{129.73}{12} \approx 11\ \text{W} \qquad \text{Equation 4.1}$$

$$\text{Power loss}_{\text{MOSFET,high voltage}} = \frac{89.70}{6} \approx 15\ \text{W} \qquad \text{Equation 4.2}$$

$$\text{Power loss}_{\text{MOSFET,low voltage}} = \frac{158.68}{4} \approx 40\ \text{W} \qquad \text{Equation 4.3}$$

One of the possible ways to manage the measured heat loss of each MOSFET is mounting a cooling system directly on them like Figure 4.2.b. Since the converter will be mounted on the wall, there is a desire to have the device as small as possible specifically a thinner system is more preferred. So, the main goal of this study is to design the cooling system in a way that adds the lowest thickness to the entire system. And the second goal is to have a very efficient system in terms of power usage and costs.

## 4.5. Cooling System Design Approach

Figure 4.2.b shows a possible forced air cooling system for the converter. The system contains a heat sink mounted on the lead frames of the MOSFETs, and 4 fans are forcing air to the chandelles of the heat sink for dissipating the heat. As already mentioned, one of the goals of this study is to have a very thin converter. In case of mounting any type of cooling system on the lead frame of the MOSFETs, for instance the proposed system in Figure 4.2.b, the space between the lead frame and the PCB may stay unused (Figure 4.3.a). Hence, in terms of using this space we need to transfer the power loss in a way that we can dissipate the heat from these available locations. A very efficient way to transfer the heat is using heat pipes. Figure 4.3.b shows that a heat pipe can connect the lead frame of the MOSFET to the heat sink in any desired location. Therefore, by mounting the heat pipe on the MOSFET we can implement a heat sink in the unused available spaces and save more space in general. Typically, the heat pipe can provide the freedom to dissipate the heat at any location on the PCB.

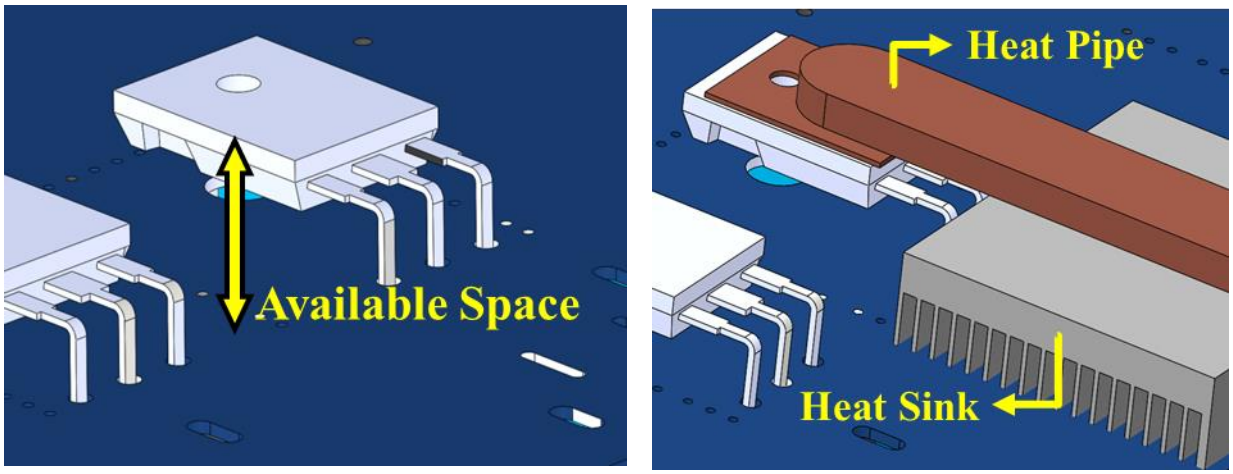


(a) (b)

Figure 4.3.a: Possible usable space between MOSFET's lead frame and the PCB, b: mounting heat pipe on the MOSFET for transferring the heat to the heat sink

Maintaining acceptable temperature for each power MOSFET requires an efficient cooling system to dissipate the heat from them. According to chapter 3, for transferring the heat from one point to another, heat pipes are very reliable. In this study, the cooling system must dissipate the transferred power loss of each MOSFET through the heat pipes to the ambient in a way that satisfies the junction temperature requirements of each MOSFET in terms of performance and reliability. In this study, the electronics thermal management is examined in three inseparable steps.

First, the thermal management system must maintain the power MOSFET junction temperature below its critical allowable point.

Second, the heat pipe module must be able to conduct the maximum possible generated heat from the corresponding MOSFET properly to the dissipating section of the cooling system.

Third, there must be efficient heat dissipation from heat pipes to the ambient.

As a result, the thermal design is influenced by the amount of heat loss, power switches size, critical junction temperature and ambient temperature, which needs to be very thin and efficient. According to chapter 3, forced air cooling is a proper selection for dissipating the range of converter's heat loss for this study.

In the next chapter, a cooling system for this converter is suggested and a model for estimating the junction temperature of the MOSFETs and overall performance of the cooling system is proposed.

# Chapter 5

# Proposed Integrated Forced Air Heat Pipe Embedded Heatsink Cooling System

## 5.1. Design Configuration

Since the cooling system needs a heat pipe for transferring the heat and a forced air cooling system for dissipating the heat, an initial idea for this converter cooling system is shown in Figure 5.1. The MOSFETs are connected to the heatsink via heat pipes, while the heat loss dissipates from the heatsink by the forced air cooling system using fan. As it is shown in Figure 5.1, thermal management for all the MOSFETs applied with the same approach, accordingly thermal model and design process for all the three sides are the same but different geometries. Therefore, to avoid repeatable contents only the inverter part is taken for the design process explanations. Besides, based on Table 4.1, the MOSFETs in inverter side have higher heat loss, so it is a better practice to design the cooling system with more strict constraints.

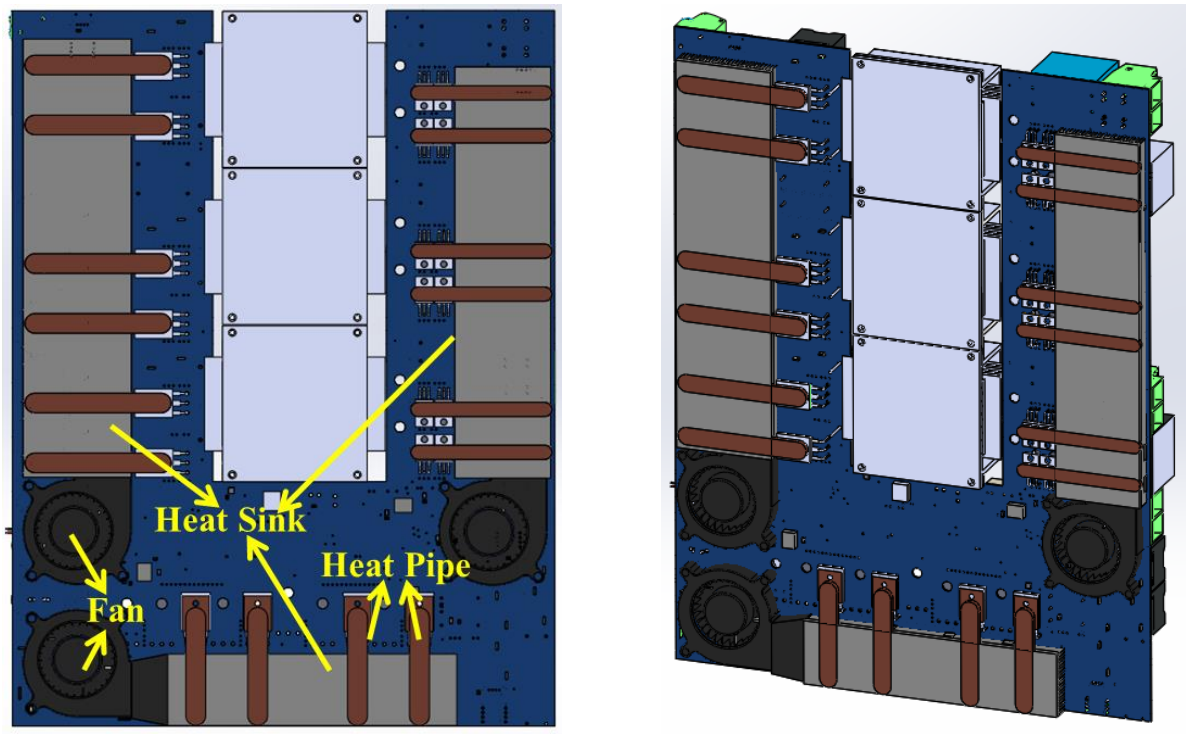


(a) (b)

Figure 5.1.a: Front view and, b: 3D view of the proposed cooling system for the converter

Two cooling system is suggested for this study in Figure 5.2. Both designs are very similar, the only difference is the heat pipes in Figure 5.2.a are embedded with two heat sinks. However, in Figure 5.2.b, there is only the bottom heat sink for the heat dissipation. As it can be seen, the MOSFETs are connected to the heatsink with the heat pips. And the fan directs the entire air flow to the channels of the heatsinks through a duct. A thin copper plate with the same foot print as MOSFET is soldered to the heat pipe so we can mount the MOSFET to the heat pipes with screws easily.

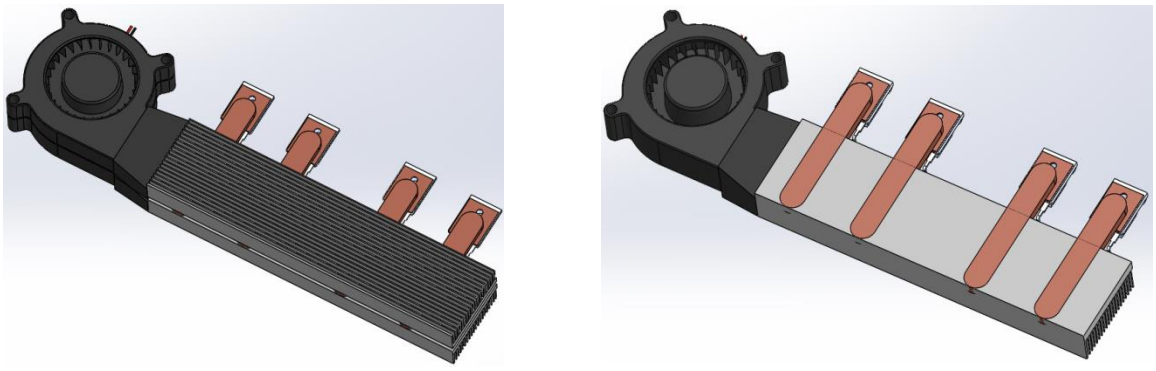

(a) (b)

Figure 5.2.a: 3D design of the cooling system with two heat sinks, b: with only one heat sink in the heat dissipation section

In order to design the cooling system to prevent the MOSFETs junction from overheating, it is necessary to dissipate the heat loss with an efficient rate, and to have an efficient heat dissipation rate the cooling system should have a low thermal resistance. Since the MOSFET and heat pipe module in Figure 5.2 has a repeated pattern in the entire cooling system, we only need to study the thermal performance of one MOSFET in an integrated heat pipe heatsink (Figure 5.3) and then expand the results for the entire system.

The design in Figure 5.3.b is suggested for the cases that the space between the MOSFETs lead frame and PCB is enough for heat dissipation. Figure 5.3.a is suggested for more strict and harsh constraints. This sandwich design is very similar to Figure 5.3.b, but another similar heatsink is added on top of the heat pipe.

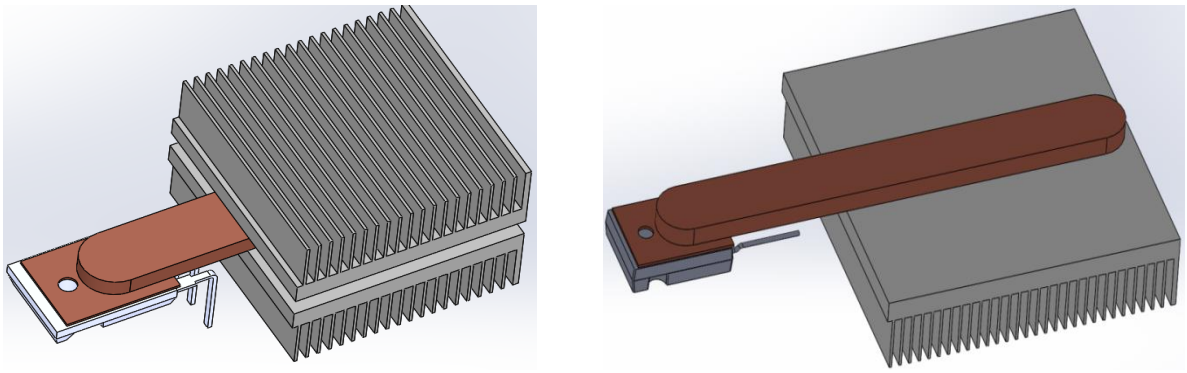

(a) (b)

Figure 5.3: Single MOSFET with a: sandwich heat-pipe heatsink 3D design, b: single heat-pipe heat sink 3D design

## 5.2. Thermal Model Schematics

### 5.2.1.Single Heat Source

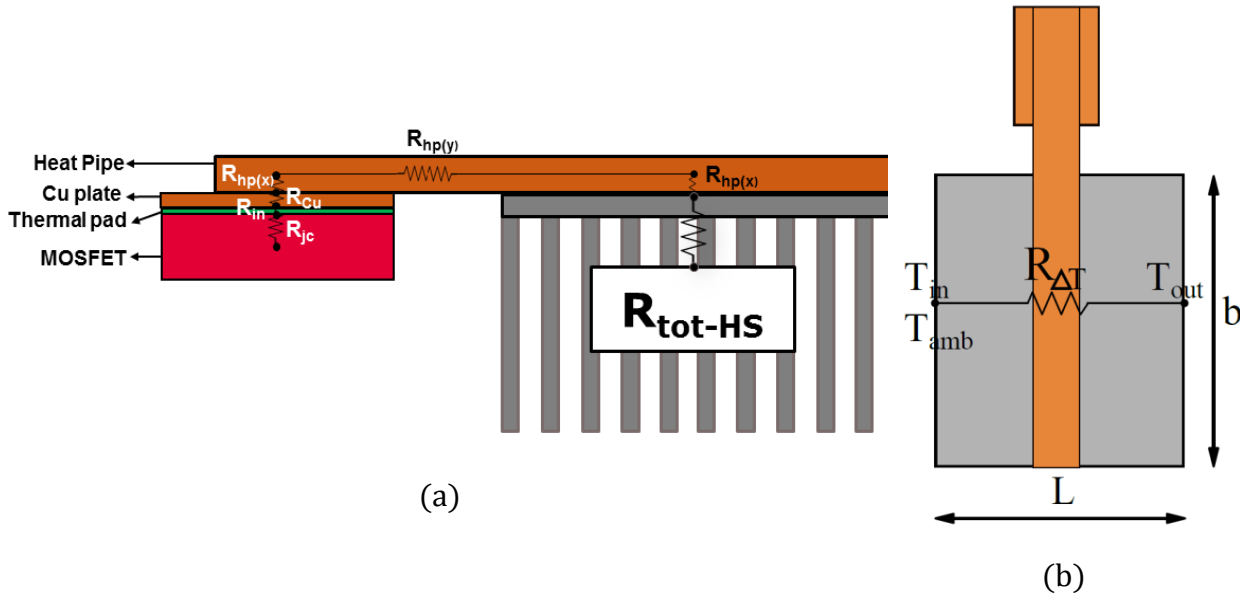


(a) (b)

Figure 5.4.a: Thermal network schematic form junction of heat source to the ambient, b: Thermal network for the temperature rise of air flow through the heatsink channel

The schematic of thermal resistance network for Figure 5.3.a from single MOSFET's junction to the ambient is shown in Figure 5.4. Therefore, total thermal resistance from junction to the ambient can be calculated using Equation 5.1.

$$R_{total} = R_{jc} + R_{in} + R_{Cu} + R_{hp(x)} + R_{hp(y)} + R_{hp(x)} + R_{tot-HS} \qquad \text{Equation 5.1}$$

According to Table 5.1, we have the thermal resistances from MOSFET's junction to the surface of heat-pipe and we need to find the resistance of each section or model the thermal network in order to be able to design the entire cooling system.

Table 5.1: The known thermal resistances

| | |
|---|---|
| $R_{jc} = 0.27\ [\frac{K}{W}]$ | Thermal resistance from junction to the lead frame of MOSFET. It is provided by the manufacturer [60] |
| $R_{in} = 0.12\ [\frac{K.in^2}{W}]$ | Thermal resistance of thermal pad. It is provided by the manufacturer [63] |
| $R_{Cu} = 0.008[\frac{K}{W}]$ | Thermal resistance of copper plate. It is calculated using thermal conductivity correlation $R_{Cu} = \frac{t}{\lambda_{cu}.A}$, where $t$ is thickness, $\lambda$ is thermal conductivity and $A$ area of thermal conductivity. |

Thermal network schematic of the sandwich heat-pipe heatsink cooling system design is shown in Figure 5.5. The only difference is the additional thermal resistance of heat pipe in x direction and the resistance of the heatsink system, which is in series with the same resistances of same parts at the bottom. This design leads to almost double improvement compare to the same cooling system with only one heatsink. The total resistance is obtained using Equation 5.2.

$$R_{total} = R_{jc} + R_{in} + R_{Cu} + R_{hp(x)} + R_{hp(y)} + \frac{1}{2}(R_{hp(x)} + R_{tot-HS}) \qquad \text{Equation 5.2}$$

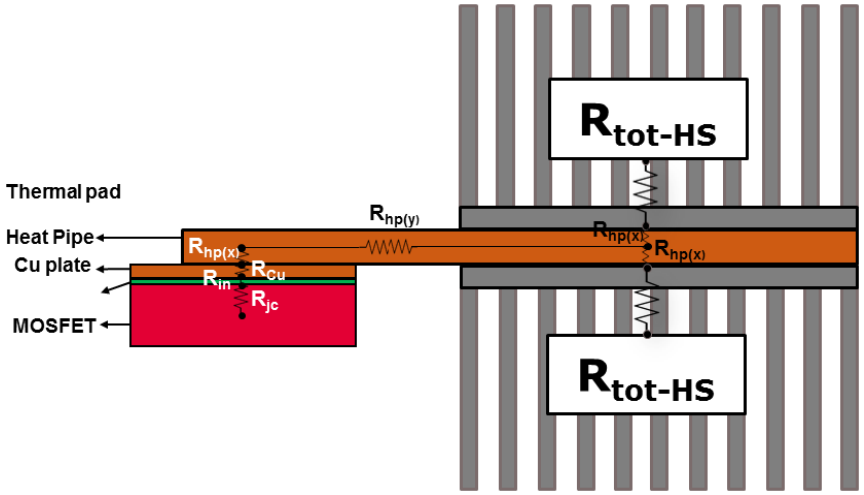


Figure 5.5: Thermal network schematic for the sandwich heat-pipe heatsink cooling system design

## 5.2.2.Multiple Heat Sources

Since all the modules of MOSFET-heat-pipes have the same configurations, we can use the thermal network that is described in Figure 5.4.a, and connect each heat source module to the nearby ones by considering Figure 5.4.b. In other words, we can simply assume that the outlet temperature of air flow for each node that is highlighted with dashed yellow lines in Figure 5.6 is the same as inlet temperature for the next node. So by this assumption, thermal model for the entire system can be modeled in two dimensions, one from junction to the heatsink through the heat-pipe (Figure 5.4.a or Figure 5.5) and the other connects each module to the next one by considering four nodes containing heat source modules as it is shown in Figure 5.6. This assumption can be used for any multiple heat source problems.

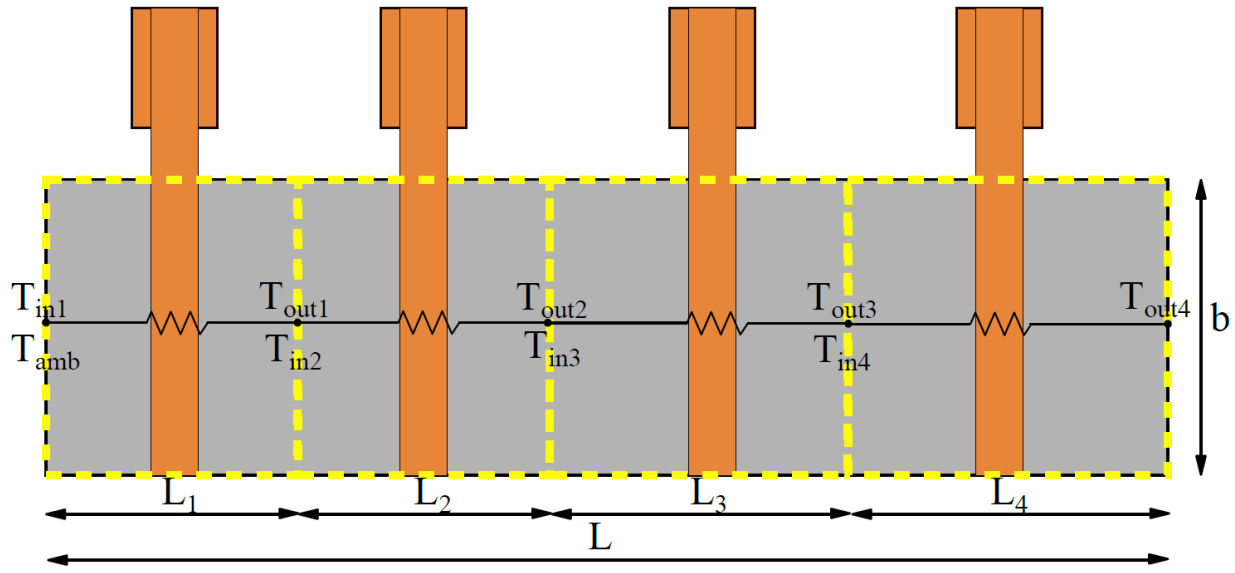


Figure 5.6: Thermal network of multiple heat sources connects each module to the nearby one in a forced air cooling system

## 5.3. Heat Pipes Design Criteria

Since this research study is not concentrating on heat pipes design, several heat pipes which are compatible to the cooling system requirements have been chosen from off the shelf. The selected heat pipes are tested and at the end the best heat pipe is taken for the design process of the entire cooling system. In the following paragraphs the steps that been considered during selection of heat pipes are explained.

### 5.3.1.Working Fluid and Casing Material

The goal of this cooling system is to solve thermal issues of the power semiconductors in the converter. As it is stated in data sheet of the MOSFET [60], the maximum allowable junction temperature of this MOSFET is 150 ℃ which equals to 423 Kelvin. According to Table 3.1, the operating temperature range for group three is compatible for this research study. Also, we already mentioned that copper is mostly selected as the heat pipe casing material for the operating temperature range of $(0,200)°C$. Hence, water as the working fluid and copper as the heat pipe casing material are compatible for this study.

Among the heat pipes with copper as the casing material and water as the working fluid, there is a wide range of heat pipes that are off the shelf in [64].

### 5.3.2.Heat Pipe Type

Although the converter is mounted on the wall, the MOSFETs on the low and high voltage side of the converter are mounted horizontally compare to inverter side (Figure 4.2). Therefore, gravity cannot assist these heat pipes for the MOSFET-heat-pipe modules at low voltage and high voltage sides to direct back the condensed working fluid toward the evaporator end.

According to [65], the performance of heat pipes is dependent on their orientation and the type of wick that is used for the interior of the heat pipe. So, it is important to choose the proper wick structure type for the heat pipes based on their applications. Based on [65], the performance of the heat pipes are not affected so much with sintered metal powder wick structure type for the heat flux of less than 25 W comparing to other types of wick structures. However, the heat flux with high power range (more than 25 W) is better to be mounted in a way that the gravity can help

the capillary force. And in our application, by considering Table 4.1, only the power loss of MOSFETs in inverter side is more than 25 W and since they are mounted vertically in this side, gravity helps for moving back the condensed working fluid to the evaporator side. The power loss in high and low voltage side is lower than 25 W (15 and 11 W, respectively (Table 4.1)), so the sintered metal powder wick structure is adequate for this application in any direction.

Since the MOSFETs need to be mounted on the heat pipes, among the flat heat pipe and round heat pipe, flat heat pipe is the best option due to easier mounting and it also provides more contact surface area between the MOSFET and the heat pipe. The surface area of TO-247 packages is $15 \times 20$ millimeters, so the maximum heat pipe width can be 15 mm and the minimum heat flux capability should be 40 W based on the maximum possible heat loss according to Table 4.1.

## 5.3.3. Conclusion

Three different heat pipes that satisfy the maximum heat flux, operating temperature range, compatible wick structure, casing material and working fluid are selected from off the shelf components [65].The specifications of these four heat pipes are shown in Table 5.2. The outer heat-pipe dimensions guide is shown in Figure 5.7.


Figure 5.7: Flat heat-pipe dimenstions guide [65]

Table 5.2: Selected heat pipes specifications

| Heat-pipe number | Length $[mm]$ | Width $[mm]$ | Height $[mm]$ | Wick type | Working fluid | Temperature range [℃] | MAX heat flux $[W]$ |
|---|---|---|---|---|---|---|---|
| 1 | 100 | 8 | 3 | Sintered | Distilled $H_2O$ | $30-120$ | 70 |
| 2 | 100 | 8 | 3 | Sintered | Distilled $H_2O$ | $30-120$ | 48 |
| 3 | 100 | 11.2 | 3.5 | Sintered | Distilled $H_2O$ | $30-120$ | 61 |

Since thermal resistance of the heat pipes are not stated in their data sheet, it is necessary to test each heat pipe and find the thermal resistance of them in real application. The characterization of each heat pipe has been explained in chapter 6.

## 5.4. Forced Air Cooling

The goal of the analysis is to determine the heat sink geometry and a device setup which allow enough heat dissipation for that specific device in desired working condition.

The heat sinks can be meshed by many 3D thermal resistances which can involve a complex modeling. In addition, convective heat transfer problems can be solved using differential equations, that unfortunately this type of calculations is very time-consuming [5].

For simple analytical analysis, that is not more than one heat source involved; it is useful to use the one-dimensional method of equivalent resistances. Even though, as an alternative, empirical equations can be used for different geometries for the heat sink [6]. These equations generally define the problems based on three normalized parameters called Reynolds number (Re) (normalized fluid flow), Nusselt number (Nu) (normalized convective heat transfer) and Prandtl number (Pr) (fluid characteristics). These empirical equations are accurate and very useful to

simply describe complex convective heat transfer problems in dependency of geometric parameters [5].

As already mentioned, the global thermal resistance can be calculated from the partial thermal resistances of each part (Figure 5.4) using Equation 5.1, and by having total thermal resistance, it is possible to monitor the temperature of MOSFET's junction using Equation 5.3.

$$T_j - T_{amb} = R_{total} \times Q \qquad \text{Equation 5.3}$$

Thermal resistance of $R_{jc}$, $R_{in}$ $and$ $R_{Cu}$ are already known. Thermal resistance of heat pipes can be measured by characterizing them which is done in chapter 6. So, we need to develop a model to estimate the thermal resistance of the forced air cooled heatsink ($R_{tot-HS}$) part.

## 5.4.1. Single Heat Source Thermal Model

Finding the thermal resistance of the forced air cooled heatsink which follows by convective heat transfer problem can be calculated by solving the five differential equations; the Navier Stokes equation which describes the fluid flow in three dimensions, mass conversion and energy conversion equations. Since these equations are very time-consuming, empirical equations which are achieved by experiments and analytical solutions of heat transfer differential equations are used in our model. Empirical equations are very accurate, they simplify, describe and solve the convective heat transfer problems applying three normalized parameters of fluid flow (Reynolds number Re), fluid characteristics (Prandtl number Pr) and convection effectivity (Nusselt number Nu) [6].

In forced air cooled heatsink systems, the geometry of the fin and heatsink describe the pressure drop inside the channels while the fan direct the air flow through the channels. In this

regard, the air flow behaves based on the channel's geometries and the fan characteristic. Generally, the fan pressure drop at different air flows is provided by the manufacturer. As it is shown in Figure 5.8 the operating point of the fan can be obtained at the point where the heat sink channel pressure drop and the fan pressure drop multiplied by the heat sink's fin spacing ration (k) curve converge [43].

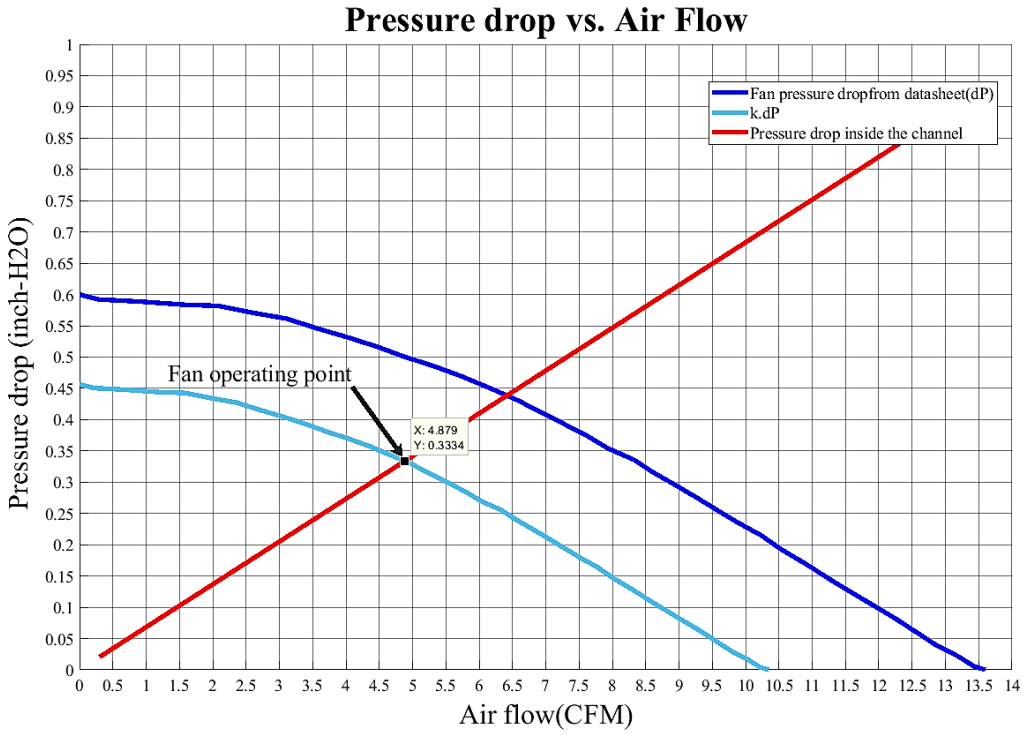


Figure 5.8: Finding the fan operating point according to the pressure drop of the fan and heat sinks channel

A single channel and fin of a parallel plate fin heatsink is shown in Figure 5.9, this figure describes the thermal network for transferring heat from heat sink surface into the air through its channels. Since the geometry of the fins and channels are all the same in the entire heat sink, the results for one single fin can be extended over the entire heatsink composed of any number of fins [43]. Following the networks shown in Figure 5.9, the total thermal resistance from the surface of the heat sink to ambient air in the fan inlet can be obtained from Equation 5.4.

$$R_{tot-HS} = R_{tot-Fin} + R_{tot-conv} + R_{\Delta T} \qquad \text{Equation 5.4}$$

The term $R_{tot-Fin}$ is the result of conductive heat flow through the fins and $R_{tot-conv}$ is because of convection heat transfer from the fin surfaces into the air and is defined by Equation 5.5.

$$R_{tot-Fin} + R_{tot-conv} = \frac{1}{n}\left(R_{th,d} + \left(\frac{1}{R_{th,a}} + \frac{1}{\frac{1}{2}\left(R_{th,fin} + R_{th,ch}\right)}\right)^{-1}\right) \qquad \text{Equation 5.5}$$

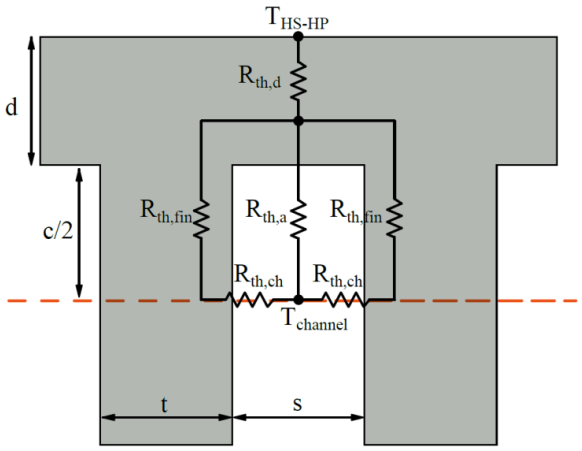


Figure 5.9: Thermal network for describing the convective heat transfer through a single channel of a parallel plane fin heat sink

Since the air along the channel from inlet to outlet heats up, the term $R_{\Delta T}$ (shown in Figure 5.4.b) should be considered to apply the air temperature rise into the calculations by using Equation 5.6.

$$R_{\Delta T} = \frac{0.5}{\rho_{air}\, c_{P,air}\, V} \qquad \text{Equation 5.6}$$

Table 5.3: Equations for obtaining thermal resistance of the heat sink

| | | |
|---|---|---|
| $A_{hs} = s \times c$ | Surface area of the channel normal to the air flow | Equation 5.7 |
| $k = s/(b\ /\ n)$ | Fin spacing ration | Equation 5.8 |
| $d_h = \frac{4\ A}{P} = \frac{2\ s\ c}{s + c}$ | Hydraulic diameter | Equation 5.9 |
| $Re = \frac{2\ \times V}{n \times (s + c) \times v_{Air}}$ | Reynolds number | Equation 5.10 |
| $ab = L/s$ | Length ratio coefficient | Equation 5.11 |
| $C = 1.24 \times ab + 13.27$ | Came from linear fit between the two points close to $ab$ ratio | Equation 5.12 |
| $k\ dP_{fan}(V) = dP_{laminar}(V_{lam}) \rightarrow V$ | Air flow at fan's operating point | Equation 5.13 |
| $dP_{laminar} = \frac{2 \times \left(\frac{C}{Re}\right) \times L}{\frac{d_h \times \rho \times V}{2 \times n \times s \times c}}$ | Laminar pressure drop | Equation 5.14 |
| $\lambda_{HS} = \lambda_{copper}$ | Thermal conductivity of the heatsink | Equation 5.15 |
| $x^* = \frac{L}{D_h\ Re\ Pr}$ | Effective length used in Nusselt number calculation | Equation 5.16 |
| $Nu_{m,T} = 7.55 + \frac{0.024\ (x^*)^{-1.14}}{1 + 0.0358(x^*)^{-0.64} Pr^{0.17}}$ | Nusselt number for parallel plate fins | Equation 5.17 |
| $h = \frac{Nu_{m,T} \times \lambda_{air}}{d_h}$ | Thermal conductivity of the heat sink | Equation 5.18 |
| $R_{th,ch} = 1/(h \times L \times c)$ | Thermal resistance caused from convective heat transfer through fin surface | Equation 5.19 |
| $R_{th,a} = 1/(h \times L \times s)$ | Thermal resistance caused from convective heat transfer through based plate exposing to air flow | Equation 5.20 |
| $R_{th,fin} = c/(t \times L \times \lambda_{hs})$ | Thermal resistance caused from conductive heat transfer through the fin thickness | Equation 5.21 |
| $R_{th,d} = d/(1/n\ \times A_{hs} \times \lambda_{hs})$ | Thermal resistance caused from convective heat transfer through based plate thickness | Equation 5.22 |

The procedure of obtaining the total thermal resistance needs the calculation of thermal conductivity of the heat sink, which needs to find the Nusselt number initially.

Following equations in Table 5.3 can lead us to calculate the Nusselt number, accordingly finding the thermal conductivity is feasible and consequently calculation of total thermal resistance is possible. Therefore, applying total thermal resistance in Equation 5.3 follows by calculation of junction temperature.

In addition, considering Figure 5.4.b and equation ($R_{\Delta T}$) leads us to find the outlet temperature of the air flow (Equation 5.23). The temperature at the inlet of channel equals to the ambient temperature.

$$T_{out} = R_{\Delta T} \times Q + T_{in} \qquad \text{Equation 5.23}$$

## 5.4.2. Multiple Heat Sources Thermal Model

As it is already explained in this chapter, for the cases that multiple heat sources are on a heatsink the effect of each module can be separated into a node (Figure 5.6), and each node can be studied as an individual heatsink system and connect each individual node to the nearby one by taking the temperature rise of air flow inside the channels into account.

The term $R_{tot-Fin} + R_{tot-conv}$ is effected by node's length ($L_i$) and can be calculated by applying each nodes length into equations in Table 5.3. Consequently, junction temperature of each module can be calculated using Equation 5.24, while inlet temperature of each node equals to outlet temperature of previous node (Equation 5.25).

$$T_j(i) = R_{total}(i) \times Q(i) + T_{in}(i) \quad \text{Equation 5.24}$$

$$\begin{cases} T_{in}(i) = T_{out}(i-1) \\ T_{in}(1) = T_{amb} \; i = [1, \dots, n] \end{cases} \quad \text{Equation 5.25}$$

# Chapter 6

# Thermal Model Simulation Verification and Experimental Validation

## 6.1. Introduction

In this chapter, the thermal model proposed in chapter 5 is verified with ANSYS Icepack simulation and then an experimental setup is built and tested to validate the model experimentally. Initially, the thermal model parameters from the actual converter that are needed for the validation is explained and the values for solving the model are illustrated. Next, the heat-pipes are characterized in order to find their actual resistances and utilized the results for estimating the junction temperature in analytical model and simulation. Afterwards, a setup for validating the model is built and tested at different ranges of power losses.

## 6.2. Thermal Model Parameters Values

In order to validate the thermal model, it is needed to find the parameters that are applied in the actual setup and apply them in the model.

The MOSFETs that are used for the actual inverter are TO-247 packages [60]. And since the thermal evaluation of the cooling system is the goal of these tests, the same approach as [66] is taken for experimental tests. So, instead of using heat dummies or actual MOSFETs, resistors with the same packaging and foot print as the MOSFETs are used. Each resistor has one ohm resistance with the accuracy of 1% [67]. So, by loading the power to the resistors up to the maximum level of heat loss for the inverter we can evaluate the performance of the developed thermal model with the actual setup.

The setup is tested in McMaster Automotive Resource Center's lab. The room temperature during the tests was $25 \pm 2$ ℃. The air properties at $25$ ℃ is shown in Table 6.1.

Table 6.1: Air properties at $25$ ℃

| | |
|---|---|
| Prandtl number ( Pr ) | 0.703 |
| Air density ( ρ) | 1.1614 [ kg / m^3 ] |
| Air viscosity ( ν ) | $1.84 \times 10^{-5}$ [$m^2/s$] |
| Air thermal conductivity ( λ ) | $0.0261$ [$W/m.K$] |
| Specific heat ( $c_\rho$ ) | $1005$ [$J/kg.K$] |

The thermal resistance of the MOSFET from junction to the lead frame that is mounted on the heat pipe according to [60] and the thermal resistance of the pad [63] that is used to prevent

the short circuit and also improving the connection between the MOSFET and the heat-pipe are shown in Table 6.2.

Table 6.2: Thermal properties from data sheets

| | | |
|---|---|---|
| $R_{j-c}$ | 0.27 [℃/$W$] | Junction to lead frame thermal resistance of the MOSFET [60] |
| $R_{in}$ | 0.12 [$K\ in^2/W$] | Thermal pad's resistance [63] |

# 6.3. Heat Pipe Characterization

## 6.3.1. Characterization Setup Description

Since the manufacturer didn't provide the thermal conductivity of the each heat pip in the data sheet [64], it is necessary to characterize them in order to find the thermal resistance in the real application. The 1 Ω resister that is described in previous sub chapter is used for the experiments. Therefore, the heat-pipes can receive a certain amount of heat by loading the resistor to different ranges of power. Having the heat pipes heated with a known amount of power loss can lead us to study the performance of each heat pipe and find the thermal resistance of them. The effective thermal resistance of each heat pipe can be asset by measuring the temperature at the evaporator and condenser part. The temperature of the adiabatic part is also measured in order to evaluate the overall heat pipe's performance. The temperature measurements have been done using T-type thermocouples [68]. The measurement points for the evaporator (point e), adiabatic (point a), and condenser (point c) are shown in Figure 6.1.

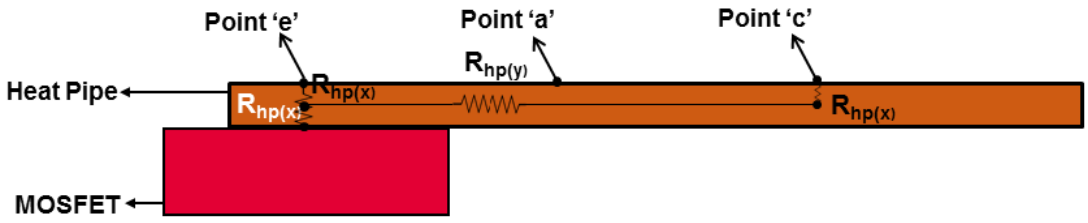


Figure 6.1: The location of thermocouples on the heat-pipe at the evaporator (point e), adiabatic (point a), and condenser (point c) sections

By applying current to the resistor, the heat loss can be calculated using Equation 6.2. And, by measuring the temperature of point 'e' and 'c' we can calculate the thermal resistance of the heat pipe using Equation 6.2 and Equation 6.3.

$$\text{Power loss} = V \times I \qquad \text{Equation 6.1}$$

$$R_{eff-Hp} = R_{hp(x)} + R_{hp(y)} + R_{hp(x)} \qquad \text{Equation 6.2}$$

$$R_{eff-Hp} = \frac{\text{Power loss}}{T_e - T_c} \qquad \text{Equation 6.3}$$

Figure 6.2 shows the configuration of this experimental setup test. At the evaporator section the resistor is mounted on the heat pipe, and the heatsink is in contact with the heat pipe at the condenser section. A very high conductive thermal paste is used between the heat pipe and heat sink to assure a better contact between them. For preventing any heat loss from the setup to the ambient and directing all the heat to the heat sink, the evaporator and adiabatic part is insulated with high temperature fiberglass insulation blanket during the tests. The fan that is used for this setup in order to provide forced air cooling is a DC blower with the maximum volumetric air flow

of 13.6 CFM [69]. During the experiments, two power supplies are used; one for the fan operation and the other for applying current load to the resistor.

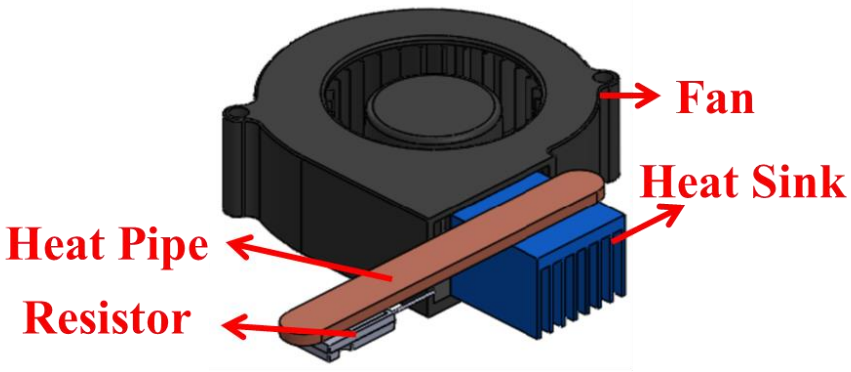


Figure 6.2: Configuration of the heat pipes characterization setup

In order to mount the resistors on the heat pipe a very thin copper part with the same foot print area of the resistor is machined and soldered to the heat pipe (Figure 6.3.a), and the resistor is secured on the heat pipe by screwing down the MOSFET to the thin copper plate and using a nut at the bottom of the copper plate (Figure 6.3.b).

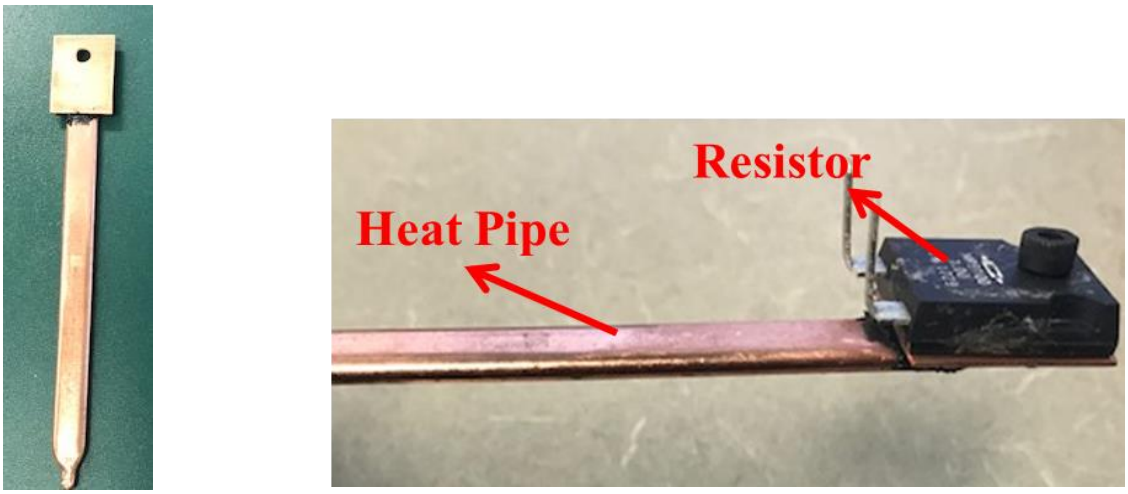


(a) (b)

Figure 6.3.a: soldered copper plate on the heat pipe, b: mounted resistor on the heat pipe

Soldering the copper plate on the heat pipe is a very challenging process since the heat pipe is already evacuated and built. During soldering process, a sufficient amount of heat is needed to increase the temperature of the soldering paste up to the melting point, on the other hand, the heat pipe has a limited allowable heat flux and in case of exceeding its level the heat pipe will damage and is no longer functional for its purpose. Similarly, the heat pipes with lower maximum heat flux limitation during soldering the copper plates got damaged and no longer were suitable for the experiments. As a result, all the tests have been continued by securing the MOSFETs on the heat pipe using a clamp (Figure 6.4.a). High temperature fiberglass insulation blanket is used around the MOSFET and evaporator part to make sure that all the heat loss dissipates through the heat pipe (Figure 6.4.b). The clamp pressure is consistent in all the tests.

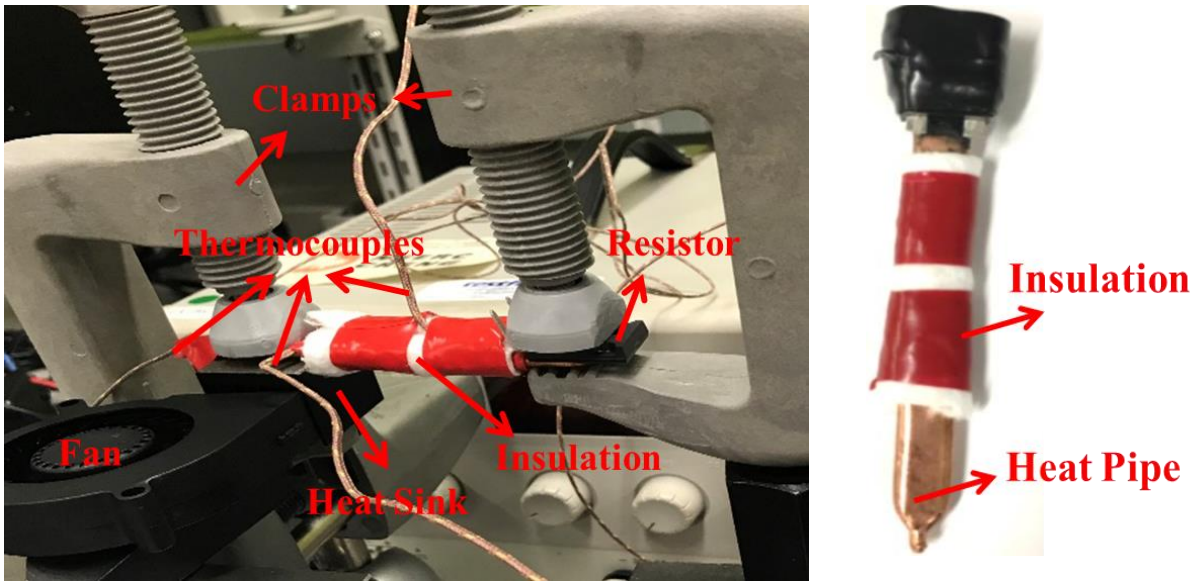


(a) (b)

Figure 6.4.a: Resistor is clamped on the heat-pipe at the evaporator part and the heatsink is clamped to the heat-pipe at the condenser part, b: Heat pipe is insulated using high temperature fiberglass layar

## 6.3.2.Characterization Test Process

Since the heat pipes should be functional for all the power loss ranges that the inverter might face, the tests have been done for five different power losses from a very small heat loss up to the highest possible heat loss that the inverter might experience (2.25, 9, 20.25, 36, 40 watts). The temperature of evaporator, adiabatic and condenser sections are monitored during each test and all the tests were continued until reaching the steady state condition.

## 6.3.3.Results and Discussion

Figure 6.5, Figure 6.6 and Figure 6.7 show the temperature of condenser, evaporator and adiabatic section while applying different power loss to heat pipe number one, two and three, respectively. As it can be seen the temperature of each section increases by increasing the power loss. Since the thermocouple at evaporator section is close to the power heat source, the measured temperature is higher than the adiabatic and condenser section. Similarly, since the thermocouple at condenser end is close to the heat sink, the temperature at this point is lower than adiabatic and evaporator section.

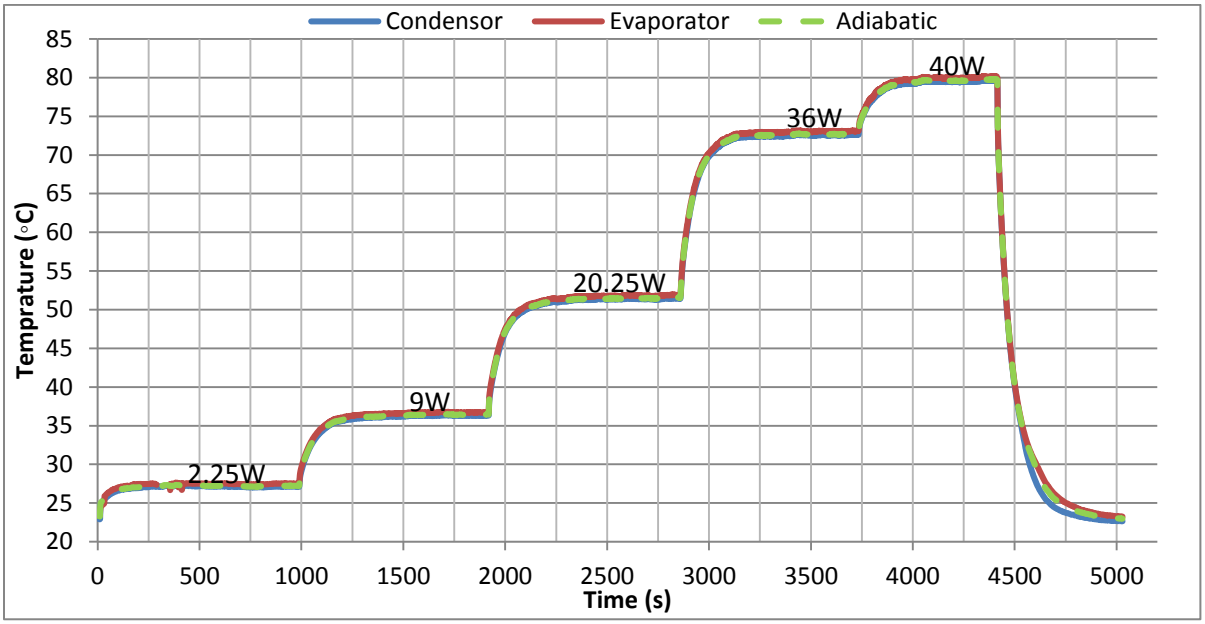


Figure 6.5: Temperature behavior of condenser, evaporator and adiabatic sections for heat pipe number one versus time at different power losses

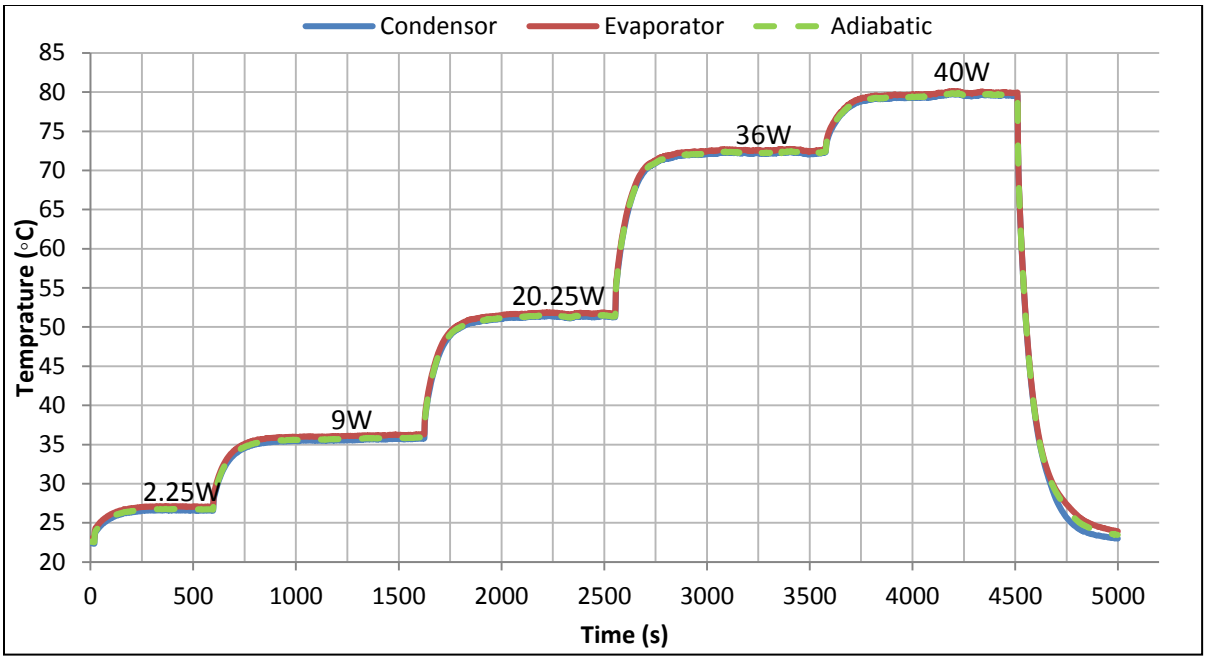


Figure 6.6: Temperature behavior of condenser, evaporator and adiabatic sections for heat pipe number two versus time at different power losses

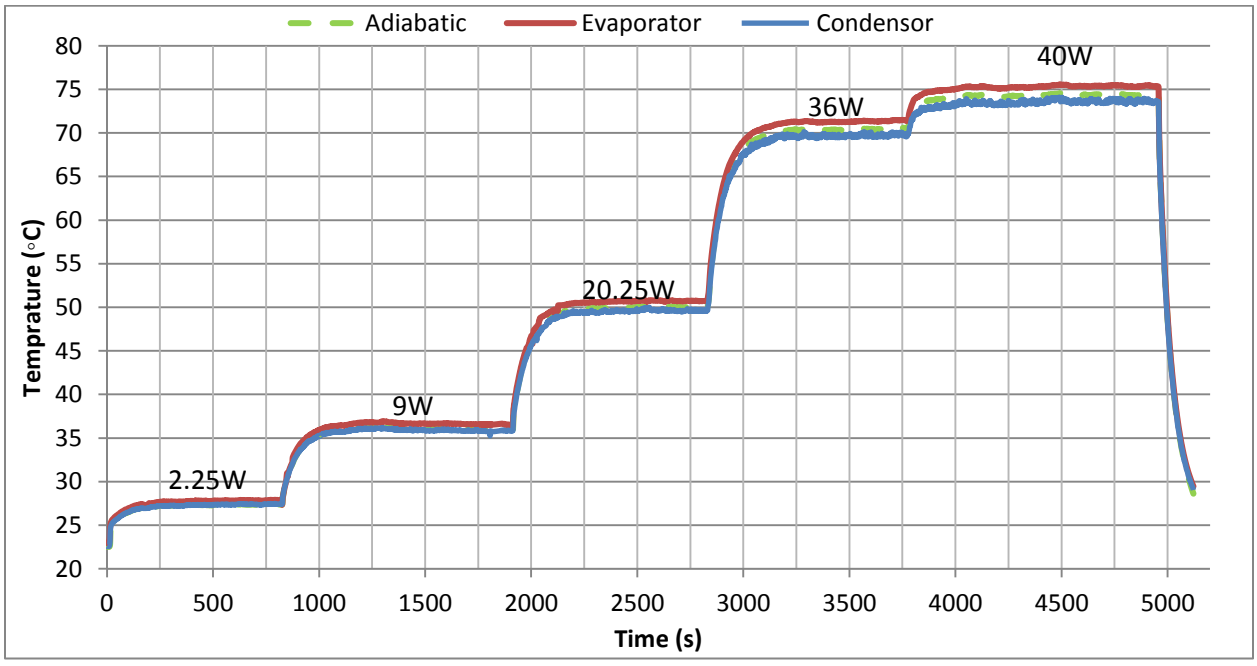


Figure 6.7: Temperature behavior of condenser, evaporator and adiabatic sections for heat pipe number three versus time at different power losses

By comparing the maximum temperatures that are reached at each power loss stage for these three heat pipes, heat pipe number three has lower maximum temperature and the reason is because it has 11 millimeter of width and the other two heat pipes are 8 millimeters wide with the same length as heat pipe number three, which means heat pipe number three has bigger surface area for dissipating the heat at the condenser section. In addition, since the cross section area of heat-pipe number three is $11.2 \times 3.5 = 39.2\ \mathrm{mm}^2$compare to heat pipes number one and two which is $8 \times 3 = 24\ \mathrm{mm}^2$, heat pipe number three is able to transfer the more amount of heat at the same time, which means higher rate of heat transfer and as a result lower temperature on the heat pipe.

By applying the measured temperature at condenser and evaporator section in Equation 6.3, thermal resistance of each heat pipe can be calculated. Calculated thermal resistances of each heat pipe at different ranges of power loss are shown in Table 6.3.

Table 6.3: Calculated thermal resistance of each heat pipe for different power losses

| Power Loss [W] | HP #1 [K/W] | HP #2 [K/W] | HP #3 [K/W] |
|---|---|---|---|
| 2.25 | 0.253 | 0.327 | 0.321 |
| 9 | 0.15 | 0.175 | 0.197 |
| 20.25 | 0.1 | 0.101 | 0.162 |
| 36 | 0.082 | 0.065 | 0.156 |
| 40 | 0.078 | 0.059 | 0.153 |

Figure 6.8 compares the performance of each heat pipe together for the applied power losses. At 2.25 watts heat loss, performance of all the heat pipes is relatively bad. Although by increasing the power loss, thermal resistance decreases which is due to the existence of enough heat for working fluid evaporation and higher vapor pressure for moving faster toward the condenser section. However, the thermal resistance of each heat pipe at the heat loss of more than 20.25 watts is almost consistent for different power losses, which means the heat pipes reached the minimum point of heat that is needed for their optimal performance.

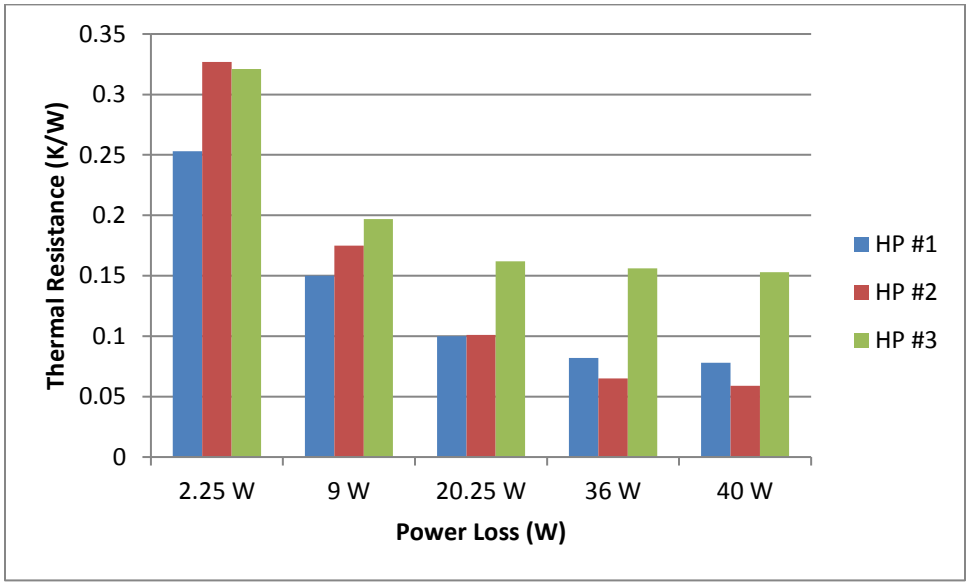


Figure 6.8: Thermal resistance of each heat-pipe at different power losses

Heat pipe number one and two have the same dimensions but different maximum allowable heat flux due to their different interior design. Considering Figure 6.8, heat pipe number two has lower thermal resistance and better overall performance compare to heat pipe number one. Specifically, it has the lowest thermal resistance during its operation while applying more than 20.25 watts heat. Although heat pipe number three has the highest thermal resistance, we learned

that mounting the MOSFET on the 11-millimeter width heat pipe is easier during characterizing the heat pipes, and also the complete heat extraction from and to the heat pipe is more guaranteed with the bigger surface area of the 11 millimeters width in comparison to the 8 millimeters width. In addition, because it has bigger width, it transfers and dissipates the heat in bigger area, which means higher heat transfer and dissipation rate; hence better overall performance can be achieved with heat pipe number 3.

In summary, heat pipe number three, two and one is the priority of our selection based on their overall performance for transferring the heat loss of the inverter's MOSFETs to the heatsink.

## 6.4. Experimental Validation

### 6.4.1. Experimental Setup Description

In order to validate the thermal model experimentally a setup for multiple heat sources is built and tested. The setup has to resistors that are mounted on heat-pipes parallel to each other. The heat-pipes are embedded between to similar heat sinks and the air is flowing to the heat sinks' channels with a DC blower through a duct. The 3D model of the setup is designed in Solid works (Figure 6.9.a), and the actual raw setup is shown in Figure 6.9.b.

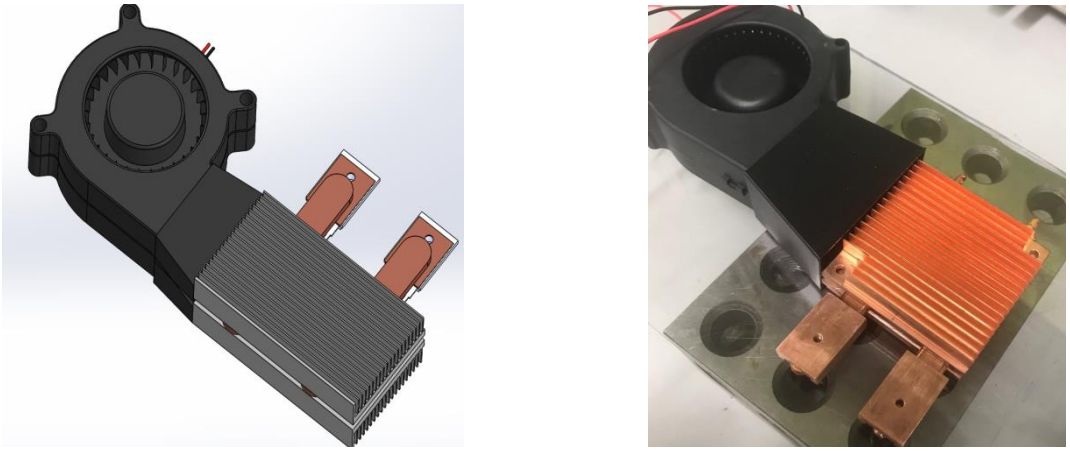

(a) (b)

Figure 6.9.a: The 3D design of the setup in Solid works, b: The actual setup that is used for experimental tests

Since soldering copper plates on the heat pipes is so challenging, a copper block is machined in a way that one side of the block is very flush and smooth so a MOSFET can be mounted with screw on this side and the other side of the block is a groove with the same width as the heat pipe so the heat pipe can slid inside the block's groove (Figure 6.10). The resistor mounted on one side of the copper block and the heat pipe inside the groove on the other side of the block is shown in Figure 6.11.

(a) (b)

Figure 6.10.a: A groove with the same width as the heat pipe is machined on one side of the copper block, b: the heat pipe is slid inside the groove

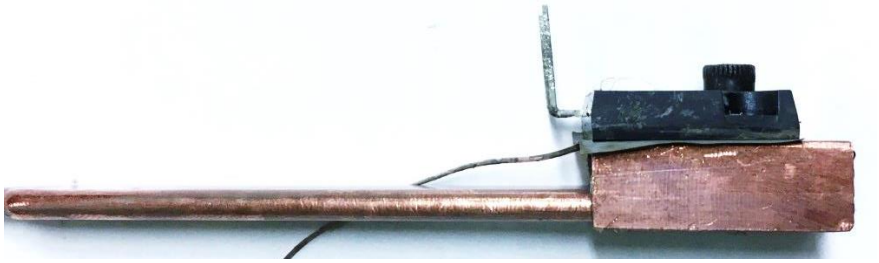

Figure 6.11: The resistor is mounted on one side of the copper block with screw and the heat pipe is slide inside the block's groove on the other side

In order to direct the air flow of the blower into the heat sinks' channels and prevent the air dissipation to outside of the cooling system, a duct is designed. The duct beginning is the same as the fan's opening's output and it ends with the same area as the cross section of the embedded heat-pipes-heat sinks system. The duct is designed in Solid works and manufactured with 3D printer (Figure 6.12).

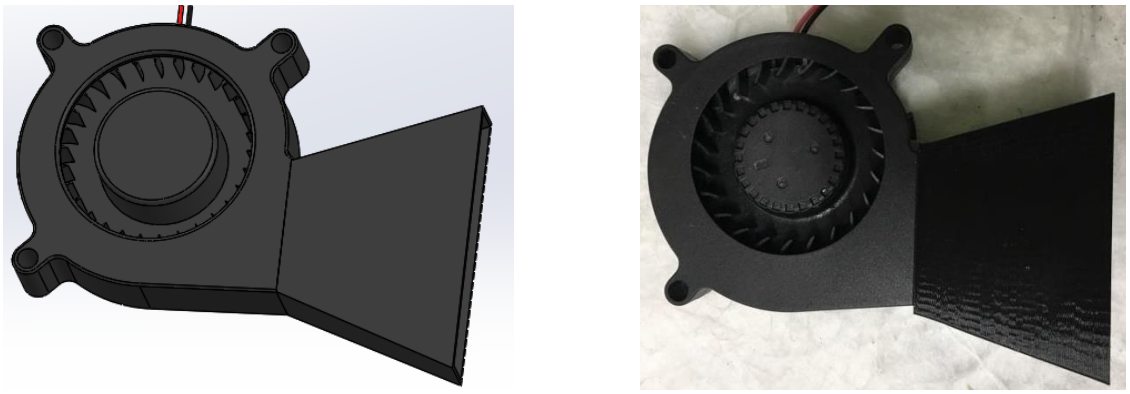

(a) (b)

Figure 6.12.a: the 3D design and b: the 3D printed duct with the assembled blower to it

Having the MOSFET's lead frame temperature leads us to estimate the junction temperature by applying the thermal resistance of junction to lead frame from data sheet using Equation 6.4.

$$T_j = T_c + P \times R_{j-c} \qquad \text{Equation 6.4}$$

In order to measure the lead frame's temperature of the resistor, the same approach as [66] is applied. A very small groove with the same diameter as the thermocouple (0.08 mm) [68] is created on the surface of the copper block, so the thermocouple can reach the middle of the lead frame which is approximately under the resistor's junction area and the groove is created, so a flush surface can be provided for the resistor's mounting purpose. A very conductive thermal paste is used around the thermocouple inside the groove for eliminating possible air pockets. After mounting the thermocouple inside the block's groove, the resistor is secured with a screw on top of the block. A same thermal pad as the actual inverter's setup is used between the resistor and the copper block to insure the electrical insulation and also prevents possible roughness between the surface and the resistor's lead frame. The mounted resistors on the copper blocks with the thermal pad between them and installed thermocouples under the resistors are shown in Figure 6.13.

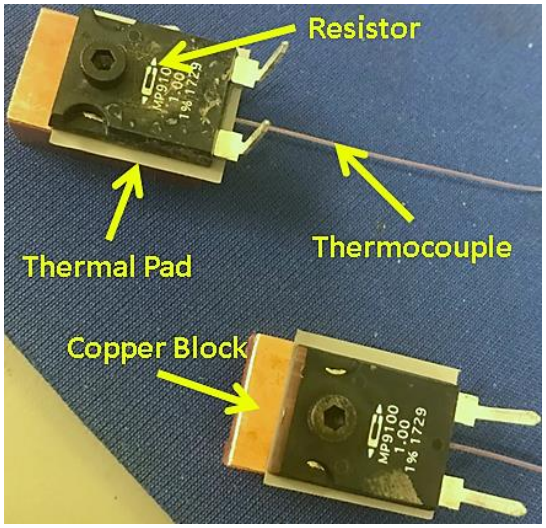


Figure 6.13: A thermocouple is installed in a created small groove on top of the copper block for each resistor

Several thermocouples are mounted with Kapton tape on the heat sinks in order to evaluate the performance of the cooling system (Figure 6.14.a). The resistors and the cooling system are insulated with high temperature fiber glass layers to prevent the heat dissipation out of the system (Figure 6.14-b). The heat pipes are embedded between the two heat sinks using silver thermal paste with high thermal conductivity. The embedded heat pipes heat sinks system is pressed using a clamp during the tests to insure the proper contacts between the heat pipes and the heat sinks (Figure 6.15).

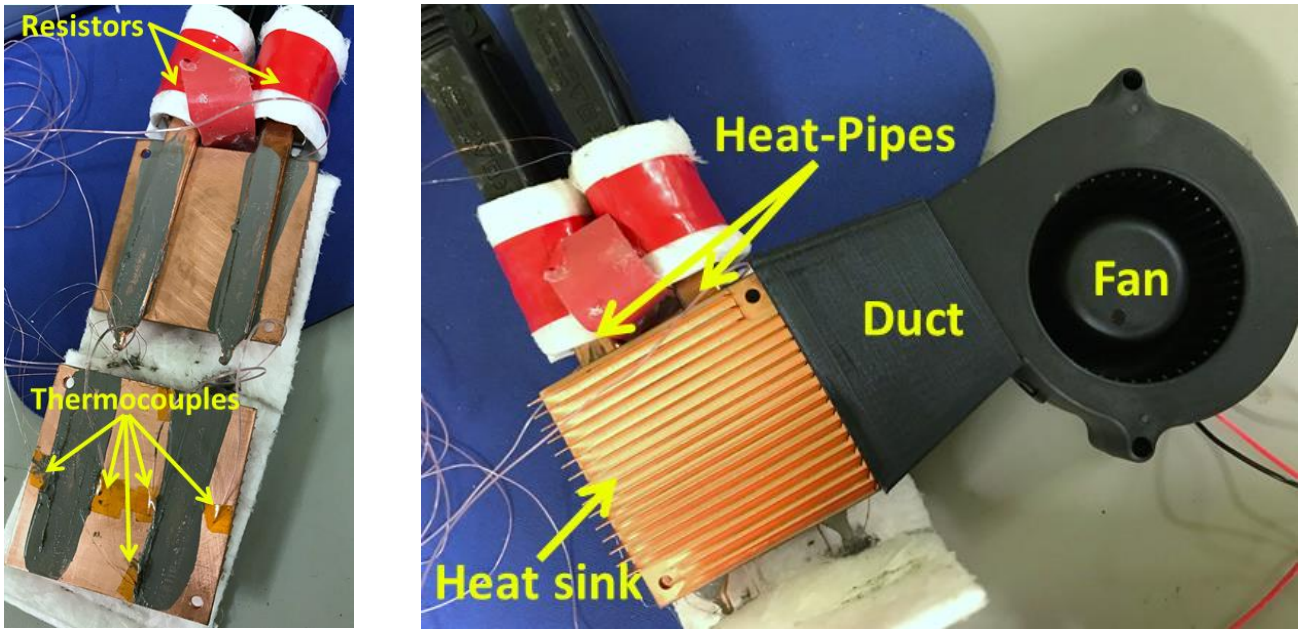


(a) (b)

Figure 6.14.a: thermocouples are fixed on different locations of the heat sink, b: the setup is insulated suing fiber glass layers

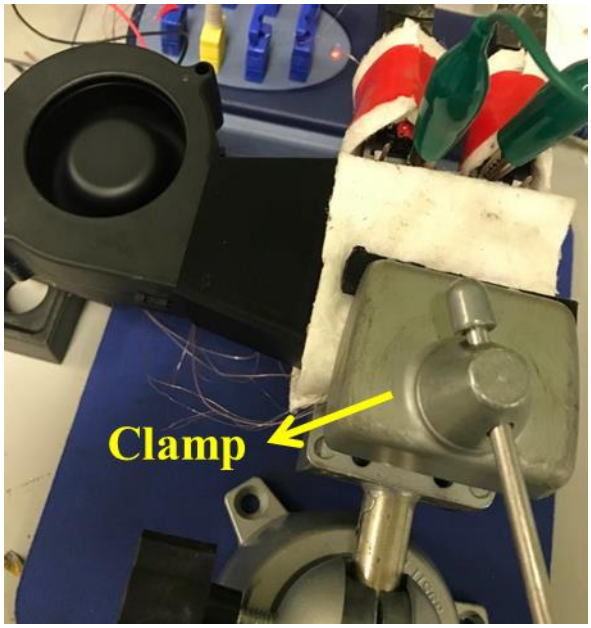


Figure 6.15: Final setup used for experimental tests

## 6.4.2.Experimental Test Process

Initially the power supply is turned on for the blower in order to provide the force air flow to the cooling system. The resistors are connected in series to another power supply, so by applying voltage to the two end of the circuit an equal current flow through the resistors and causes heat loss from their lead frames. The voltage and current is read from the power supply, so we can calculate the heat loss of each resistor using Equation 6.5.

$$P_{loss} = \frac{V \times I}{\text{number of resistors in series}} \qquad \text{Equation 6.5}$$

The resistors are loaded for a very small amount of power loss up to the highest possible heat loss that a MOSFET might achieve during the inverter's performance. The temperature at different points of the heat sink, the lead frame of the resistors, the air flow at the inlet and outlet

of embedded heat pipe heat sink system is monitored with the installed thermocouples that are shown with their numbers in Figure 6.16. All the tests are continued until reaching the steady state condition.

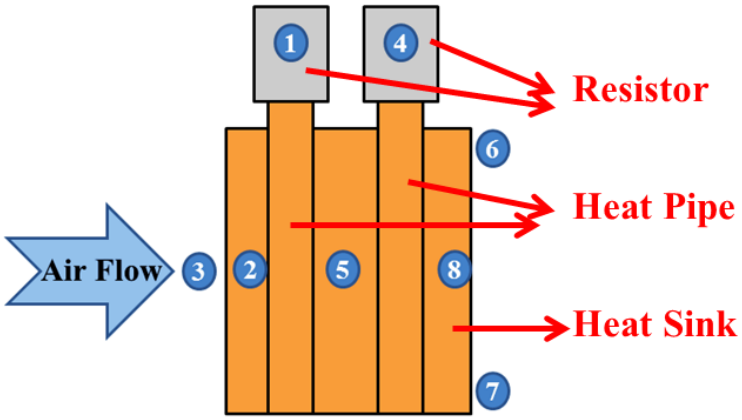


Figure 6.16: Thermocouples locations on the setup

## 6.4.3.Experimental Test Results

The measured temperature for the located thermocouples for power losses of 3.8, 15.3, 22.6 and 43 W is shown in Figure 6.17. Each channel is measuring the temperature of corresponding point's number that is shown in Figure 6.16.

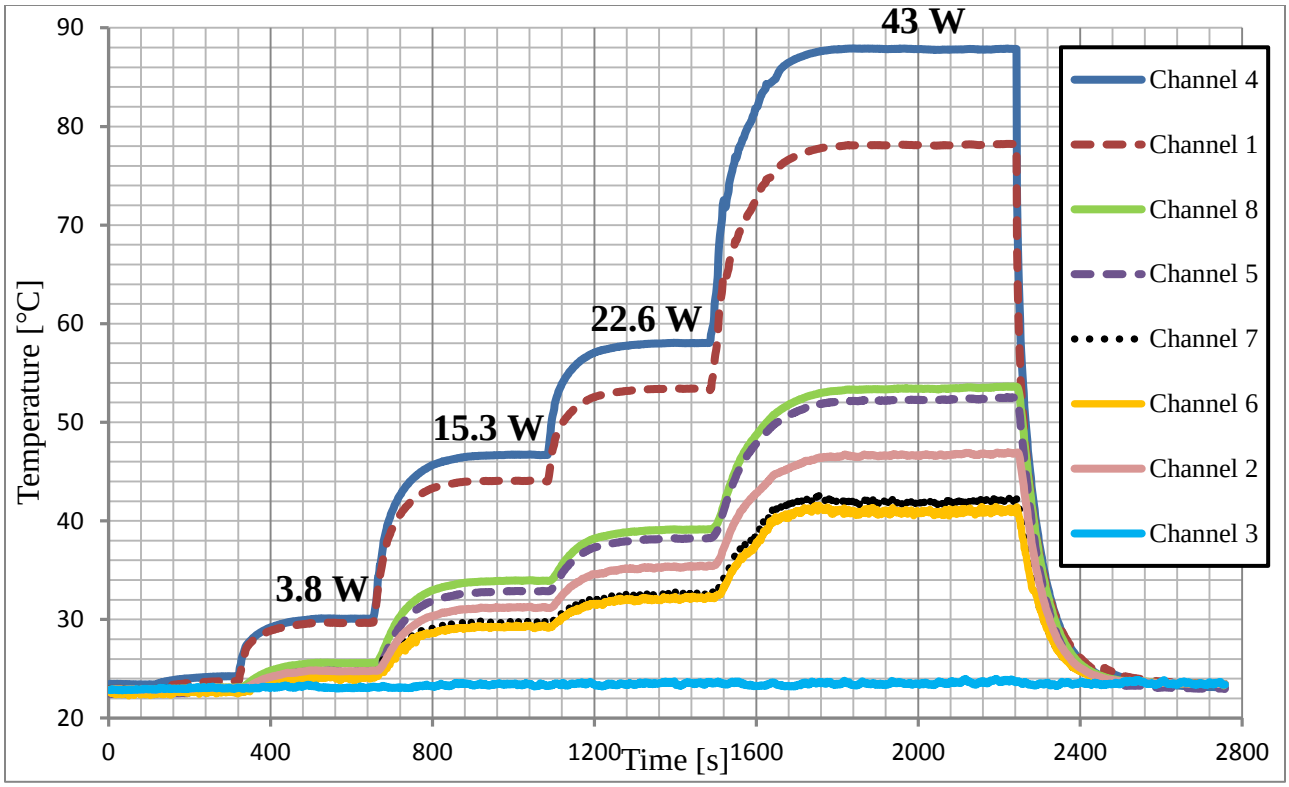


Figure 6.17: Temperature measurements for different power loss ranges at different points of the system

Channels 1 and 4 are measuring the temperature at the lead frame of the first (near to the inlet air flow) and second resistors, respectively. Channel 3 measures the inlet air flow's temperature; the inlet temperature is assumed to be constant and equal to the average of measured inlet temperatures for the entire test period. Channel 7 and 6 monitor the temperature of the outlet air flow of the top heat sink near to the resistors side and the bottom heatsink far from the resistors side, respectively. It is assumed that the temperature of the outlet air flow is equal to the average of measured temperatures from thermocouples number 7 and 6.

The temperatures of the first and second resistors, inlet and outlet air flow for different power losses at steady state condition is shown in Table 6.4.

Table 6.4: Measured temperature at different points for different power losses in steady state condition

| Power Loss [W] | Inlet air flow temperature [℃] Channel #3 | First resistor temperature [℃] Channel #1 | Second resistor temperature [℃] Channel #4 | Outlet air flow outlet temperature, top HS [℃] Channel #7 | Outlet air flow temperature, bottom HS [℃] Channel #6 | Averaged outlet air flow temperature [℃] |
|---|---|---|---|---|---|---|
| 43 | 23.37 | 78.12 | 87.83 | 41.99 | 40.93 | 41.46 |
| 22.6 | 23.37 | 53.40 | 58.02 | 32.62 | 32.12 | 32.37 |
| 15.3 | 23.37 | 44.06 | 46.69 | 29.74 | 29.25 | 29.50 |
| 3.8 | 23.37 | 29.66 | 30.08 | 24.16 | 24.10 | 24.13 |

## 6.5. ANSYS Icepack Simulation Verification

A model same as the experimental setup is simulated in ANSYS Icepack with the same air properties. The simulation is run for the same power losses as the experimental test and the temperature of the resistors' lead frames and outlet temperature are monitored. The outlet temperature is obtained by taking an average of the mean temperature for the top and bottom heat sinks temperature contour. The temperature contour for outlet air flow of the top and bottom heat sinks at 43 W power loss is shown in Figure 6.18.

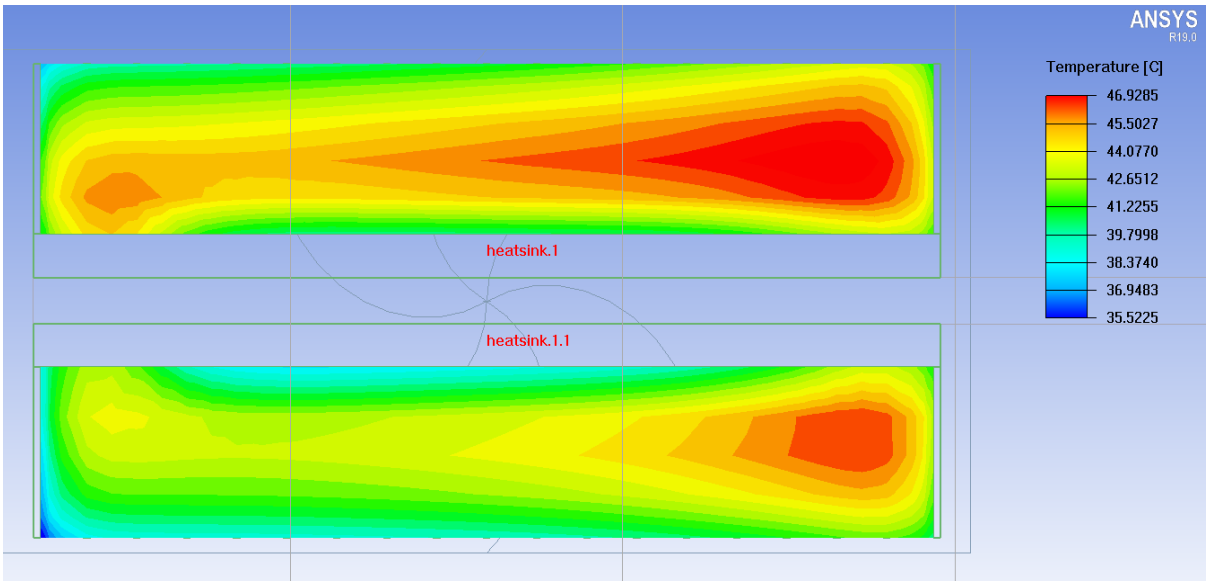


Figure 6.18: Temperature contour of the outlet air flow for the top and bottom heat sinks' channels at 43 watts power loss

The temperature contours of the entire simulated cooling system at 43 watts power loss is shown in Figure 6.19.

The model is simulated and run for the power losses of 3.8,15.3,22,6 and 43 watts . The obtained temperatures for the resistor lead frames, inlet and outlet air flow of the heat sinks channels are shown in Table 6.5.

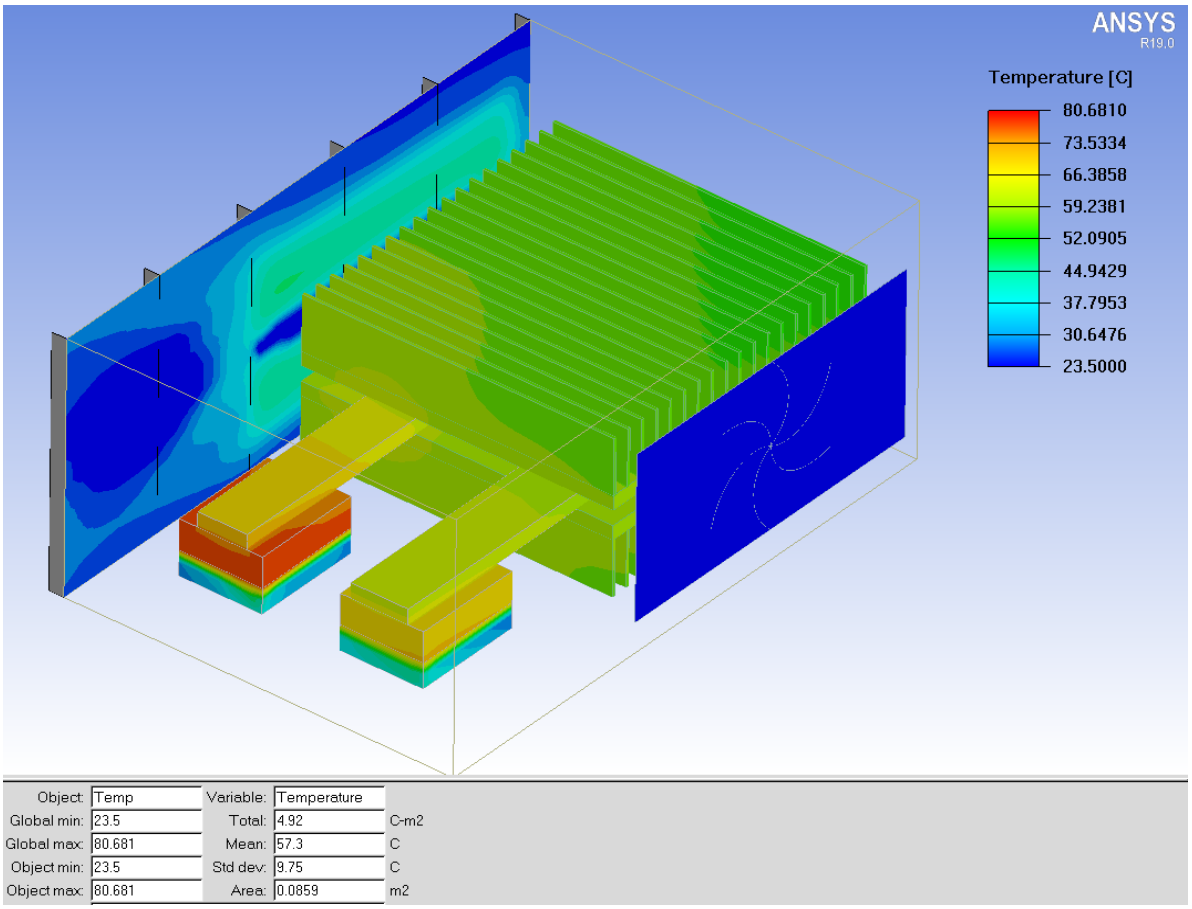


Figure 6.19: Temperature contours for the entire forced air heat-pipes embedded heat sinks cooling system at 43 watts power loss in ANSYS Icepack

Table 6.5: Obtained temperature at different points for different power losses in ANSYS Icepack simulation

| Power Loss [W] | Air flow inlet temperature [℃] | First resistor temperature [℃] | Second resistor temperature [℃] | Averaged air flow outlet temperatures [℃] |
|---|---|---|---|---|
| 43 | 23.50 | 72.49 | 80.68 | $(42.9 + 44.5)/2) = 43.70$ |
| 22.6 | 23.50 | 49.27 | 53.57 | $(33.7 + 34.6)/2 = 34.15$ |
| 15.3 | 23.50 | 40.95 | 43.86 | $(30.4 + 31.0)/2 = 30.7$ |
| 3.8 | 23.50 | 27.83 | 28.56 | $(25.2 + 25.4)/2 = 25.3$ |

## 6.6. Thermal Model Results

For validating the thermal model that is proposed in chapter 5, the experimental setup that is proposed in this chapter is implemented in the model. The model is run for the power losses of $3.8, 15.3, 22.6$ and $43\ watts$. The achieved temperatures for the resistor's lead frames and outlet air flow are shown in Table 6.6.

Table 6.6: Thermal model temperature results at different points for different power losses

| Power Loss [W] | Air flow inlet temperature [℃] | First resistor temperature [℃] | Second resistor temperature [℃] | Outlet air flow temperature [℃] |
|---|---|---|---|---|
| 43 | 23.50 | 71.92 | 80.82 | 46.57 |
| 22.6 | 23.50 | 48.98 | 53.63 | 35.64 |
| 15.3 | 23.50 | 40.73 | 43.89 | 31.71 |
| 3.8 | 23.50 | 27.78 | 28.57 | 25.54 |

## 6.7. Comparison

In order to examine the performance of our thermal model, Table 6.7-Table 6.10 are presented to compare the results of experimental tests and ANSYS simulation to our proposed thermal model at different power losses. As it can be seen, the thermal model has very close results to the ANSYS simulation. However, the results compare to experimental tests is not as close as ASNYS simulation.

Table 6.7: Comparison of thermal model with experimental test and ANSYS simulation results at 43 W power loss

| Power loss 43 W | First resistor ℃ | Second resistor ℃ | Output air flow ℃ |
|---|---|---|---|
| Experimental | 78.12 | 87.83 | 41.46 |
| ANSYS | 72.49 | 80.68 | 43.7 |
| Analytical | 71.92 | 80.82 | 46.57 |

Table 6.8: Comparison of thermal model with experimental test and ANSYS simulation results at 22.6 W power loss

| Power loss 22.6 W | First resistor ℃ | Second resistor ℃ | Output air flow ℃ |
|---|---|---|---|
| Experimental | 53.4 | 58.02 | 32.37 |
| ANSYS | 49.27 | 53.57 | 34.15 |
| Analytical | 48.98 | 53.63 | 35.64 |

Table 6.9: Comparison of thermal model with experimental test and ANSYS simulation results at 15.3 W power loss

| Power loss 15.3 W | First resistor ℃ | Second resistor ℃ | Output air flow ℃ |
|---|---|---|---|
| Experimental | 44.06 | 46.69 | 29.5 |
| ANSYS | 40.95 | 43.86 | 30.7 |
| Analytical | 40.73 | 43.89 | 31.71 |

Table 6.10: Comparison of thermal model with experimental test and ANSYS simulation results at 3.8 W power loss

| Power loss 3.8 W | First resistor ℃ | Second resistor ℃ | Output air flow ℃ |
|---|---|---|---|
| Experimental | 29.66 | 30.08 | 24.13 |
| ANSYS | 27.83 | 28.56 | 25.3 |
| Analytical | 27.78 | 28.57 | 25.54 |

# 6.8. Conclusions

For better understanding of our thermal model performance, the accuracy of the model is studied by calculating the error of the thermal model compare to ANSYS and experimental results at different power losses using Equation 6.6.

$$\%\text{Error} = \frac{T_{\text{ANSYS or experiments}} - T_{\text{model}}}{T_{\text{model}}} \times 100 \qquad \text{Equation 6.6}$$

The calculated errors for different power losses compare to experimental and ANSYS results are shown in Table 6.11. As it can be seen, the error of the model to the ANSYS results is very low, which is highlighted with green. However, the error of the model compare to experimental results is higher than ANSYS due to the following reasons:

- The resistors that are used for creating heat loss have an uncertainty of 1%, which can lead us to power loss calculations error.
- The power supply's current and voltage measurements show only one decimal of the numbers, which also can lead us to power loss calculations error.

- The thermocouples have some errors that can lead to an uncertainty for the temperature measurements.
- The cooling system components may not have perfect contacts, which lead to higher resistance, which follows by higher temperature measurements.

Table 6.11: Calculated error of thermal model temperature measurements for the resistors and outlet air flow compare to experimental and ANSYS results at different power losses.

| | | % Error | | |
|---|---|---|---|---|
| Power loss | Error in | First resistor | Second resistor | Output air flow |
| 43 W | Experimental | 8.62 | 8.67 | 10.97 |
| | ANSYS | 0.79 | 0.17 | 6.16 |
| 22.6 W | Experimental | 9.02 | 8.19 | 9.18 |
| | ANSYS | 0.59 | 0.11 | 4.18 |
| 15.3 W | Experimental | 8.18 | 6.38 | 6.97 |
| | ANSYS | 0.54 | 0.07 | 3.19 |
| 3.8 W | Experimental | 6.77 | 5.29 | 5.52 |
| | ANSYS | 0.18 | 0.04 | 0.94 |

The error for output air flow's temperature is higher. This is mainly because the surface area of the resistors lead frame is smaller than the output channels, so assuming the lead frame as a point and measuring one point of the lead frame is more acceptable than considering the entire heat sink's cross section area as one point knowing that the air temperature near the heat loss side is few degrees higher than the outer side (see Figure 6.18). According to [70], in case of using empirical equations for modeling the thermal network and assuming that the air flow inside the channel is fully developed the error below 12% is acceptable

In summary, the proposed thermal model in chapter 5 can estimate the temperature of the MOSFET's lead frame and output air flow perfectly with the error of less than 10% in a full range of heat loss. However, the thermal model has better performance in lower power losses.

# Chapter 7

# Cooling System Optimization

## 7.1. Optimization Process and Algorithms

An optimization process is finding the maximum or minimum of a function relative to a set of parameters, which represents a range of choices available that satisfies a set of constraints. The function provides comparison of the different choices, so it can verify the best option. An optimization is usually developed as an iteration process following a specific algorithm.

It is accepted that the behavior of nature is always in its optimum performance. The main reason that researchers developed several nature-based algorithms is its capability to solve different optimization problems effectively. There are several such algorithms, including Particle Swarm Optimization (PSO), Genetic Algorithm (GA), Artificial Bee Colony (ABC), Ant Colony Optimization (ACO), etc. [1]

Particle Swarm Optimization (PSO) is inspired by behavior of bird flock or fish school that searching for food. John Holland introduced the Genetic Algorithm (GA) based on the concept of Darwin's theory of evolution; ABC optimization method works on the foraging behavior of a honey bee, ACO simulates the behavior of an ant in searching a path between the source of food and the ant's colony. [1]

All of the evolutionary optimization algorithms require common controlling parameters like population size, number of generations, etc. In addition to common controlling parameters, each algorithm has its own algorithm-specific control parameters. The most commonly used evolutionary optimization methods are the Genetic Algorithm (GA) and Particle Swarm Optimization. Nonetheless, GA determines almost the optimal solution for a complex problem that includes large number of variables and constraints. Determining the optimum controlling parameters including crossover and mutation rates cause some difficulties for this method, since changing the controlling parameters can affect the algorithm performance drastically. Similarly, in the case of using PSO algorithm, controlling parameters such as inertia weight, social and cognitive coefficients play huge roles on the algorithm effectiveness [1]. Therefore, another optimization technique which requires less algorithm controlling parameters to work is of more interest to search for the optimum design of the cooling system of this research.

In 2011, R.V. Rao proposed a new optimization method, Teaching–Learning-Based Optimization (TLBO), which is based on the influence of a teacher on the output of learners in a class. This method is for seeking global solutions for continuous non-linear functions, which also has low computations and high consistency [1]. The implementation of TLBO requires only determining the common controlling parameters such as population size and number of generations, so there is no need for any of the algorithm-specific controlling parameters which leads to robust results [2].

In this chapter, TLBO algorithm is implemented for finding the optimal design of the cooling system. Also, in order to investigate the effectiveness and robustness of TLBO we implemented one of the classic optimization methods. Therefore, this thesis compares the results of each optimization method.

Among the two very widely-used optimization algorithms, which are GA and PSO, for comparing with TLBO method, PSO is selected. Both PSO and TLBO use the best solution of the iteration to change the existing solution in the population, so they both have increasing convergence rate compare to other algorithms, so it is worth to compare their convergence rate to each other. In addition, PSO has fewer computations and lines of code over GA, however, Genetic Algorithm is normally implemented in the problems with large number of variables but we are dealing with only five different variables in the optimization process [71].

## 7.2. Teaching Learning Based Optimization (TLBO)

TLBO method is based on the influence of a teacher on the output of learners in a class, that the output can be considered as the grades. The teacher is considered as the most knowledgeable person in the class who shares his or her knowledge with the learners. So, the quality of a teacher influences the grades of the learners. TLBO is a population-based optimization algorithm that utilize a population of solutions that proceed to the most desired solution. In contrast with other population-based optimization techniques, there are no algorithm controlling-parameters involved in TLBO, which makes the implementation simpler. The process of TLBO is divided into two sections, first section is the Teacher Phase, where the learners learn from the teacher and the second one is the Learner Phase, where the learners learn and improve their level of knowledge through interaction with other learners in the class (Figure 7.1)[1].

### 7.2.1. Teacher Phase

A class can be defined with the level of the teacher's knowledge ($T_i$ ), the mean of learners' grades ($M_i$) , and the level of each learner's knowledge ($X_i$).

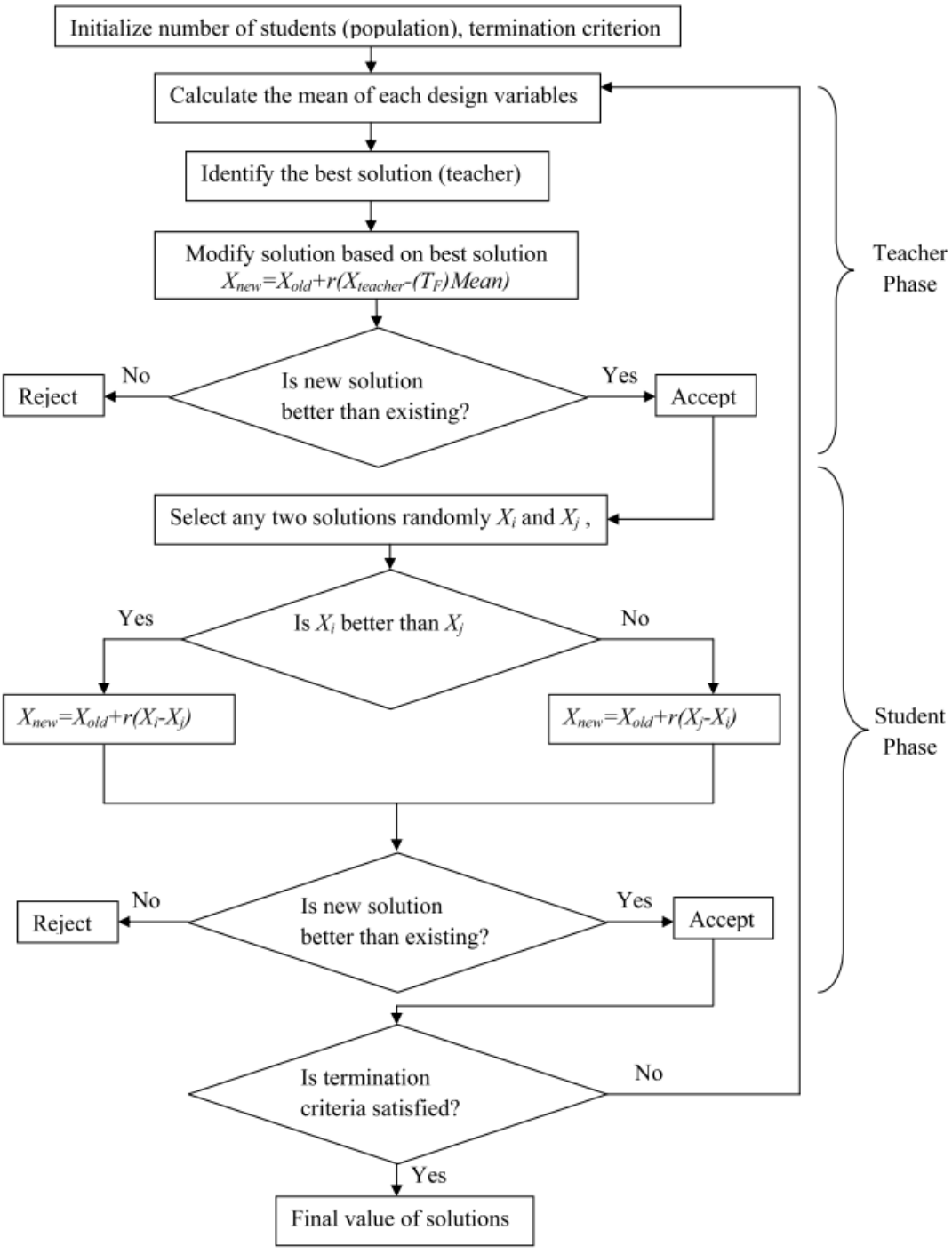


Figure 7.1: Teaching Learning Based Optimization (TLBO) flow chart [1]

Every teacher ($T_i$ ) tries to improve the level of the entire class ($M_i$) close to its own level ($M_{new}$). So, the solution can be updated according to the difference between the existing and new mean of the class (Equation 7.1). Since the teacher might be able to change the mean or not, a teaching factor ($T_F$) is assigned that can be either 1 or 2 using Equation 7.2, and $r_i$is a random number between [0,1]. And the new level of each student ($X_{new,i}$) can be improved according to the mean difference using Equation 7.3.

$$\Delta_{mean} = r_i \times (M_{new} - T_F M_i) \quad \text{Equation 7.1}$$

$$T_F = \text{round}[1 + \text{rand}(0,1)] \quad \text{Equation 7.2}$$

$$X_{new,i} = X_{old,i} + \Delta_{mean} \quad \text{Equation 7.3}$$

## 7.2.2.Learner Phase

Students' knowledge can be improved either through the inputs from their teacher or interaction with themselves. One grade ($X_i$ ) will improve if the student learns something form another student who has higher level of knowledge. So, for a class with a population of $P_n$, learners' level of knowledge will modify with the following instruction.

For $i = 1: P_n$

If $f(X_i) < f(X_j)$; $X_{new,i} = X_{old,i} + r_i \times (X_i - X_j)$

Else $X_{new,i} = X_{old,i} + r_i \times (X_j - X_i)$

End if

End for

Accept $X_{new}$ , if gives better results for the objective function.

## 7.3. Particle Swarm Optimization (PSO)

Particle swarm optimization (PSO) is an evolutionary computation technique developed by Kennedy and Eberhart in 1995 [72]. This algorithm simulates the movement of flocks or birds searching for food. In PSO, objective function determines the fitness of each individual's solution. Each solution is described as a particle in the search space. The particles fly through the search space to find the minimized or maximized value returned by the objective function [56]. Typically, the particles are located randomly in the search space and they evaluate their fitness at their position. Afterwards, each particle moves to a new location that can upgrade its fitness over the previous position. The movement is based on the particle's own experience and other particles in the group (swarm). Hence, PSO algorithm consists of a swarm that includes n particles, and each particle's position represents a possible solution according to the fitness function. Each particles moves toward a new location according to three factors; its own inertial, its own most optimal position, the entire swarm's most optimal solution [73]. The position (x) and speed (v) of each particle is defined by Equation 7.4 and Equation 7.5.

$$x_i^{k+1} = x_i^k + v_i^{k+1} \qquad \text{Equation 7.4}$$

$$v_i^{k+1} = w.v_i^k + c_1.r_1^k\left(pbest_i^k - x_i^k\right) + c_2.r_2^k\left(gbest_i^k - x_i^k\right) \qquad \text{Equation 7.5}$$

$pbest_i^k$ and $gbest_i^k$ resprsent personal and global best positions of the $i^{th}$ particle at its $k^{th}$ iteration, w is the inertial weight, $c_1$ is the personal learning coefficient and causes the particle to move toward its personal best, $c_2$ is the global learning coefficient that leads the particle toward the best position the swarm has been experienced. $r_1^k$ and $r_2^k$are random numbers in the range of

[0,1] [73]. Inertia weight, personal and global learning coefficients, and maximum value of velocity are the PSO controlling parameters that need to be tuned in the algorithm in order to proceed to the optimum solutions.

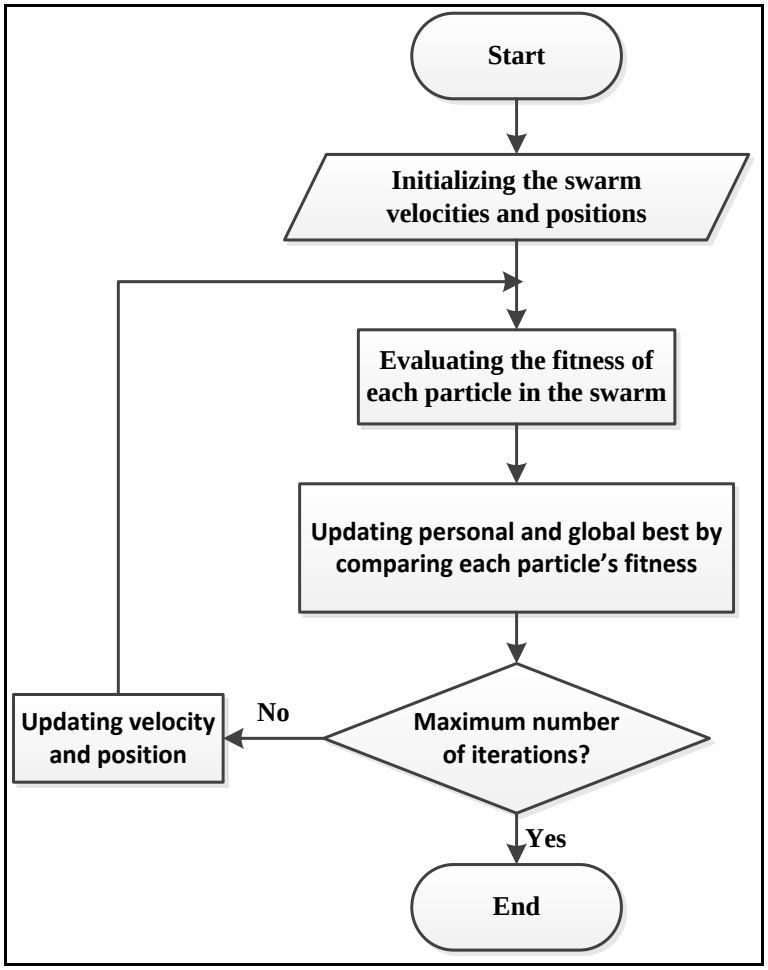


Figure 7.2: Flow chart of Particle Swarm Optimization (PSO)

Basically, PSO algorithm initially create a number (number of population) of particles. Position and velocity of each particle are given randomly. Then, it evaluates the fitness of each particle. After that, it compares personal and global bests and updates them. Then, it updates each particle's velocity and position for the specified maximum iteration number times (Figure 7.2).

## 7.4. Optimization Problem

In general, an optimization problem consists of a set of variables that define an objective function. These variables during the optimization process will be tuned in order to maximize or minimize the objective function according to the goal of optimization. In addition, there might be a set of constraints which define some boundaries that formulate the borders between the feasible and non-feasible solutions in the design space. In this section, the objectives, variables, constraints of the design of our cooling system is explained and the optimal design is found by applying TLBO and PSO algorithms.

### 7.4.1. Design Variables

Since the heat pipes have been already selected and the dimensions are fixed, the optimization has freedom only on the design of forced air-cooling part which consists of the design of the heat sink and selecting the proper fan.

The top and side view of the cooling system is shown in Figure 7.3. There are many variables that can be considered for the optimization of the heat sink such as thickness and number of fins, dimensions and material of the heat sink, air flow velocity. However, we limit the optimization problem to the geometrical variables and fan selection based on the off the shelf components. The heat sink design variables in this study are thickness (t), height (c) and number (N) of the fins, width (b) and base plate thickness (d) of the heat sink.

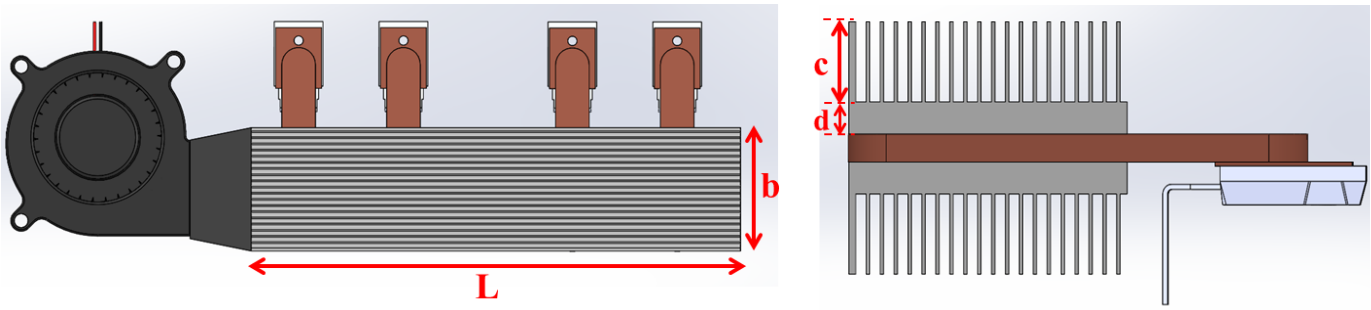


(a) (b)

Figure 7.3.a: Top view and .b: Side view of the cooling system

Since the maximum possible height for the heatsink is equal to 30 mm due to packaging constraints of the entire converter, five different fans that are compatible with the size of the heat sink and the converter's packaging are selected from off the shelf. The characteristics of all the five fans are provided in Table 7.1.

Table 7.1: The characteristics of all the five fans

| Fan number | Fan manufacturing name | Input voltage range [Vdc] | Input power [W] | Air flow [CFM] | Static pressure [inch H2O] |
|---|---|---|---|---|---|
| 1 | BM-7530B-134 | [6-13.8] | 3.6 | 13.6 | 0.60 |
| 2 | BM-7530B-224 | [10-27.6] | 1.9 | 9.6 | 0.27 |
| 3 | B5020 | 5/12/24 | 1.4 | 6 | 0.2 |
| 4 | CBM-5015V-140 | [4.5-13.8] | 0.78 | 3.5 | 0.40 |
| 5 | CBM-6015V-150 | [4.5-13.8] | 1.25 | 5.7 | 0.44 |

## 7.4.2. Constraints

The constraints are due to different reasons; for example, the dimensions of the heat sink cannot exceed some limits due to converter packaging size, minimum fin thickness and spacing

cannot be lower than a limit due to fabrication process. Also, the design should maintain in a way that the power semiconductor devices junction temperature ($T_j$) does not exceed the maximum allowed temperature. Also, the cooling system should manage thermal dissipation of maximum possible MOSFETs heat loss which is 40 Watts for each MOSFET. The constraints boundaries are shown in Table 7.2.

Table 7.2: Optimization problem constraints

| | Fin thickness(t) [mm] | Fin height (c) [mm] | Heat sink width (b) [mm] | Base plate thickness (d) [mm] | Number of fins (N) | Junction temperature ($T_j$) [℃] | Heat loss (q) [w] |
|---|---|---|---|---|---|---|---|
| Min | 0.5 | 5 | 10 | 2 | 5 | - | 0 |
| Max | 1 | 20 | 50 | 10 | 25 | 150 | 40 |

## 7.4.3. Objectives

The optimization in cooling system can minimize the weight, the volume, the height, the price or maximizing the power density for the desired working conditions. The goal of this research is to design a cooling system for the power converter with the lowest volume, power consumption and maximum efficiency. As it is already mentioned in chapter 3, the previous studies mostly concentrate on maximizing the power density and minimizing the weight of the cooling systems in power converters. However, optimizing the heat sink's geometries in order to achieve higher power efficiency of commercially available fans in forced air-cooling systems has not been done in previous researches. In this thesis, the heat sink design is optimized in order to achieve higher power efficiency for possible commercially available fans while minimizing the volume of the entire converter.

Since the converter is already built and has fixed dimensions, it is preferred to have the cooling system within the converter packaging dimensions limits. Since the heat sinks length and width boundaries are selected to be within the converter's length and width limits, the only variable that effects the converter's total volume is the height of the heat sink. Therefore, minimization of the heat sink's height is one of this optimization problem objectives. The height of the heat sink describes by the sum of height of the fins and base plate thickness. Another goal of this optimization is maximizing the efficiency of the cooling system. As it is explained in chapter 3, the operating point of a fan is dependent on the design of the heat sink. On the other hand, designing a heat sink with the lowest volume may lead the operating point of the fan for a lower value which is followed by lower efficiency of the system. Therefore, finding the cooling system for the lowest volume and highest efficiency has an opposite impact on each other. Therefore, studying the fan mechanical power consumption for each heat sink design is necessary to find the maximum efficiency. The efficiency of the cooling system can be defined using Equation 3.4. Therefore, the objective functions for this study is minimizing the heat sink height and maximizing the cooling system efficiency (Table 7.3).

Table 7.3: Optimization problem objective functions

| | |
|---|---|
| Minimizing heat sink height | $2 \times (c + d)$ |
| Maximizing cooling system efficiency | $\eta_f = \frac{P_{mech,out}}{P_{elec,in}}$ |

## 7.4.4.Optimization Configurations

The selection of different fans and number of fins are the discrete design variables in this optimization problem. So, finding the optimal design has been done in two steps in this study:

1. Applying the optimization algorithm in a loop of number of fins within its limits
2. Repeating first step for each fan

Since, the minimum volume of the converter is more of interest in this study compare to the efficiency, the minimum height (local optimum design) of the heat sink based on the optimization constraints and variables is found for different number of fins. Afterwards, the corresponding efficiency values for each founded minimum height are compared together to investigate the best optimal design (global optimum design) for minimum height and maximum efficiency. This process is repeated for all the five fans and at the end the global and local optimum designs for all the fans are studied and compared together to find the most desired design.

The optimization has been run for 5 different fans using TLBO and PSO algorithm. For all configurations, the number of iterations and populations is 200 and 20, respectively. The PSO controlling parameters are defined based on the studies that have been done on stability and convergence in multidimensional complex spaces for PSO problems in [74] and shown in Table 7.4.

Table 7.4: PSO controlling parameters

| | |
|---|---|
| Inertia weight | 0.72984 |
| Personal learning coefficient ($c_1$) | 1.49618 |
| Global learning coefficient ($c_2$) | 1.49618 |
| Maximum velocity | $0.02 \times (Variables_{max} - Variables_{min})$ |

## 7.4.5. Results

### 7.4.5.1. TLBO

Initially, TLBO algorithm is run for each fan. The results are sorted according to the number of fins in Table 7.5-Table 7.9. The running time for all the cases is almost 85 seconds. The results include the design variables of fins thickness (t), fin height (c), number of fins (N), base plate thickness (d), heat sink width (b), a number of heat sink design properties for evaluation such as total volume of the heat sink (V), operating point of the volumetric air flow (Q), junction temperature of all the four MOSFETs ($T_j$ ), the ration of fin spacing and fin thickness ($\frac{s}{t}$). This ration determines the difficulty of manufacturing, higher ration means easier manufacturing. Lastly, the values for the objective functions including heat sink height and power efficiency of the cooling system ($\eta_{power}$ ) are illustrated. It can be concluded that in all the designs for the various fans, the values for base plate and fin thickness are constant and is at the lowest range of their boundary condition. However, the width of the heat sink and height of the fin changes drastically since they influence heat dissipation surface area more than the fin and base plate thickness.

Figure 7.4 shows the objective functions values that are achieved applying TLBO algorithm for different number of fins. All the designs for corresponding points are valid, however the achieved height and efficiency do not have a defined relation together. As it is shown in Figure 7.4, the green boxes are highlighted the best achieved heights and efficiencies among the entire optimal feasible designs. For fan number one, the heights for 10 to 15 number of fins are the lowest, however, the efficiency is the best for fin number of (5,6,7,8,11,12), which concludes that the achieved optimal designs for number of fins of 11 and 12 are the best and since we specified higher

priority for the lower heat sink height over higher efficiency in the optimization process, the design for 12 number of fins considered as the global best optimum design. The global optimum design is highlighted with green in Table 7.5 for this problem.

Table 7.5: Values of objective functions, design variables, constraints and design evaluation for optimal design of the heat sink with fan number 1 using TLBO

| Fan #1 | | | | Power loss=40 watts | | | | | Running Time= 84.79 s | | | | |
|---|---|---|---|---|---|---|---|---|---|---|---|---|---|
| Decision variable | | | | | Evaluation | | | | | | | Objective Function | |
| **N** | t | c | b | d | $s/t$ | V | Q | $T_j$ | | | | Height | $\eta_{Power}$ |
| **-** | [mm] | [mm] | [mm] | [mm] | - | [lit] | [CFM] | [°C] | [°C] | [°C] | [°C] | [mm] | [%] |
| **5** | 0.5 | 18.65 | 21.23 | 2 | 7.29 | 0.137 | 7.13 | 150.00 | 147.17 | 144.22 | 150.00 | 20.65 | 6.59 |
| **6** | 0.5 | 14.93 | 26.31 | 2 | 7.60 | 0.139 | 7.14 | 150.00 | 147.16 | 144.21 | 149.98 | 16.93 | 6.34 |
| **7** | 0.5 | 12.42 | 31.72 | 2 | 7.92 | 0.143 | 7.13 | 149.98 | 147.16 | 144.22 | 150.00 | 14.42 | 6.05 |
| **8** | 0.5 | 10.60 | 37.60 | 2 | 8.28 | 0.148 | 7.14 | 150.00 | 147.17 | 144.21 | 149.99 | 12.60 | 5.71 |
| **9** | 0.5 | 9.21 | 43.89 | 2 | 8.64 | 0.154 | 7.12 | 149.94 | 147.13 | 144.21 | 150.00 | 11.21 | 5.36 |
| **10** | 0.5 | 8.16 | 49.93 | 2 | 8.89 | 0.158 | 7.01 | 149.16 | 146.64 | 144.00 | 150.00 | 10.16 | 5.11 |
| **11** | 0.5 | 7.76 | 49.98 | 2 | 8.00 | 0.152 | 6.20 | 142.60 | 142.50 | 142.28 | 150.00 | 9.76 | 5.44 |
| **12** | 0.5 | 7.62 | 49.93 | 2 | 7.24 | 0.150 | 5.50 | 135.48 | 138.00 | 140.42 | 150.00 | 9.62 | 5.41 |
| **13** | 0.5 | 7.68 | 50 | 2 | 6.62 | 0.151 | 4.95 | 128.27 | 133.43 | 138.50 | 149.95 | 9.68 | 5.18 |
| **14** | 0.5 | 7.91 | 50 | 2 | 6.07 | 0.155 | 4.49 | 121.13 | 128.92 | 136.62 | 149.95 | 9.91 | 4.91 |
| **15** | 0.5 | 8.30 | 49.96 | 2 | 5.59 | 0.161 | 4.12 | 114.22 | 124.57 | 134.85 | 150.00 | 10.30 | 4.64 |
| **16** | 0.5 | 8.85 | 50 | 2 | 5.19 | 0.169 | 3.84 | 107.84 | 120.52 | 133.14 | 149.94 | 10.85 | 4.39 |
| **17** | 0.5 | 9.57 | 49.97 | 2 | 4.82 | 0.180 | 3.60 | 102.02 | 116.86 | 131.65 | 150.00 | 11.57 | 4.17 |
| **18** | 0.5 | 10.45 | 50 | 2 | 4.50 | 0.194 | 3.43 | 96.85 | 113.55 | 130.21 | 149.88 | 12.45 | 3.98 |
| **19** | 0.5 | 11.52 | 50 | 2 | 4.21 | 0.211 | 3.28 | 92.37 | 110.75 | 129.10 | 149.97 | 13.52 | 3.83 |
| **20** | 0.5 | 12.85 | 50 | 2 | 3.95 | 0.232 | 3.17 | 88.44 | 108.23 | 127.99 | 149.86 | 14.85 | 3.72 |
| **21** | 0.5 | 14.42 | 50 | 2 | 3.71 | 0.256 | 3.07 | 85.19 | 106.23 | 127.24 | 150.00 | 16.42 | 3.63 |
| **22** | 0.5 | 16.26 | 50 | 2 | 3.50 | 0.285 | 3.00 | 82.46 | 104.51 | 126.53 | 150.00 | 18.26 | 3.55 |
| **23** | 0.5 | 18.52 | 50 | 2 | 3.30 | 0.320 | 2.94 | 80.17 | 103.03 | 125.87 | 149.92 | 20.52 | 3.49 |

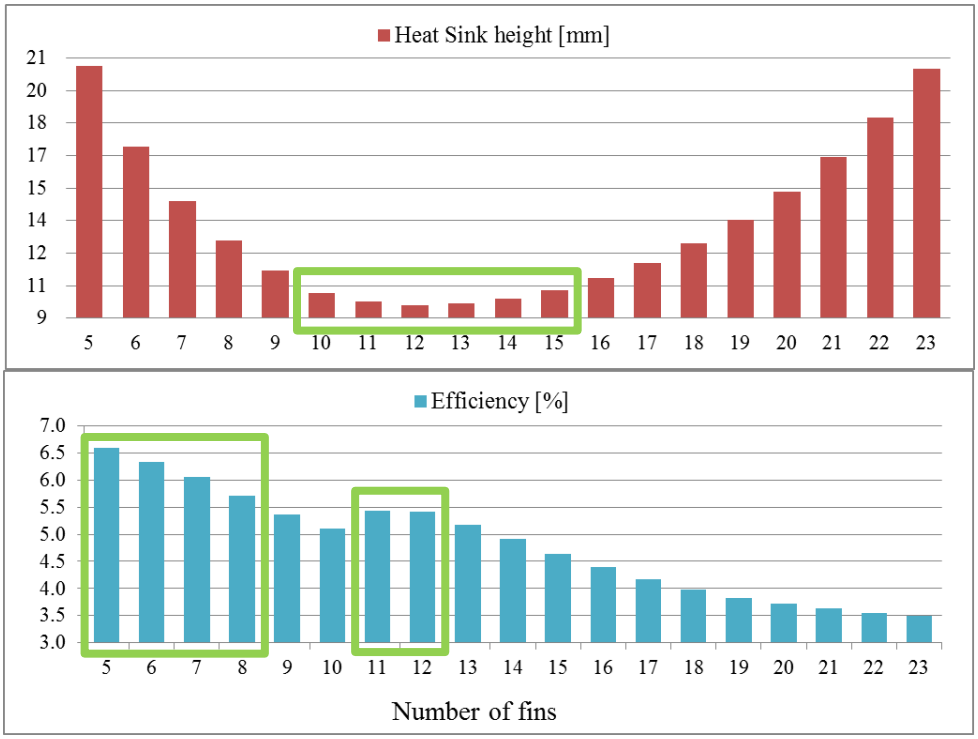


Figure 7.4: Optimal height and efficiency that are achieved for design of the heat sink with fan number 1 using TLBO

Figure 7.5 shows the objective functions values that are achieved applying TLBO algorithm for different number of fins using fan number two. The best achieved heights and efficiencies among the entire optimal feasible designs are highlighted with the green boxes. In this problem, the heights for 10 to 13 number of fins are the lowest. Also, the efficiency is the best for fin number of 11-17, which concludes that the achieved optimal designs for number of fins of 11,12 and 13 are the best designs. However, due to higher priority for the lower heat sink height over higher efficiency in the optimization process, the design for fin number of 12 is found as the global best. The global optimum design for fan number 2 is highlighted with green in Table 7.6.

Table 7.6: Values of objective functions, design variables, constraints and design evaluation for optimal design of the heat sink with fan number 2 using TLBO

| Fan #2 | | | | | Power loss=40 watts | | | | | Running Time= 84.86 s | | | |
|---|---|---|---|---|---|---|---|---|---|---|---|---|---|
| Decision variable | | | | | Evaluation | | | | | | | Objective Function | |
| N | t | c | b | d | $s/t$ | V | Q | $T_j$ | | | | Height | $\eta_{Power}$ |
| - | [mm] | [mm] | [mm] | [mm] | - | [lit] | [CFM] | [°C] | [°C] | [°C] | [°C] | [mm] | [%] |
| 7 | 0.5 | 17.96 | 37.44 | 2 | 9.55 | 0.233 | 6.36 | 144.07 | 143.42 | 142.67 | 150.00 | 19.96 | 2.51 |
| 8 | 0.5 | 15.37 | 43.59 | 2 | 9.77 | 0.236 | 6.28 | 143.36 | 142.98 | 142.48 | 150.00 | 17.37 | 2.45 |
| 9 | 0.5 | 13.42 | 49.94 | 2 | 9.99 | 0.240 | 6.20 | 142.63 | 142.52 | 142.29 | 150.00 | 15.42 | 2.39 |
| 10 | 0.5 | 12.28 | 49.96 | 2 | 8.89 | 0.223 | 5.55 | 136.03 | 138.35 | 140.56 | 150.00 | 14.28 | 2.89 |
| 11 | 0.5 | 11.76 | 50.00 | 2 | 8.00 | 0.215 | 4.99 | 128.92 | 133.84 | 138.67 | 149.96 | 13.76 | 3.20 |
| 12 | 0.5 | 11.71 | 49.94 | 2 | 7.24 | 0.214 | 4.51 | 121.49 | 129.16 | 136.75 | 150.00 | 13.71 | 3.33 |
| 13 | 0.5 | 12.04 | 50.00 | 2 | 6.62 | 0.219 | 4.13 | 114.26 | 124.57 | 134.82 | 149.94 | 14.04 | 3.34 |
| 14 | 0.5 | 12.71 | 49.94 | 2 | 6.06 | 0.229 | 3.81 | 107.36 | 120.24 | 133.05 | 150.00 | 14.71 | 3.29 |
| 15 | 0.5 | 13.68 | 49.99 | 2 | 5.60 | 0.245 | 3.57 | 101.20 | 116.34 | 131.44 | 150.00 | 15.68 | 3.20 |
| 16 | 0.5 | 15.04 | 50.00 | 2 | 5.19 | 0.266 | 3.39 | 95.65 | 112.78 | 129.88 | 149.84 | 17.04 | 3.12 |
| 17 | 0.5 | 16.75 | 50.00 | 2 | 4.82 | 0.292 | 3.24 | 90.95 | 109.81 | 128.65 | 149.85 | 18.75 | 3.04 |
| 18 | 0.5 | 18.85 | 50.00 | 2 | 4.50 | 0.325 | 3.13 | 87.02 | 107.33 | 127.62 | 149.85 | 20.85 | 2.98 |

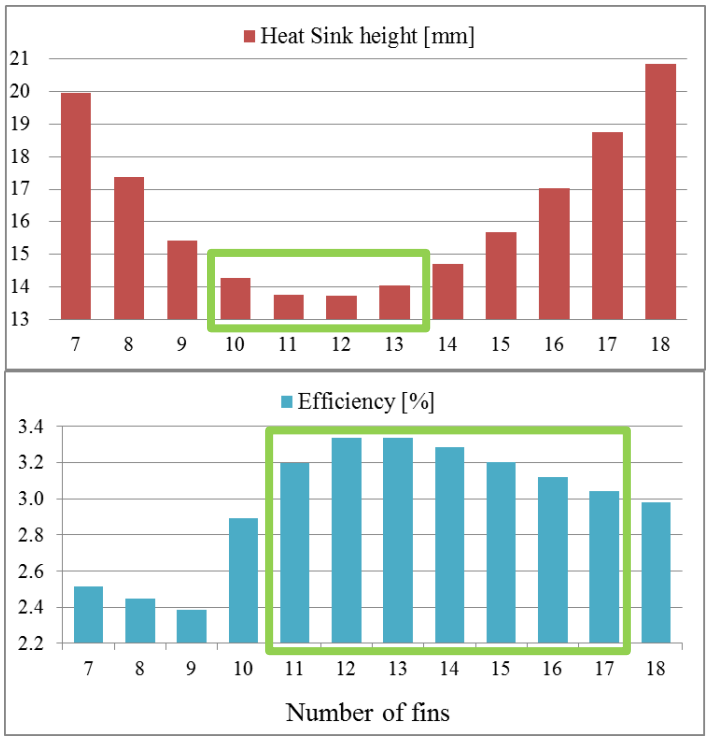


Figure 7.5: Optimal height and efficiency that are achieved for design of the heat sink with fan number 2 using TLBO

For the optimization problem using fan number 3, the algorithm did not find any feasible design. Table 7.7 shows the best design values that are achieved using fan number 3. As it can be seen, the junction temperature that are achieved are all more than 150 °C which is the maximum allowable temperature for the MOSFETs, and this is the reason that algorithm cannot find any feasible designs.

Table 7.7: Values of objective functions, design variables, constraints and design evaluation for optimal design of the heat sink with fan number 3 using TLBO

| Fan #3 | | | | | Power loss=40 watts | | | | Running Time= 74.28 s | | | | |
|---|---|---|---|---|---|---|---|---|---|---|---|---|---|
| Decision variable | | | | | Evaluation | | | | | | | Objective Function | |
| N | t | c | b | d | $s/t$ | V | Q | $T_j$ | | | | Height | $\eta_{Power}$ |
| - | [mm] | [mm] | [mm] | [mm] | - | [lit] | [CFM] | [°C] | [°C] | [°C] | [°C] | [mm] | [%] |
| 10 | 0.5 | 20.00 | 49.98 | 2 | 8.90 | 0.343 | 3.91 | 121.66 | 132.05 | 142.36 | 158.16 | 22.00 | 0.88 |
| 11 | 0.5 | 20.00 | 49.97 | 2 | 7.99 | 0.343 | 3.71 | 113.45 | 126.04 | 138.57 | 155.76 | 22.00 | 1.04 |
| 12 | 0.5 | 20.00 | 49.95 | 2 | 7.24 | 0.343 | 3.51 | 107.16 | 121.87 | 136.54 | 155.20 | 22.00 | 1.21 |
| 13 | 0.5 | 20.00 | 49.98 | 2 | 6.61 | 0.343 | 3.30 | 102.38 | 119.21 | 135.99 | 156.23 | 22.00 | 1.37 |
| 14 | 0.5 | 20.00 | 49.94 | 2 | 6.06 | 0.343 | 3.09 | 98.75 | 117.73 | 136.67 | 158.63 | 22.00 | 1.53 |

Similarly, no feasible design point is found while applying fan number 4. Table 7.8 shows the optimization results for fan number 4. As it can be seen, the junction temperature that are achieved are all more than 150 °C and algorithm cannot specify them as feasible design points. According to Table 7.2, fan number 3 can provide higher volumetric air flow (6 CFM) in comparison to fan number 4 (3.5 CFM), and this causes achieving lower junction temperature for the best designs that are found for fan number 3 over fan number 4.

Table 7.8: Values of objective functions, design variables, constraints and design evaluation for optimal design of the heat sink with fan number 4 using TLBO

| Fan #4 | | | | Power loss=40 watts | | | | | Running Time= 87.72 s | | | | |
|---|---|---|---|---|---|---|---|---|---|---|---|---|---|
| Decision variable | | | | | Evaluation | | | | | | | Objective Function | |
| N | t | c | b | d | $^{s}/_{t}$ | V | Q | $T_j$ | | | | Height | $\eta_{Power}$ |
| - | [mm] | [mm] | [mm] | [mm] | - | [lit] | [CFM] | [°C] | [°C] | [°C] | [°C] | [mm] | [%] |
| 13 | 0.5 | 15.64 | 50.00 | 2 | 6.62 | 0.275 | 2.35 | 116.67 | 141.37 | 166.03 | 194.85 | 17.64 | 1.72 |
| 14 | 0.5 | 16.44 | 50.00 | 2 | 6.07 | 0.288 | 2.28 | 110.20 | 136.77 | 163.30 | 193.34 | 18.44 | 1.93 |
| 15 | 0.5 | 18.47 | 50.00 | 2 | 5.60 | 0.319 | 2.26 | 103.20 | 131.15 | 159.07 | 189.82 | 20.47 | 2.05 |
| 16 | 0.5 | 17.87 | 50.00 | 2 | 5.19 | 0.310 | 2.13 | 101.75 | 132.01 | 162.23 | 195.01 | 19.87 | 2.35 |
| 17 | 0.5 | 19.94 | 50.00 | 2 | 4.82 | 0.342 | 2.10 | 97.26 | 128.77 | 160.24 | 193.82 | 21.94 | 2.45 |

Table 7.9 shows the best design values that are achieved using fan number 5. The objective functions values are sorted based on the number of fins in Figure 7.6. The best achieved heights and efficiencies among the entire optimal feasible designs are highlighted with the green boxes. In this problem, the heights for 12 to 14 number of fins are the lowest. Also, the efficiency is the best for fin number of 13-17, which concludes that the achieved optimal designs for number of fins of 13 and 14 are the best designs. However, since lower heat sink height is preferred over higher efficiency in the optimization process, the design for fin number of 13 is found as the global best and is highlighted with green in Table 7.9.

Table 7.9: Values of objective functions, design variables, constraints and design evaluation for optimal design of the heat sink with fan number 5 using TLBO

| Fan #5 | | | | Power loss=40 watts | | | | Running Time= 84.06 s | | | | | |
|---|---|---|---|---|---|---|---|---|---|---|---|---|---|
| Decision variable | | | | | Evaluation | | | | | | | Objective Function | |
| N | t | c | b | d | $s/t$ | V | Q | $T_j$ | | | | Height | $\eta_{Power}$ |
| - | [mm] | [mm] | [mm] | [mm] | - | [lit] | [CFM] | [°C] | [°C] | [°C] | [°C] | [mm] | [%] |
| **10** | 0.5 | 20 | 46.51 | 2 | 8.20 | 0.319 | 4.22 | 117.04 | 126.56 | 136.01 | 150.63 | 22.00 | 1.56 |
| **11** | 0.5 | 18.39 | 49.97 | 2 | 7.99 | 0.318 | 4.14 | 114.54 | 124.77 | 134.93 | 150.00 | 20.39 | 1.66 |
| **12** | 0.5 | 17.25 | 49.96 | 2 | 7.24 | 0.300 | 3.92 | 109.89 | 121.83 | 133.71 | 150.00 | 19.25 | 2.13 |
| **13** | 0.5 | 16.77 | 49.92 | 2 | 6.60 | 0.292 | 3.72 | 105.16 | 118.85 | 132.47 | 150.00 | 18.77 | 2.52 |
| **14** | 0.5 | 16.91 | 49.94 | 2 | 6.06 | 0.295 | 3.55 | 100.43 | 115.86 | 131.23 | 150.00 | 18.91 | 2.87 |
| **15** | 0.5 | 17.52 | 49.94 | 2 | 5.59 | 0.304 | 3.39 | 95.97 | 113.03 | 130.06 | 150.00 | 19.52 | 3.12 |
| **16** | 0.5 | 18.59 | 50 | 2 | 5.19 | 0.321 | 3.27 | 91.89 | 110.44 | 128.96 | 149.95 | 20.59 | 3.31 |
| **17** | 0.5 | 20 | 50 | 2 | 4.82 | 0.343 | 3.15 | 88.39 | 108.32 | 128.23 | 150.22 | 22.00 | 3.46 |

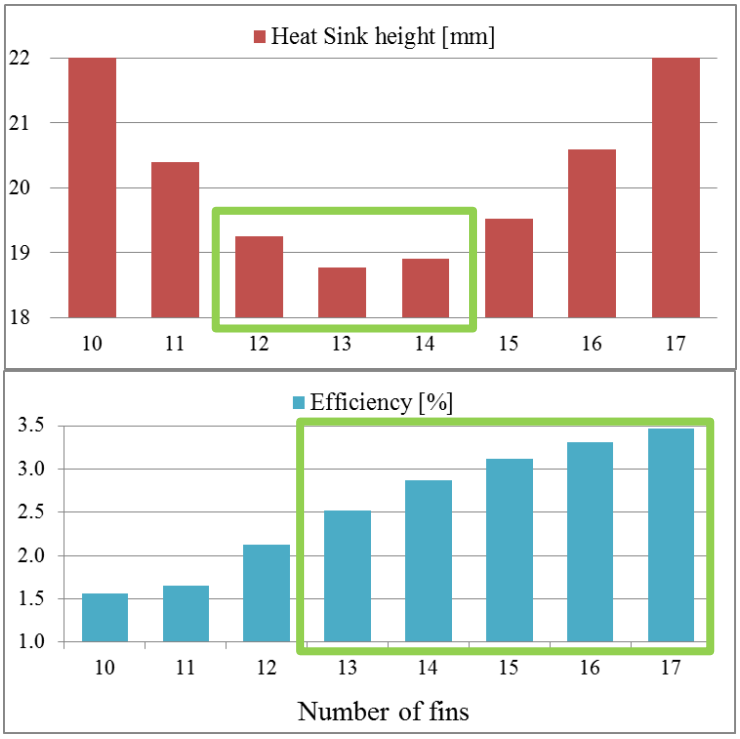


Figure 7.6: Optimal height and efficiency that are achieved for design of the heat sink with fan number 5 using TLBO

Figure 7.7 compares the achieved heat sink height versus the efficiency for each fan in the entire optimization problem. According to Table 7.2, fan number 1, 2 and 5 has the volumetric air flow of 13.7, 9.6 and 5.7, respectively, so they can provide better heat dissipation in this order respectively. Also, since fan number 1 has higher effectiveness it can provide more design points compare to fan number 2 and 5. According to Figure 7.7, fan number1 can provide the lowest height and highest efficiency, however, it consumes more power during its operation (3.6 W). Although fan number 5 provides lowest efficiency with relatively high height, it consumes only 1.25 W for its operation, which means 65% lower power consumption than fan number 1 and 34% lower than fan number 2. The global best point for each fan is specified with green points and is shown in Table 7.10.

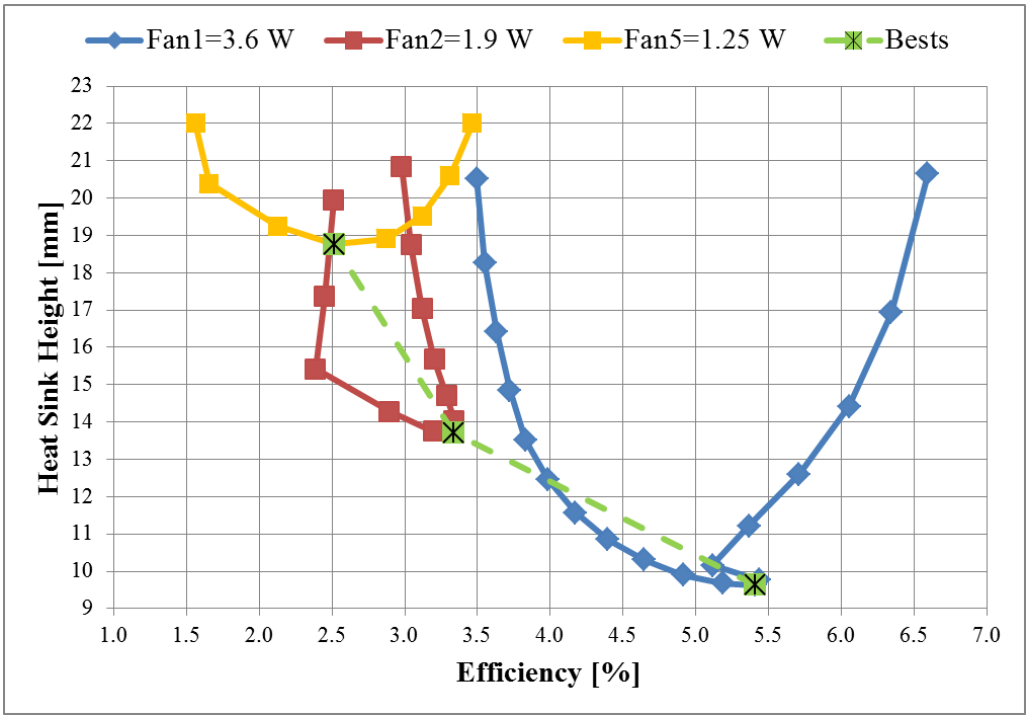


Figure 7.7: Heat sink height versus efficiency for feasible optimal designs for the entire optimization problem based on applied fans using TLBO

Table 7.10: The global optimum design for each fan using TLBO

| Fan number | Efficiency [%] | Heat sink height [mm] | N | t [mm] | c[mm] | b[mm] | d[mm] |
|---|---|---|---|---|---|---|---|
| 1 | 5.41 | 9.62 | 12 | 0.5 | 7.62 | 49.93 | 2 |
| 2 | 3.33 | 13.71 | 12 | 0.5 | 11.71 | 49.94 | 2 |
| 5 | 2.52 | 18.77 | 13 | 0.5 | 16.77 | 49.92 | 2 |

### 7.4.5.2. PSO

In order to examine the performance of TLBO algorithm, we did the optimization for fan number 1,2 and 5 applying PSO algorithm. The running time for each problem for all the evaluations took approximately 45 seconds. The results including design variables, objective functions, and heat sink design properties for evaluation applying PSO method for each fan are shown in Table 7.11-Table 7.13. The most optimal design considering that lower heat sink height is preferred over the higher efficiency is highlighted with green for fan number 1,2 and 5 in Table 7.11, Table 7.12 and Table 7.13, respectively.

Table 7.11: Values of objective functions, design variables, constraints and design evaluation for optimal design of the heat sink with fan number 1 using PSO

| Fan #1 | | | | | Power loss=40 watts | | | | Running Time= 45.46 s | | | | | |
|---|---|---|---|---|---|---|---|---|---|---|---|---|---|---|
| Decision variable | | | | | Evaluation | | | | | | | | Objective Function | |
| N | t | c | b | d | $^{s}/_{t}$ | V | Q | $T_j$ | | | | | Height | $\eta_{Power}$ |
| - | [mm] | [mm] | [mm] | [mm] | - | [lit] | [CFM] | [°C] | [°C] | [°C] | [°C] | | [mm] | [%] |
| 5 | 0.82 | 19.05 | 24.31 | 2 | 4.70 | 0.160 | 7.13 | 150.00 | 147.17 | 144.22 | 150.00 | | 21.05 | 5.10 |
| 6 | 0.65 | 15.11 | 28.06 | 2 | 5.97 | 0.150 | 7.14 | 150.00 | 147.16 | 144.21 | 149.97 | | 17.11 | 5.62 |
| 7 | 0.76 | 12.75 | 35.07 | 2 | 5.43 | 0.161 | 7.13 | 150.00 | 147.17 | 144.22 | 149.99 | | 14.75 | 4.95 |
| 8 | 0.79 | 10.94 | 41.75 | 2 | 5.51 | 0.168 | 7.14 | 150.00 | 147.17 | 144.21 | 149.98 | | 12.94 | 4.60 |
| 9 | 0.72 | 9.44 | 47.55 | 2 | 6.21 | 0.170 | 7.13 | 150.00 | 147.17 | 144.22 | 150.00 | | 11.44 | 4.54 |
| 10 | 0.5 | 8.16 | 49.93 | 2 | 8.89 | 0.158 | 7.01 | 149.16 | 146.64 | 144.00 | 150.00 | | 10.16 | 5.11 |
| 11 | 0.5 | 7.76 | 49.98 | 2 | 8.00 | 0.152 | 6.20 | 142.59 | 142.49 | 142.28 | 150.00 | | 9.76 | 5.44 |
| 12 | 0.5 | 7.62 | 49.93 | 2 | 7.24 | 0.150 | 5.50 | 135.48 | 138.00 | 140.42 | 150.00 | | 9.62 | 5.41 |
| 13 | 0.5 | 7.68 | 50 | 2 | 6.62 | 0.151 | 4.95 | 128.27 | 133.43 | 138.50 | 149.95 | | 9.68 | 5.18 |
| 14 | 0.5 | 7.91 | 50.00 | 2 | 6.07 | 0.155 | 4.49 | 121.13 | 128.92 | 136.62 | 149.95 | | 9.91 | 4.91 |
| 15 | 0.50 | 8.30 | 49.96 | 2 | 5.59 | 0.161 | 4.12 | 114.22 | 124.57 | 134.85 | 150.00 | | 10.30 | 4.64 |
| 16 | 0.5 | 8.85 | 50 | 2 | 5.19 | 0.169 | 3.84 | 107.84 | 120.52 | 133.14 | 149.94 | | 10.85 | 4.39 |
| 17 | 0.5 | 9.57 | 49.97 | 2 | 4.82 | 0.180 | 3.60 | 102.02 | 116.86 | 131.65 | 150.00 | | 11.57 | 4.17 |
| 18 | 0.5 | 10.45 | 50 | 2 | 4.50 | 0.194 | 3.43 | 96.85 | 113.55 | 130.21 | 149.88 | | 12.45 | 3.98 |
| 19 | 0.5 | 11.52 | 50 | 2 | 4.21 | 0.211 | 3.28 | 92.37 | 110.75 | 129.10 | 149.97 | | 13.52 | 3.83 |
| 20 | 0.5 | 12.85 | 50 | 2 | 3.95 | 0.232 | 3.17 | 88.44 | 108.23 | 127.99 | 149.86 | | 14.85 | 3.72 |
| 21 | 0.5 | 14.42 | 50 | 2 | 3.71 | 0.256 | 3.07 | 85.19 | 106.23 | 127.24 | 150.00 | | 16.42 | 3.63 |
| 22 | 0.5 | 16.26 | 50 | 2 | 3.50 | 0.285 | 3.00 | 82.46 | 104.51 | 126.53 | 150.00 | | 18.26 | 3.55 |
| 23 | 0.5 | 18.52 | 50.00 | 2 | 3.30 | 0.320 | 2.94 | 80.17 | 103.03 | 125.87 | 149.92 | | 20.52 | 3.49 |

Table 7.12: Values of objective functions, design variables, constraints and design evaluation for optimal design of the heat sink with fan number 2 using PSO

| Fan #2 | | | | | Power loss=40 watts | | | | Running Time= 45.20 s | | | | |
|---|---|---|---|---|---|---|---|---|---|---|---|---|---|
| Decision variable | | | | | Evaluation | | | | | | | Objective Function | |
| N | t | c | b | d | $s/t$ | V | Q | $T_j$ | | | | Height | $\eta_{Power}$ |
| - | [mm] | [mm] | [mm] | [mm] | - | [lit] | [CFM] | [°C] | [°C] | [°C] | [°C] | [mm] | [%] |
| 7 | 0.5 | 17.97 | 37.58 | 2 | 9.58 | 0.234 | 6.38 | 144.19 | 143.50 | 142.69 | 149.98 | 19.97 | 2.49 |
| 8 | 0.5 | 15.37 | 43.76 | 2 | 9.81 | 0.237 | 6.30 | 143.52 | 143.08 | 142.53 | 150.00 | 17.37 | 2.43 |
| 9 | 0.5 | 13.42 | 49.94 | 2 | 9.99 | 0.240 | 6.20 | 142.63 | 142.52 | 142.29 | 150.00 | 15.42 | 2.39 |
| 10 | 0.5 | 12.28 | 49.96 | 2 | 8.89 | 0.223 | 5.55 | 136.03 | 138.35 | 140.56 | 150.00 | 14.28 | 2.89 |
| 11 | 0.5 | 11.76 | 50.00 | 2 | 8.00 | 0.215 | 4.99 | 128.92 | 133.84 | 138.67 | 149.96 | 13.76 | 3.20 |
| 12 | 0.5 | 11.71 | 49.94 | 2 | 7.24 | 0.214 | 4.51 | 121.49 | 129.16 | 136.75 | 150.00 | 13.71 | 3.33 |
| 13 | 0.5 | 12.04 | 50.00 | 2 | 6.62 | 0.219 | 4.13 | 114.26 | 124.57 | 134.82 | 149.94 | 14.04 | 3.34 |
| 14 | 0.5 | 12.71 | 49.94 | 2 | 6.06 | 0.229 | 3.81 | 107.36 | 120.24 | 133.05 | 150.00 | 14.71 | 3.29 |
| 15 | 0.5 | 13.68 | 49.99 | 2 | 5.60 | 0.245 | 3.57 | 101.20 | 116.34 | 131.44 | 150.00 | 15.68 | 3.20 |
| 16 | 0.5 | 15.04 | 50.00 | 2 | 5.19 | 0.266 | 3.39 | 95.65 | 112.78 | 129.88 | 149.84 | 17.04 | 3.12 |
| 17 | 0.5 | 16.75 | 50.00 | 2 | 4.82 | 0.292 | 3.24 | 90.95 | 109.81 | 128.65 | 149.85 | 18.75 | 3.04 |
| 18 | 0.5 | 18.85 | 50.00 | 2 | 4.50 | 0.325 | 3.13 | 87.02 | 107.33 | 127.62 | 149.85 | 20.85 | 2.98 |

Table 7.13: Values of objective functions, design variables, constraints and design evaluation for optimal design of the heat sink with fan number 5 using PSO

| Fan #5 | | | | | Power loss=40 watts | | | | Running Time= 45.31 s | | | | |
|---|---|---|---|---|---|---|---|---|---|---|---|---|---|
| Decision variable | | | | | Evaluation | | | | | | | Objective Function | |
| N | t | c | b | d | $s/t$ | V | Q | $T_j$ | | | | Height | $\eta_{Power}$ |
| - | [mm] | [mm] | [mm] | [mm] | - | [lit] | [CFM] | [°C] | [°C] | [°C] | [°C] | [mm] | [%] |
| **10** | 0.5 | 20.00 | 47.18 | 2 | 8.34 | 0.324 | 4.24 | 117.59 | 126.91 | 136.17 | 150.65 | 22.00 | 1.49 |
| **11** | 0.5 | 18.39 | 49.97 | 2 | 7.99 | 0.318 | 4.14 | 114.54 | 124.77 | 134.93 | 150.00 | 20.39 | 1.66 |
| **12** | 0.5 | 17.25 | 49.96 | 2 | 7.24 | 0.300 | 3.92 | 109.89 | 121.83 | 133.71 | 150.00 | 19.25 | 2.13 |
| **13** | 0.5 | 16.77 | 49.92 | 2 | 6.60 | 0.292 | 3.72 | 105.16 | 118.85 | 132.47 | 150.00 | 18.77 | 2.52 |
| **14** | 0.50 | 16.91 | 49.94 | 2 | 6.06 | 0.295 | 3.55 | 100.43 | 115.86 | 131.23 | 150.00 | 18.91 | 2.87 |
| **15** | 0.5 | 17.52 | 49.94 | 2 | 5.59 | 0.304 | 3.39 | 95.97 | 113.03 | 130.06 | 150.00 | 19.52 | 3.12 |
| **16** | 0.5 | 18.59 | 50 | 2 | 5.19 | 0.321 | 3.27 | 91.89 | 110.44 | 128.96 | 149.95 | 20.59 | 3.31 |
| **17** | 0.5 | 20.00 | 50 | 2 | 4.82 | 0.343 | 3.15 | 88.39 | 108.32 | 128.23 | 150.22 | 22.00 | 3.46 |

Figure 7.8 compares the achieved heat sink height versus the efficiency for each fan in the entire optimization problem using PSO. The global best point for each fan is specified with green points and connected to each other with green dashed line in Figure 7.8 and is shown in Table 7.14.

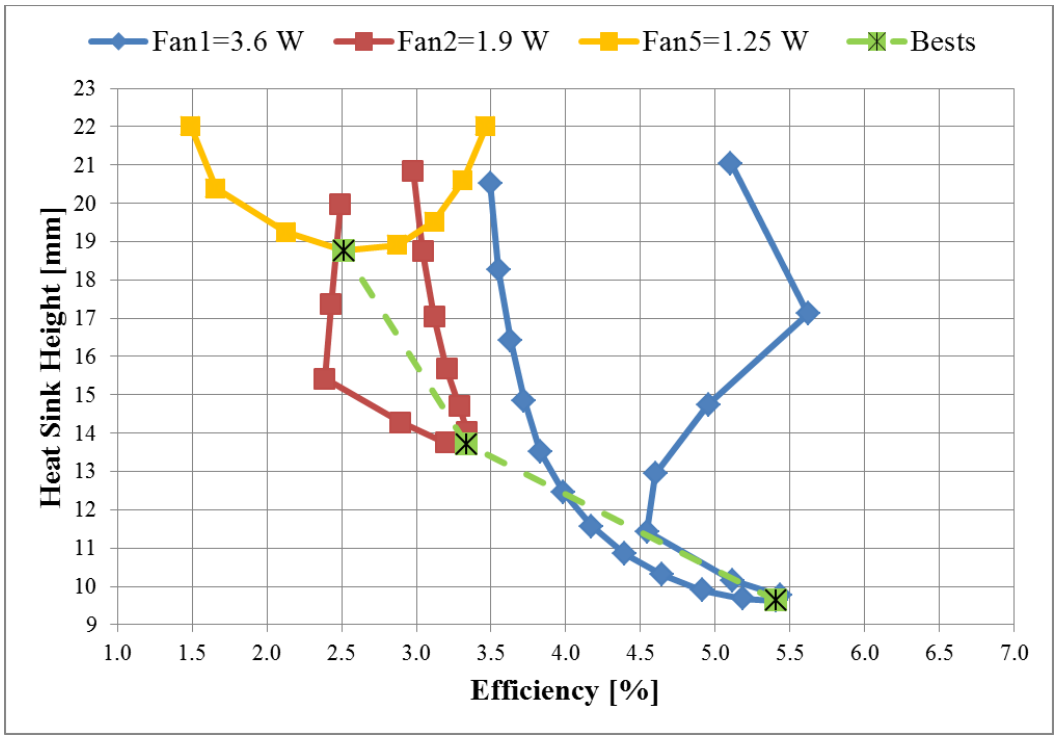


Figure 7.8: Heat sink height versus efficiency for feasible optimal designs for the entire optimization problem based on applied fans using PSO

Table 7.14: The global optimum design for each fan using PSO

| Fan number | Efficiency [%] | Heat sink height [mm] | N | t [mm] | c[mm] | b[mm] | d[mm] |
|---|---|---|---|---|---|---|---|
| 1 | 5.41 | 9.62 | 12 | 0.5 | 7.62 | 49.93 | 2 |
| 2 | 3.33 | 13.71 | 12 | 0.5 | 11.71 | 49.94 | 2 |
| 5 | 2.52 | 18.77 | 13 | 0.5 | 16.77 | 49.92 | 2 |

### 7.4.5.3. Comparison

For evaluating the performance of TLBO algorithm, the results from TLBO and PSO are compared. The objective function value (heat sink height) convergence during the entire optimization for all the evaluations are observed. Figure 7.9: Convergence plots for finding the minimum height as the optimal heat sink design using the TLBO and PSO algorithms applying fan number 1Figure 7.9-Figure 7.11 compare the convergence plot of TLBO to PSO for each fan. As it can be seen, the convergence rate of TLBO is much faster than PSO in earlier evaluations. However, with the increase in the number of evaluations the convergence of both algorithms becomes to the almost same level.

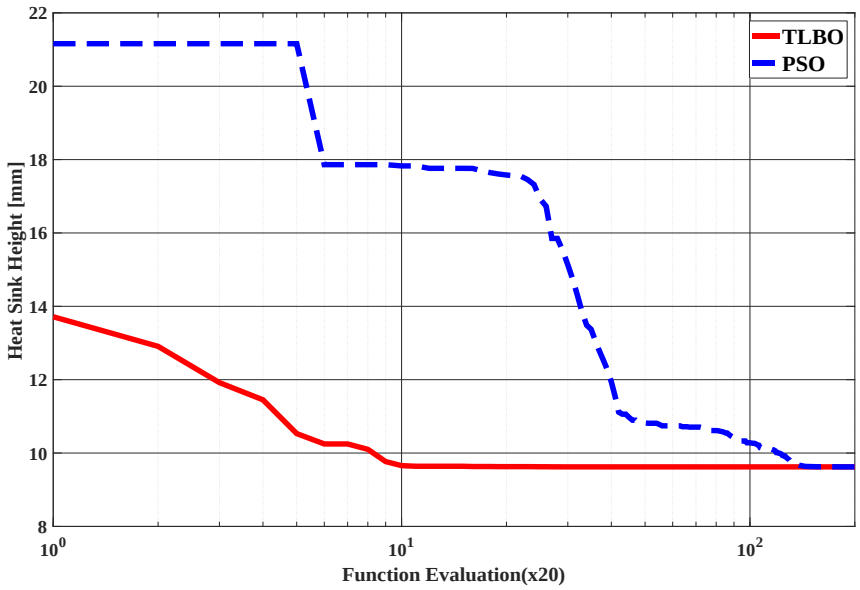


Figure 7.9: Convergence plots for finding the minimum height as the optimal heat sink design using the TLBO and PSO algorithms applying fan number 1

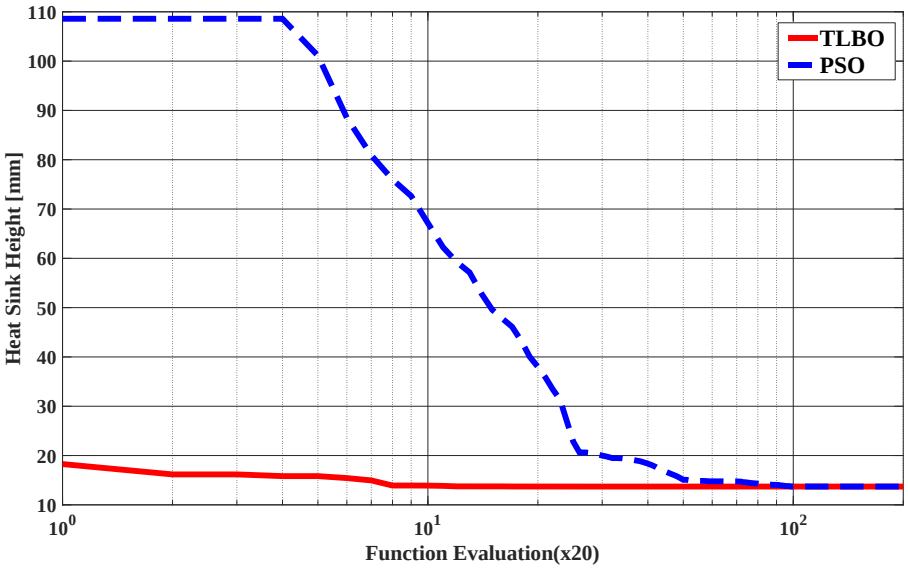


Figure 7.10: Convergence plots for finding the minimum height as the optimal heat sink design using the TLBO and PSO algorithms applying fan number 2

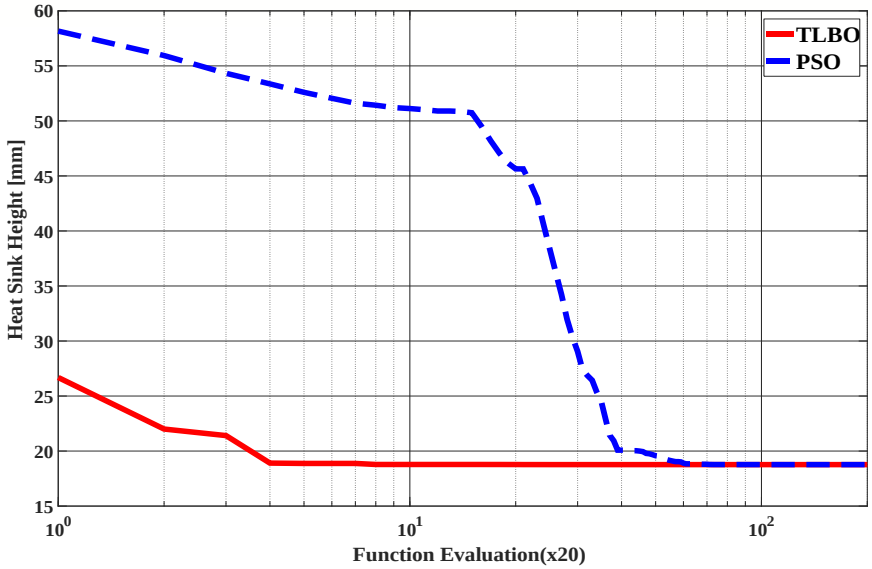


Figure 7.11: Convergence plots for finding the minimum height as the optimal heat sink design using the TLBO and PSO algorithms applying fan number 5

Figure 7.12 compares the objective values of the optimum designs for each fan achieved by TLBO to PSO. As it can be seen, the results for fan number 2 and 5 are nearly the same for each algorithm. By comparing the results for fan number 1, it is shown that PSO was not be able to find the optimum designs at some number of fins. Even though, by comparing Table 7.14 and Table 7.10 the global best points that are achieved for each fan for both algorithms are the same, the PSO didn't produce the best results for some number of fins. Therefore, it is observed that TLBO appeared to have better performance than PSO in the entire optimization process in terms of producing better results and faster convergence rate which means it can find the best solutions in lower number of generations. In addition, the computational time for TLBO in different studied cases was almost 85 seconds and for PSO was 45 seconds, therefore PSO needs lower amount of time for the same number of population and iteration size compare to TLBO.

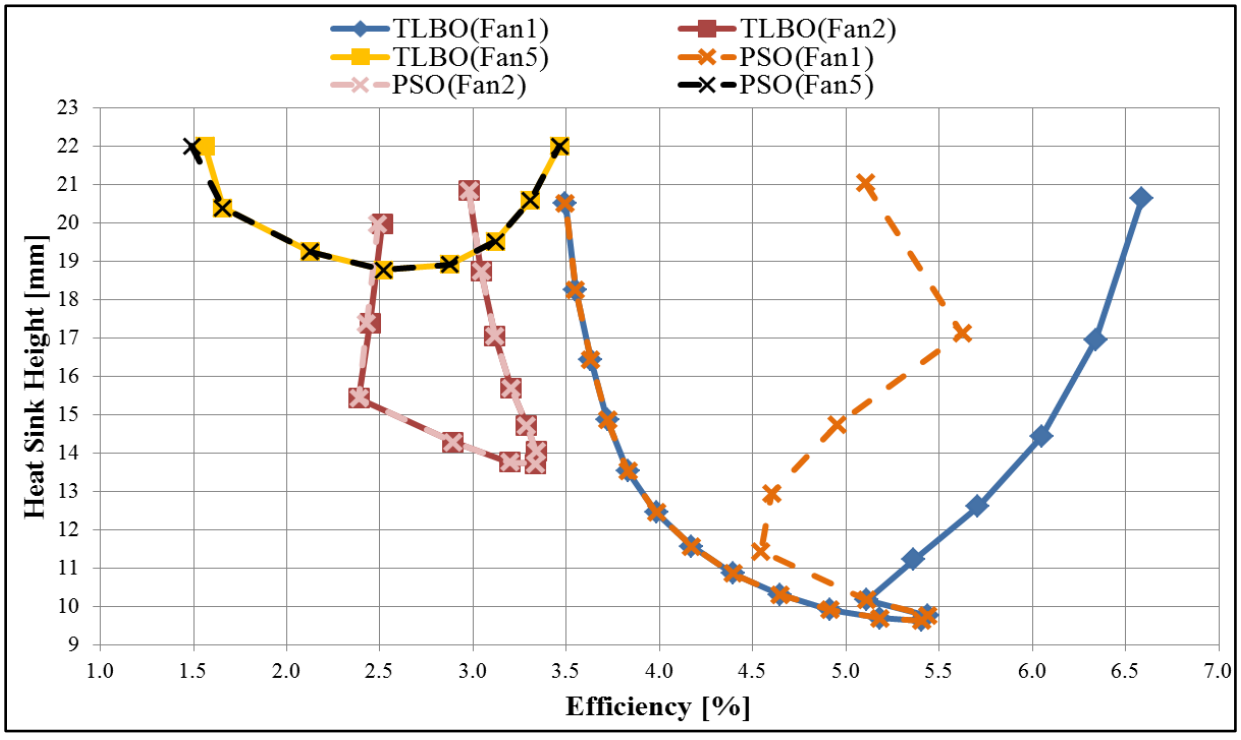


Figure 7.12: The heat sink height versus efficiency for feasible optimal designs of the entire optimization problem applying TLBO and PSO for different fans

## 7.5. Verification with ANSYS Icepack

The global optimal point that is achieved from the optimization process is selected for verifying the design performance. A model with the same design parameters as the global optimum point and optimization designs working condition is simulated in ANSYS Icepack (Figure 7.13).

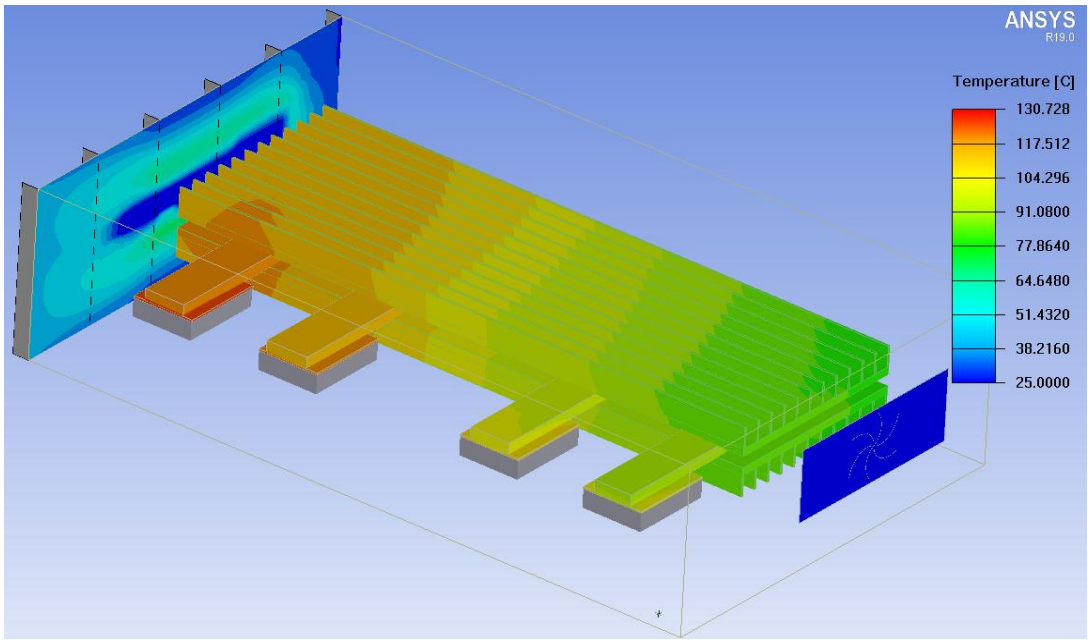


Figure 7.13: Temperature contours for the global optimum point at 40 watts power loss in ANSYS Icepack

The simulation is run for the power loss of 40 watts using fan number 1, and the temperature of the MOSFETs lead frames are observed. The difference between the obtained lead frames temperature from optimization and ANSYS are examined using Equation 6.6. The values for the lead frames temperature achieved from ANSYS and the optimization process and their difference are presented in Table 7.15. The difference in the values of the model and ANSYS is

due to the reason that in the thermal model each MOSFET is considered in one segment so the entire cooling system is divided into 4 segments, and the temperature of each of the lead frames is evaluated as a point in the area of the corresponding node. However, in the ANSYS the number of nodes is a lot more, so the results is more accurate. However, the results difference for the last two MOSFETs which are more critical for the temperature constraints is less than 2%, which means the model is very accurate and adequate for finding the optimal design.

Table 7.15: Lead frames temperature obtained from optimization process and ANSYS for global optimal design at 40 W power loss and the calculated difference between the values

| | 1st MOSFET | 2nd MOSFET | 3rd MOSFET | 4th MOSFET |
|---|---|---|---|---|
| Optimization | 118.05 | 120.6 | 123.04 | 132.64 |
| ANSYS | 104.21 | 111.05 | 124.81 | 130.73 |
| Difference [%] | 13.28 | 8.60 | 1.42 | 1.46 |

# Chapter 8

# Conclusions and Future Work

## 8.1. Conclusions

In this thesis, an integrated forced air heat pipe embedded heat sink cooling system is designed for a converter using in smart home applications. The biggest advantages of the proposed cooling system over previous researches are presented as followed.

Integrating passive and active cooling methods in order to design a very compact, small, power efficient cooling system by using heat pipes, plate-fin heat sinks and fans. It is concluded that the heat pipes during different power loads behave differently in terms of heat transfer rate thus characterization of the heat pipes is necessary in order to find their thermal resistance before implementing them in the design. In addition, integrating fans with heat sinks may drop the efficiency of the fan performance due to the change in cross section area thus a comprehensive thermal model for the proposed cooling system is developed. The thermal model is expanded for cases with multiple heat sources.

A simulation model is built in ANSYS Icepack and the accuracy of the developed thermal model compare to the simulation was more than 99%. In addition, a setup was built and tested for different power loss ranges in combination with multiple heat sources for validating the developed thermal model experimentally, and it has been found that the error between the thermal model and the experimental results was less than 10%.

The validated thermal model was applied in Teaching Learning Based Optimization (TLBO) and Particle Swarm Optimization (PSS) algorithms for finding the optimum cooling system design. It was found that the results found by TLBO is very robust compare to PSO in terms of finding the optimum results and having faster convergence rate. Furthermore, two of the most controversial issues in power converters packaging, volume and efficiency, were discussed during the optimization process for six different design parameters of number of fins, fin height, fin thickness, heat sink width, base plate thickness and fan selection options, under temperature, manufacturability and packaging size constraints.

Finally, the most optimum design that is found from the optimization process is simulated in ANSYS and verified with the optimization results.

## 8.2. Future Work

As mentioned in chapter 6, heat pipes performance might change or destroy when the copper plate is soldered to the heat pipe during the soldering process. Soldering the copper plate to the heat pipe during heat pipe manufacturing before evacuating step is of an interest, since it makes the assembly of the MOSFET-heat pipe module much easier without declining the heat pipe performance.

In addition, the accuracy of the thermal model is strongly affected by the number of nodes that is specified for the entire cooling system. Therefore, increasing the number of nodes along the heat sink length in the thermal model may improve the accuracy of the model.

Furthermore, the heat sink design in this thesis focuses on the plate-fin types due to simple manufacturability and lower number of design parameters in comparison to flared fins and pin fin heat sinks. However, the heat sink performance can improve using pin-fin heat sinks or by flaring the fins.

Finally, the power converters can be designed using Insulated Metal Substrate (IMS) boards instead of Printed Circuit (PC) boards due to their better performance in terms of higher thermal conductivity and heat dissipation capability. Therefore, by using IMS boards it is possible to dissipate power components heat loss with the help of the board as a connection between the components lead frame and the cooling system.

# References

[1] R. V. Rao, V. J. Savsani, and D. P. Vakharia, "Teaching-learning-based optimization: A novel method for constrained mechanical design optimization problems," *Comput. Aided Des.*, vol. 43, no. 3, pp. 303–315, 2011.

[2] R. V. Rao and V. Patel, "Multi-objective optimization of heat exchangers using a modified teaching-learning-based optimization algorithm," *Appl. Math. Model.*, vol. 37, no. 3, pp. 1147–1162, 2013.

[3] J. M. Maza-Ortega, E. Acha, S. García, and A. Gómez-Expósito, "Overview of power electronics technology and applications in power generation transmission and distribution," *J. Mod. Power Syst. Clean Energy*, vol. 5, no. 4, pp. 499–514, 2017.

[4] E. Schütt and K. Skön, "Thermal management and design optimization for a high power LED work light," *Thesis*, p. 72, 2014.

[5] S. S. Anandan and V. Ramalingam, "Thermal management of electronics: A review of literature," *Therm. Sci.*, vol. 12, no. 2, pp. 5–25, 2008.

[6] F. P. Incropera, D. P. DeWitt, T. L. Bergman, and A. S. Lavine, *Fundamentals of Heat and Mass Transfer*. 2007.

[7] E. Laloya, O. Lucía, H. Sarnago, and J. M. Burdío, "Heat management in power converters: from state-of-the-art to future ultra high efficiency systems ," *IEEE Trans.*

*Power Electron.*, vol. 31, no. 11, pp. 7896–7908, 2016.

[8] N. B. Geetha and R. Velraj, “Passive cooling methods for energy efficient buildings with and without thermal energy storage - A review,” *Energy Educ. Sci. Technol. Part A Energy Sci. Res.*, vol. 29, no. 2, pp. 913–946, 2012.

[9] D. Sabatino and K. Yoder, “Pyrolytic graphite heat sinks: A study of circuit board applications,” *IEEE Trans. Components, Packag. Manuf. Technol.*, vol. 4, no. 6, pp. 999–1009, 2014.

[10] B. R. Prasher, “Thermal Interface Materials : Historical Perspective , Status , and Future Directions,” *Proc. IEEE*, vol. 94, no. 8, pp. 1571–1586, 2006.

[11] I. Sauciuc *et al.*, “Carbon based thermal interface material for high performance cooling applications,” *Thermomechanical Phenom. Electron. Syst. -Proceedings Intersoc. Conf.*, pp. 426–434, 2014.

[12] H. Akeiber *et al.*, “A review on phase change material (PCM) for sustainable passive cooling in building envelopes,” *Renew. Sustain. Energy Rev.*, vol. 60, pp. 1470–1497, 2016.

[13] S. K. Saha and P. Dutta, “Thermal management of electronics using PCM-based heat sink subjected to cyclic heat load,” *IEEE Trans. Components, Packag. Manuf. Technol.*, vol. 2, no. 3, pp. 464–473, 2012.

[14] Y. C. Weng, H. P. Cho, C. C. Chang, and S. L. Chen, “Heat pipe with PCM for electronic cooling,” *Appl. Energy*, vol. 88, no. 5, pp. 1825–1833, 2011.

[15] J. Jaguemont, N. Omar, P. Van den Bossche, and J. Mierlo, “Phase-change materials

(PCM) for automotive applications: A review," *Appl. Therm. Eng.*, vol. 132, pp. 308–320, 2018.

[16] A. Waqas and Z. Ud Din, "Phase change material (PCM) storage for free cooling of buildings - A review," *Renew. Sustain. Energy Rev.*, vol. 18, pp. 607–625, 2013.

[17] D. Deng, J. ping Cheng, S. chang Zhang, and F. gen Ge, "Theoretical and experimental validation study on automotive air-conditioning based on heat pipe and LNG cold energy for LNG-fueled heavy vehicles," *Heat Mass Transf. und Stoffuebertragung*, vol. 53, no. 8, pp. 2551–2558, 2017.

[18] H. Jouhara and R. Meskimmon, "Heat pipe based thermal management systems for energy-efficient data centres," *Energy*, vol. 77, no. October 2008, pp. 265–270, 2014.

[19] P. Cong, V. R. Gaddam, D. P. Olson, T. V. Smith, E. R. Scott, and L. L. Perz, "SENSING TEMPERATURE WITHIN MEDICAL DEVICES," *US Pat. 9,882,420 B2*, vol. 2, 2018.

[20] X. Chen, H. Ye, X. Fan, T. Ren, and G. Zhang, "A review of small heat pipes for electronics," *Appl. Therm. Eng.*, vol. 96, pp. 1–17, 2016.

[21] A. Blinov, D. Vinnikov, and T. Lehtla, "Cooling Methods for High-Power Electronic Systems," *Sci. J. Riga Tech. Univ. Power Electr. Eng.*, vol. 29, pp. 79–86, 2011.

[22] Y. P. Zhang, X. L. Yu, Q. K. Feng, and R. T. Zhang, "Thermal performance study of integrated cold plate with power module," *Appl. Therm. Eng.*, vol. 29, no. 17–18, pp. 3568–3573, 2009.

[23] H. Ohta, T. Mizukoshi, T. Yoshida, and Y. Shinmoto, "Fundamental experiments for the development of high-performance cold plates in a feasability study on space solar power

system," *Microgravity Sci. Technol.*, vol. 17, no. 3, pp. 75–81, 2005.

[24] K. Ebrahimi, G. F. Jones, and A. S. Fleischer, "A review of data center cooling technology, operating conditions and the corresponding low-grade waste heat recovery opportunities," *Renew. Sustain. Energy Rev.*, vol. 31, pp. 622–638, 2014.

[25] J. Jörg, S. Taraborrelli, G. Sarriegui, R. W. De Doncker, R. Kneer, and W. Rohlfs, "Direct single impinging jet cooling of a mosfet power electronic module," *IEEE Trans. Power Electron.*, vol. 33, no. 5, pp. 4224–4237, 2018.

[26] J. Kim, "Spray cooling heat transfer: The state of the art," *Int. J. Heat Fluid Flow*, vol. 28, no. 4, pp. 753–767, 2007.

[27] G. Righetti, C. Zilio, S. Mancin, and G. A. Longo, "Heat Pipe Finned Heat Exchanger for Heat Recovery: Experimental Results and Modeling," *Heat Transf. Eng.*, vol. 39, no. 12, pp. 1011–1023, 2018.

[28] H. Jouhara, A. Chauhan, T. Nannou, S. Almahmoud, and B. Delpech, "Heat pipe based systems - Advances and applications," *Energy*, vol. 128, pp. 729–754, 2017.

[29] C. W. Chan, E. Siqueiros, M. Royapoor, and A. P. Roskilly, "Heat utilisation technologies : A critical review of heat pipes," *Renew. Sustain. Energy Rev.*, vol. 50, pp. 615–627, 2015.

[30] S. T. Tu, H. Zhang, and W. W. Zhou, "Corrosion failures of high temperature heat pipes," *Eng. Fail. Anal.*, vol. 6, no. 6, pp. 363–370, 1999.

[31] X. Yang, Y. Y. Yan, and D. Mullen, "Recent developments of lightweight, high performance heat pipes," *Appl. Therm. Eng.*, vol. 33–34, no. 1, pp. 1–14, 2012.

[32] A. Kraus, A. Bar-Cohen, and A. A. Wative, *Cooling Electronic Equipment*, vol. 4. Wiley, 2006.

[33] C. Karatekin and O. Kökkaya, "Comparative analysis of different cooling fin types for countering LED luminaires' heat problems," *Turkish J. Electr. Eng. Comput. Sci.*, vol. 26, no. 1, pp. 454–466, 2018.

[34] Y. Peles, A. Koşar, C. Mishra, C. J. Kuo, and B. Schneider, "Forced convective heat transfer across a pin fin micro heat sink," *Int. J. Heat Mass Transf.*, vol. 48, no. 17, pp. 3615–3627, 2005.

[35] K. J. T. Assel Sakanova, "Comparison of pin-fin and finned shape heat sink for power electronics in future aircraft," *Appl. Therm. Eng. J.*, vol. 15, no. 3, pp. 434–447, 2018.

[36] D. Yang, Y. Wang, G. Ding, Z. Jin, J. Zhao, and G. Wang, "Numerical and experimental analysis of cooling performance of single-phase array microchannel heat sinks with different pin-fin configurations," *Appl. Therm. Eng.*, vol. 112, pp. 1547–1556, 2017.

[37] "Availble Online: https://www.abl-heatsinks.co.uk/heatsink/heatsink-selection-fin-arrangements.htm."

[38] J. Zhao, S. Huang, L. Gong, and Z. Huang, "Numerical study and optimizing on micro square pin-fin heat sink for electronic cooling," *Appl. Therm. Eng.*, vol. 93, pp. 1347–1359, 2016.

[39] P. Li, H. Yan, Q. Luo, D. Liang, and P. Li, "Numerical study on natural convection heat dissipation of flared fin heat sink for high concentrating photovoltaic module cooling," *Energy Sources, Part A Recover. Util. Environ. Eff.*, vol. 41, no. 5, pp. 573–583, 2019.

[40] M. Pierce, “Fans and Blowers - Introduction,” *Energy*, pp. 93–112, 1997.

[41] A. Engineers, “Resort Saves Money Using Rejected Heat Select Fans Using Fan Total Pressure To Save Energy,” no. July, 2011.

[42] J. Smoot, “Important Considerations When Selecting a Fan for Forced Air Cooling.”

[43] U. Drofenik and J. W. Kolar, “Analyzing the Theoretical Limits of Forced Air-Cooling by Employing Advanced Composite Materials with Thermal Conductivities #x003E; 400W/mK,” *Integr. Power Syst. (CIPS), 2006 4th Int. Conf.*, pp. 1–6, 2006.

[44] S. Schiavon and A. K. Melikov, “Introduction of a cooling-fan efficiency index,” *HVAC R Res.*, vol. 15, no. 6, pp. 1121–1144, 2009.

[45] W. Srimuang and P. Amatachaya, “A review of the applications of heat pipe heat exchangers for heat recovery,” *Renew. Sustain. Energy Rev.*, vol. 16, no. 6, pp. 4303–4315, 2012.

[46] C. Alfred S. Conte, Hollister, “COOLING MULTI-CHIP MODULES USING EMBEDDED HEAT PPES,” *United States Pat. 5,355,942*, vol. 65, no. 19, 1994.

[47] V. Barrocas, “heat pipe type cooling apparatus for semiconductor,” *United States Pat. 4,982,274*, vol. 1, no. 12, pp. 0–9, 1991.

[48] R. F. Coleman and P. E. W. Davis, “Heat pipe cooling plate,” *United States Pat. 4,880,052*, no. 19, 1989.

[49] H.-S. Li and C.-A. Hsiao, “FLAT PLATE HEAT PIPE COOLING SYSTEM FOR ELECTRONIC EQUIPMENT ENCLOSURE,” *U.S. Pat. 6,043,336.*, pp. 1–6, 2000.

[50] U. Drofenik, G. Laimer, J. W. Kolar, O. Strategy, and H. Power, “Theoretical Converter

Power Density Limits for Forced Convection Cooling," *Proc. Int. PCIM Eur. 2005 Conf.*, no. 4, pp. 608–619, 2005.

[51] U. Drofenik and J. W. Kolar, "Thermal Power Density Barriers of Converter Systems," *5th Int. Conf. Integr. Power Syst.*, vol. 1, pp. 1–5, 2008.

[52] C. Gammeter, F. Krismer, and J. W. Kolar, "Weight optimization of a cooling system composed of fan and extruded-fin heat sink," *IEEE Trans. Ind. Appl.*, vol. 51, no. 1, pp. 509–520, 2015.

[53] U. Drofenik, G. Laimer, and J. W. Kolar, "Pump characteristic based optimization of a direct water cooling system for a 10kW/500kHz Vienna rectifier," *PESC Rec. - IEEE Annu. Power Electron. Spec. Conf.*, vol. 6, no. 3, pp. 4894–4900, 2004.

[54] B. Wrzecionko, D. Bortis, and J. W. Kolar, "A 120 °c Ambient Temperature Forced Air-Cooled Normally-off SiC JFET Automotive Inverter System," *IEEE Trans. Power Electron.*, vol. 29, no. 5, pp. 2345–2358, 2014.

[55] D. Christen, M. Stojadinovic, and J. Biela, "Energy Efficient Heat Sink Design: Natural Versus Forced Convection Cooling," *IEEE Trans. Power Electron.*, vol. 32, no. 11, pp. 8693–8704, 2017.

[56] J. Blondin, "Particle Swarm Optimization Applications in Parameterization of Classifiers," *Optimization*, pp. 1–5, 2009.

[57] R. V. Rao and K. C. More, "Optimal design of the heat pipe using TLBO (teaching–learning-based optimization) algorithm," *Energy*, vol. 80, pp. 535–544, 2014.

[58] J. Wang, A. Q. Huang, W. Sung, L. Yu, and J. B. Baliga, "Smart Grid Technologies,"

*IEEE Ind. Electron. Mag.*, vol. 3, no. 2, pp. 16–23, 2009.

[59] A. Albarbar and C. Batunlu, *Thermal Analysis of Power Electronic Devices Used in Renewable Energy Systems*. 2018.

[60] N. E. Mode, "C2M0025120D Silicon Carbide Power MOSFET," pp. 1–10, 2015.

[61] N. E. Mode, "C3M0065090J Silicon Carbide Power MOSFET," no. 1, pp. 1–10, 2015.

[62] P. Summary, "Power-Transistor."

[63] H.-F. ® 300P, "Electrically Insulating, Thermally Conductive, Phase change thermal pad 300P_HENKEL 0615," no. November, 2013.

[64] Q. advanced thermal solutions I. Company, "Heat Pipes," *Data Sheet*, pp. 23–24, 2006.

[65] T. Articles, H. Pipes, T. Roles, and T. Management, "ATS Engineering eBook."

[66] R. Rodriguez, M. Alizadeh, J. Bauman, P. S. Ravi, and A. Emadi, "Performance Evaluation of Thermal Management for a 3-Phase Interleaved DC-DC Boost Converter," *2018 IEEE Transp. Electrif. Conf. Expo, ITEC 2018*, pp. 632–637, 2018.

[67] K.-P. Company, "Power Film Resistors TO-126, TO-220 and TO-247 Style," no. 541, pp. 1–2, 2002.

[68] OMEGA, "Ready-Made Insulated Thermocouples Ready-Made Insulated Thermocouples," *Data SHee*, pp. 22–23.

[69] CUI INC Company, "SERIES : CBM-75B │ DESCRIPTION : DC BLOWER," *Data Sheet*, pp. 1–7, 2017.

[70] A. Prasad and M. A. Ricklick, "A Detailed Uncertainty Analysis of Heat Transfer

Experiments using Temperature Sensitive Paint," 2017.

[71] D. Irawan, "Geometrical Optimization of Plate-Fin Heat Sink," 2016.

[72] B. Chopard and M. Tomassini, "Particle swarm optimization," *Nat. Comput. Ser.*, pp. 97–102, 2018.

[73] M. Juneja and S. K. Nagar, "Particle swarm optimization algorithm and its parameters: A review," *ICCCCM 2016 - 2nd IEEE Int. Conf. Control Comput. Commun. Mater.*, no. Iccccm, pp. 1–5, 2017.

[74] M. Clerc and J. Kennedy, "The particle swarm-explosion, stability, and convergence in a multidimensional complex space," *IEEE Trans. Evol. Comput.*, vol. 6, no. 1, pp. 58–73, 2002.